COBRA-LIKE4: A GPI-ANCHORED PROTEIN FUNCTIONING AS A MEDIATOR OF CELLULOSE ULTRASTRUCTURE IN HERBACEOUS AND WOODY PLANTS

by

Grant McNair

BSc Hons, The University of Pretoria, 2005

MSc, The University of Pretoria, 2009

A THESIS SUBMITTED IN PARTIAL FULFILLMENT OF

THE REQUIREMENTS FOR THE DEGREE OF

DOCTOR OF PHILOSOPHY

in

THE FACULTY OF GRADUATE AND POSTDOCTORAL STUDIES

(Forestry)

THE UNIVERSITY OF BRITISH COLUMBIA

(Vancouver)

January 2015

Abstract

Cellulose biosynthesis is a dynamic and specialized cellular process with multiple layers of organization. This abundant, vital polymer is synthesized by cellulose synthase complexes (CSCs) localized at the plasma membrane. Cellulose chains are extruded into the apoplast, and rapidly self-assemble into microfibrils. The mechanisms controlling organization of the product, cellulose microfibrils, are still unclear. The GPI-anchored protein COBRA (*COB*), localized at the outer leaflet of the plasma membrane, is required for normal cellulose deposition in primary cell walls. A closely related protein, COBRA-LIKE4 (COBL4), is required for secondary cell cellulose organization. Loss-of-function, in *Arabidopsis cobl4* mutants originally called *irregular xylem 6 (irx6*), results in reduced cellulose content, cellulose of lower crystallinity, and thinner secondary cell walls. To better understand COBL4 function, I investigated the chemical and ultrastructural properties of novel *irx6*-2 and *irx6*-3 alleles of *Arabidopsis*. I followed this up by demonstrating functional conservation between *COBL4* in woody (*Populus trichocarpa*) and herbaceous (*Arabidopsis*) species. A fluorescently labelled poplar COBL4, PtCOB4a, was co-localized with secondary cell wall thickenings in an inducible *Arabidopsis* protoxylem experimental system. To further refine our understanding the molecular role of COBL4, *AtCOBL4* was over-expressed in hybrid poplar, in a secondary cell wall specific manner. Increased AtCOBL4 abundance did not significantly alter cell wall derived glucose content compared to control plants; this was confirmed by the absence of a significant increase in α-cellulose. The ultra-structural characteristics of deposited cellulose, specifically cellulose DP and cellulose crystallinity, were significantly increased in a number of over expression lines relative to control trees. These findings confirm COBL4 as a protein involved in organizing cellulose biosynthesis in plants. The increased cellulose DP and subsequent proportion of crystalline cellulose suggest that COBL4, in part, affects cellulose biosynthesis efficiency. To further resolve the role that cellulose ultrastructure plays in limiting intrusive tip growth of fibre cells, we measured xylary fibre lengths of *AtCOBL4* overexpression poplar lines. Overexpression lines had on average shorter fibres than wild-type trees. This demonstrates that increased DP and the overall structural organization of cellulose, mediated by AtCOBL4, may be sufficient to restrict intrusive growth of fibre cells.

Preface

Chapters 2 and 3 of this thesis are in preparation for publication in peer-reviewed journals.

Chapter 2: Grant McNair contributed to the experimental design of the research project, performed the research, conducted the research and prepared the manuscript. Sarah Barkwill assisted in performing the research. Yoshi Watanabe and Mathias Schuetz assisted with the FRAP and confocal imaging. Mathias Schuetz from the Samuels lab generated the *VND7-VP16-GR*/cytosolic-GFP lines. Chris Ambrose from Geoff Wasteneys' lab generated and kindly provided the RFP labelled Tubulin-5α lines. Shawn Mansfield was involved in identification of the research project; design of the research project, providing the research opportunity, and with manuscript preparation. Lacey Samuels was involved in the identification of, and design of the research project, providing research opportunity, and with manuscript preparation.

Chapter 3: Grant McNair contributed to the experimental design of the research project, performed the research, conducted the research and prepared the manuscript. Sarah Barkwill assisted in performing the research. Shawn Mansfield was involved in identification of the research project; design of the research project, providing the research opportunity, and with manuscript preparation. Lacey Samuels was involved in the design of the research project, providing research opportunity, and with manuscript preparation.

Table of contents

List of tables

List of figures

List of abbreviations

AGP	Arabinogalactan protein
Asn	Asparagine
BC1	Brittle culm 1
CBM	Cellulose binding module
cDNA	Complementary deoxyribonucleic acid
CDS	Protein coding sequence
CesA	Cellulose synthase
Col-0	Columbia-0
CSC	Cellulose synthesizing complex
CSI1	Cellulose interactive 1
cYFP	Citrine yellow fluorescent protein
DCB	2,6-dichlorobenzonitrile
DI	De-ionised
DMAc	Dimethylacetamide
DNA	Deoxyribonucleic acid
DP	Degree of polymerization
DRM	Detergent resistant membrane
EtOH	Ethanol
FLA	Fasciclin-like arabinogalactan protein

FRAP	Fluorescence recovery after photo-Bleaching
FQA	Fibre quality analyzer
GAP	GPI-anchored protein
GFP	Green fluorescent protein
G-layer	Gelatinous layer
GPC	Gel permeation chromatography
GPI	Glycosylphosphatidylinositol
HPLC	High-performance liquid chromatography
KOR	Korrigan
l_d	liquid-disordered phase
l_o	liquid-ordered phase
irx	Irregular xylem
MASC	Microtubule-associated cellulose synthase compartment
MF	Microfibril
MFA	Microfibril angle
MOE	Modulus of elasticity
MOR1	Microtubule organization 1
MS	Murashige and Skoog media
MT	Microtubule
OE	Over expression

PCR	Polymerase chain reaction
QTL	Quantitative trait loci
RFP	Red fluorescent protein
RT-PCR	real-time PCR
SmaCC	Small CesA compartment
SuSy	Sucrose Synthase
T-DNA	Transfer-deoxyribonucleic acid
TW	Tension Wood
VND7	vascular-related NAC domain 7
Ws	Wassilewskija
Wt	wild-type
XET	Xyloglucan-endo-transglycosylase

Acknowledgements

I would like to first and foremost thank my co-supervisors, Shawn Mansfield and Lacey Samuels, for their invaluable guidance, training, support and kindness throughout my PhD. Being approachable and taking a keen interest in my project has made this a wonderful environment to work in. To my supervisory committee, Carl Douglas and Patrick Martone: thank you for providing opportunities for open discussion, guidance, and allowing me to draw on your expertise.

To all Mansfield lab members, past and present, thank you for your technical support and willingness to discuss topics of cell wall research, in particular, Ji Young Park, Faride Unda, James Hart and Francis De Araujo. To Samuels lab members, past and present, thank you for sharing your microscopy expertise with me and for stimulating discussions, in particular Heather McFarlane, Yoshito Watanabe and Mathias Schuetz. I also thank the UBC bio-imaging facility, for training and technical support in the art of live cell microscopy.

Funding was provided through a NSERC discovery grant (Shawn Mansfield), a NSERC create, through the Working on Walls Program (WOW), and a UBC international tuition award. WOW provided an environment and network that extended far beyond the scope of traditional academia, better preparing graduating students for careers in or outside of academia.

I would like to thank my Family; Mom, Dad, Craig, Tammy for their continued love and support. Finally, thank you Tova for your love, understanding and support throughout the completion of my PhD.

Chapter 1: Introduction

The evolution of rigid cell walls with load-bearing capacity by plants was a prerequisite for successful colonization of terrestrial environments. Cell walls can be classified as either primary walls, which surround all plant cells, or secondary cell walls that are deposited within the confines of the primary cell wall following cell expansion. Secondary cell walls are often associated with the vascular system, such as in secondary xylem (wood). Plant secondary cell walls are composed primarily of lignin, hemicelluloses and cellulose. Correct organization of newly synthesized cellulose, the major component of the cell wall, is key to maintaining structural integrity of plant cell walls. The mechanisms underpinning the ordered pattern of cellulose deposition in the cell wall are still unclear.

Proteins anchored in the outer leaflet of plasma membrane, such as GPI-anchored proteins, are ideally situated to organize newly synthesized cellulose as it is extruded from cellulose synthase complexes (CSCs). The *COBRA* gene family is a family of GPI-anchored proteins, which have been suggested to play a role in cellulose biosynthesis which has yet to be defined. The presence of at least one cellulose binding module (CBM) at the N-terminal of COBRA protein family creates the opportunity for direct interaction with cellulose at the plasma membrane cell wall interface. These structural attributes provide a means for COBRA**,** and COBRA-like proteins, to influence the organization of cellulose at the point of cellulose extrusion into the apoplastic space. However, which specific characteristics of cellulose microfibrils in secondary cell walls are influenced by COBRA-like proteins have not been defined, especially for xylem.

1.1 Plant cell walls

To correctly place COBRA proteins at their appropriate functional position in the cellulose biosynthetic machinery, it is necessary to have a clear understanding of cellulose biosynthesis in the context of cell wall structure and development. Both primary and secondary cell walls contain cellulose, hemicelluloses, and lignin.

Cellulose consists of 1,4-β-linked glucose chains that are deposited in a parallel fashion, and can form both intra- and inter-chain hydrogen bonds that ultimately result in the formation of crystalline regions within the polymer. It has been proposed that up to 24 glucan chains form an elementary fibril (Ding and Himmel, 2006; Bessueille and Bulone, 2008; Morgan *et al.*, 2013), and that these in turn rapidly coalesce to form microfibrils (MFs). The crystalline cellulose structure give rise to tightly packed cellulose chains within MFs , and it is hypothesized that the degree of polymerization (DP) of the glucose monomers within the chains may also influence the extent of crystallization (Fujita *et al.*, 2011).

Hemicelluloses are amorphous heteropolymers that vary in structure and physiochemical properties (reviewed by Scheller and Ulvskov 2010), and are distinct from pectin molecules (Caffall and Mohnen 2009). Hemicelluloses include xyloglucan, xylans, mannans and glucomannans. Xyloglucans (~23%) are the most abundant hemicellulose in primary cell walls, while xylan (~25%) are the most abundant in secondary cell walls of angiosperms, such as poplar (Varner and Lin 1989). Hemicelluloses bind directly to both hydrophobic and hydrophilic

surfaces of elementary fibres cross-linking them together providing rigidity to the cell wall (Cosgrove, 2000; Park and Cosgrove, 2012; Derba-Maceluch *et al.*, 2014; Buse-Wicher *et al.*, 2014). However, it has been found that in *Arabidopsis,* mutants that are reduced in xylan possess secondary cell walls that are thinner, have altered cell wall composition and display an irregular xylem (*irx*) phenotype (Brown *et al.*, 2005; Zhou *et al.*, 2005; Jensen *et al.*, 2010; Brown *et al.*, 2011).

A major component of the secondary cell wall is lignin. Lignin is derived from three hydroxycinnamyl alcohol monomers; *p*-coumaryl alcohol, coniferyl alcohol, and sinapyl alcohol that polymerize to form hydroxyphenyl (H), guaiacyl (G) and syringyl (S) lignin, respectively (Boerjan *et al.* 2003). The monomers are synthesized via the phenylpropanoid pathway that employs phenylalanine as a precursor. These monolignols can engage in an array of bonds via random combinatorial coupling, ultimately resulting in a macromolecule that is hydrophobic and somewhat amorphous. The primary function of lignin is thought to be structural support and waterproofing of vascular tissues to facilitate water and nutrient transport. Substantial cross-linking of the lignin polymer to either hemicelluloses or cellulose forms lignin-carbohydrate-complexes (Jeffries, 1990). Plants deficient in lignin also show an irregular xylem phenotype and have altered composition of the remaining cell wall components (Jones *et al.*, 2001; Franke *et al.*, 2002; Coleman *et al.*, 2008) that is often accompanied by impaired growth. In contrast, altering the monomer composition of lignin in a cell wall, without reducing the overall content, generally does not appear to have a dramatic effect on the growth of greenhouse grown plants (Chen and Dixon 2007).

Irregularities or aberrations in one of these cell wall components can result in changes to the proportions and arrangement of remaining cell wall components, which may further reduce the structural integrity of the cell wall.

1.1.1 Primary cell walls

Plant cell walls provide structural support and define plant cell shape. Primary and secondary cell walls each have distinct characteristics reflecting their functional roles in plant morphology and development. Primary cell walls are deposited during cell division and expansion. The primary cell wall defines the final cell shape for the majority of cell types. This requires the primary cell wall to be selectively malleable, enabling cell expansion through a process of tightly regulated plastic deformation termed anisotropic growth. This anisotropic growth underlies the diversity of plant cell morphology and function. This plasticity is achieved by substantial remodelling of cell wall components to permit isotropic and anisotropic cell expansion. Cells can elongate either by “tip growth” where growth only occurs from a single point at each the tip of a cell, or alternatively via diffuse growth where the cell wall constituents are added along the length of an expanding cell (Smith and Oppenheimer, 2005). Loosening of the cell wall matrix to facilitate expansion is achieved by the concerted activities of a suite of enzymes (expansins, cellulases, xyloglucan endo-transglycosylases, polygalactanases and pectin lyases) that modify the various polymers composing the primary cell wall (Cosgrove, 2005, Park and Cogrove, 2012).

The chemical make-up of primary cell walls is distinct from that of secondary cell walls. Primary cell walls have a lower cellulose content (30-40%) and have xyloglucan as the major hemicellulose (35%) where secondary cell walls do not. Primary cell walls can contain as much as 23% pectic material, and also contain specialized proteins (Scheller and Ulvskov, 2010). In primary cell walls, lignin is deposited in the middle lamella, and in the corners of cells destined to have a secondary cell wall (Saka and Goring, 1985). Once cell expansion has ceased, secondary cell wall deposition commences in specialized cell types, such as xylem vessels and other tracheary elements, and in fibres. Fibre cells are required for plant structural support and expand longitudinally by intrusive tip growth, which allows the cell grow in between the cells above and below the expanding fibre cells. Unlike in most situations, there appears to be an exception here to the primary cell wall defining the ultimate size of all plant cells. A thick secondary cell wall is deposited within fibre cells to provide the mechanical strength for fibre cells supportive function. This has raised a question as to whether secondary cell wall deposition takes place during intrusive tip growth or only once cell expansion has ceased. The limited research to date provides evidence of simultaneous tip growth and secondary cell wall deposition in fibre cells (Gritsch and Murphy, 2005). Assuming these processes occur simultaneously, a role has been hypothesized for the secondary cell wall in determining final fibre cell dimensions (Lev-Yudan, 1997; Gray-Mitsumune, 2004; Gritsch and Murphy, 2005). Further evidence that primary cell wall expansion alone does not determine the final length of fibre cells was provided by Gray-Mitsumune *et al.* (2008), who over expressed an α-expansin, *PttEXPA1*, in hybrid poplar. This resulted in fibres of greater diameter, but no changes to fibre length, implying that factors other than primary cell wall expansion determines final fibre cell

length. It has been proposed that secondary cell wall deposition commences at the middle of the fibre cell, extending outwards towards the tip of the cell (Lev-Yudan, 1997; Gray-Mitsumune, 2004; Gritsch and Murphy, 2005), and that this progressive outward synthesis of the secondary cell wall in fibre cells may ultimately limit or inhibit tip growth of elongating fibre cells (Gritsch and Murphy, 2005). The study of fibre cell anatomy in secondary cell wall deficient mutant plants that have wild type plant morphology and growth would provide a means to determine if secondary cell walls do indeed influence the final length of intrusively growing fibre cells. Loss-of-function *cobl4* mutants provide such a system to study intrusive fibre growth.

1.1.2 Secondary cell walls

The majority of wood is composed of secondary cell wall material. The main function of the secondary cell wall is to provide structural strength. This strength can be utilized in a number of ways by the plant, including resisting the negative pressures associated with water transport up the plant vasculature, mechanical strength needed to maintain orientated plant growth, and resistance against abiotic and biotic stress. Central to the ability of the secondary cell wall to contribute to these tasks is the coordinated and highly ordered arrangement of the major components of the secondary cell wall. The chemical composition of the secondary cell wall is characterized by greater proportions of cellulose (~45-50%), diverse hemicelluloses (~27-35%), and lignin (~25-30%). A diverse complement of glycoproteins are also present in the secondary

cell wall. The secondary cell wall consists of three distinct structural layers (S1, S2, S3), each with unique characteristics (Figure 1.1).

A wide variety of genes have been identified that contribute to the biosynthesis as well as the dynamic assembly of the final secondary cell wall architecture. The continued functional characterization of these genes and their associated loss-of-function mutant phenotypes will continue to expand our understanding of cell wall formation. The central role of cellulose, the most abundant of the cell wall polymers, in determining a wide range of cell wall attributes makes it a key component in cell wall structure and function.

1.1.3 Cellulose biosynthesis and resultant ultrastructural properties

Cellulose is synthesized by a subset of glucosyltransferases known as the cellulose synthases (CesAs), which associate in multi-protein complexes embedded in the plasma membrane. CesAs are the most thoroughly characterized in *Arabidopsis*, where 10 family members have been identified (Yin *et al.* 2009). In contrast, 18 CesAs have been identified in poplar (Yin *et al.*, 2009). CesAs have been classified into two groups based on their roles in the synthesis of either primary or secondary cell walls. To date, in *Arabidopsis*, AtCesA4, AtCesA7 and AtCesA8 have been identified, and subsequently validated, as functioning specifically in secondary cell wall formation (Brown *et al.* 2005; N.G. Taylor 2007). Loss-of-function mutants in any one of these genes manifest in the irregular xylem (*irx*) phenotype (Brown *et al.* 2005; Turner and Somerville 1997). The remaining seven CesAs function in primary cell wall deposition with varying degrees

of redundancy (Desprez *et al.* 2007; Fagard *et al.* 2000; Persson *et al.* 2007; Scheible *et al.* 2001). The CesAs self-assemble into cellulose synthase complexes (CSCs), each consisting of multiple CesA subunits. At least one of each of the secondary cell wall CesA proteins is required to form a fully functional CSC (Wightman *et al.*, 2009). The CSC catalyzes the polymerization of UDP-glucose into 1,4-β-linked glucose chains, with UDP-glucose produced by the cleavage of sucrose via sucrose synthase (SuSy) (Coleman *et al.*, 2009; Morgan *et al.*, 2013). The polymerization of UDP-glucose within a CSC is followed by the extrusion of the glucan chains that rapidly self-assemble into elementary fibrils in the apoplast. This process is thought to facilitate CSC propulsion, moving the complex through the plasma membrane (Heath, 1974; Herth and Schnepf, 1980). In *Acetobacter xylinum*, prevention of intra- and inter-molecular hydrogen bond formation between newly synthesized β-1-4 glucan chains by exposure to calcofluor white increased glucose polymerization four-fold (Herth and Schenpf, 1980). This increased polymerization rate was also associated with cellulose of a lower crystallinity (Benziman *et al.*, 1980; Haigler *et al.*, 1980). During primary cell wall cellulose deposition, recent analyses of *Atcesa1*^{aegeus} and *Atcesa3*$^{ixr1\text{-}2}$ mutants indicated that as CSC velocities increase, the crystallinity of the cellulose produced decreases (Table 1.1) (Harris *et al.*, 2012). The mechanism promoting increased CSC velocity in *Atcesa1*^{aegeus} and *Atcesa3*$^{ixr1\text{-}2}$ plants is, however, not understood. A subsequent study of the *cesA1 mutant, anisotropy1* (*any1*), observed that both CSC velocity and cellulose crystallinity were reduced (Table1.1) (Fujita *et al.*, 2013). Such confounding results may be due to altered interactions between CesAs with a CSC or with cellulose biosynthesis associated proteins. Periods of rapid growth, such as those associated with higher temperatures, also result in reduced cellulose crystallinity and increased

CSC velocity (Table 1.1) (Fujita *et al.* 2011). How the increase in CSC velocity translates into a reduction in cellulose crystallinity or how cellulose crystallinity can influence the rate of cellulose synthesis is unclear.

A number of studies in *Arabidopsis* have identified proteins, that when absent or non-functional, result in changes to cellulose crystallinity in either primary or secondary cell walls, including; *KORRIGAN*, *MICROTUBLE ORGANIZATION* 1, *COBRA* and *COBRA-LIKE* 4, *CELLULOSE SYNTHASE INTERACTIVE 1* (Brown *et al.*, 2005; Roudier *et al.*, 2005; Maloney and Mansfield, 2010; Fujita *et al.*, 2011, Gu *et al.* 2010) (Table 1.1).

Table 1.1: Summary of key cellulose mutants identified in *Arabidopsis* and their impact on cellulose biosynthesis and ultrastructure.

Gene	Gene function	Cellulose content	Cellulose crystallinity	Cellulose organization	CSC velocity	Reference
KORRIGAN $^{1°2°}$ (*jiaoyao1, jia1*)^{ŧ}	endo-1,4-β-D-glucanase	22% less crystalline cellulose ^	Reduced	Altered-cross hatching pattern lost	Reduced	Lei et al 2014, Vain *et al.* 2014
MICROTUBLE ORGANIZATION $1^{1°2°}$ (mor1-1)^{ŧ}	Establish cortical MT arrays	Similar to Wt	Increased	Similar to Wt	Increased	Fujita *et al.* 2011
CELLULOSE SYNTHASE INTERACTIVE $1^{1°}$ *(csi1)*	Physical link between MT and CSCs	50% less crystalline cellulose ^	Reduced	Altered- less uniform	Reduced	Gu *et al.* 2010, Bringmann *et al.* 2012
CesA1$^{1°}$ (cesa1 ^{aegeus})^{ŧ} and *CesA3*$^{1°}$ (cesa3 $^{ixr1-2}$)^{ŧ}	Cellulose biosynthesis	30% less cellulose	Reduced	disorganized	Increased	Harris *et al.* 2012
CesA1$^{1°}$ (*anisotropy1, any1*)^{ŧ}	Cellulose biosynthesis	Similar to Wt	Reduced	Disordered-epidermal cells only	Reduced	Fujita *et al.* 2013

$^{1°}$ primary cell wall function, $^{2°}$ secondary cell wall function
() allele name, ^{ŧ} amino acid substitution, $^{\#}$ gene knock out
^Updegraff cellulose, *wide angle x-ray diffraction

The picture created by these studies is that of a highly specialized biosynthetic machinery that is tightly regulated. How the final ultrastructure of cellulose is determined is still unclear, but perturbation of the function of a single gene involved in the cellulose biosynthetic process alters cellulose structure. Resolution of the cellulose ultrastructural changes in the loss-of-function plant lines would help resolve how each component function and the interrelationship between the various components of cellulose biosynthesis and deposition. It is likely that the action of the cellulose biosynthesis-associated proteins, in conjunction with the CSCs, determine CSC velocity, distribution and the crystallinity of cellulose synthesized for a given set of growth conditions. The COBRA gene family, having family members known to function specifically in either primary or secondary cell wall cellulose deposition, is an important example of how cellulose biosynthesis-associated proteins influence cellulose ultrastructure.

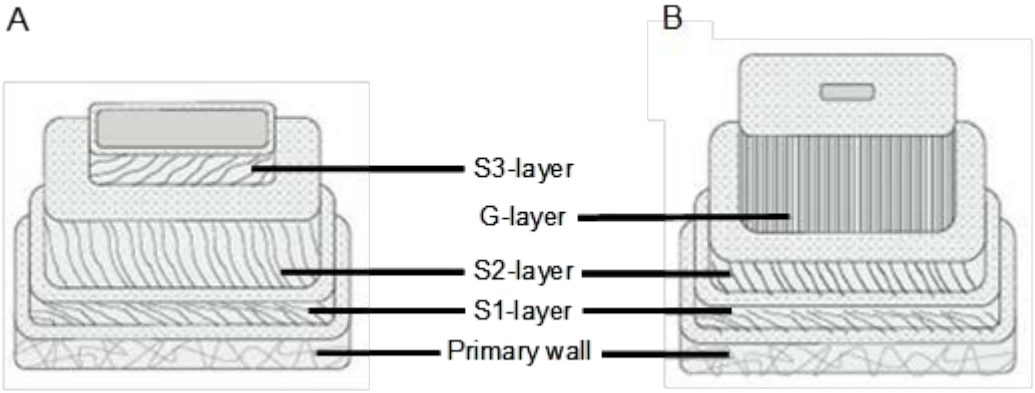

Figure 1.1: A diagrammatic representation of the differences between normal wood (A) and tension wood (B). The cell wall consists of three layers, each with a different microfibril angle. In tension wood the G-layer can replace most of the S2 and S3 layers (in some species), and is characterized by a smaller microfibril angle (Andersson-Gunnerås *et al.* 2006)

In addition to crystallinity, cellulose microfibril angle (MFA), which is defined as the angle between the longitudinal plane of growth and that of the MF, is an important property of cell walls. Once cell expansion in the primary cell wall is complete, the cortical microtubules (MT) reorganize into a helical pattern that corresponds to the cellulose microfibril angle (Funada *et al.*, 2001; Chaffey *et al.*, 2002). In secondary cell walls, the MFA plays an important role in determining its mechanical strength and rigidity, where a large MFA facilitates cell flexibility, while a smaller angle increases cell strength and rigidity (Barnett and Bonham, 2004).

1.1.4 Microtubules and cellulose deposition

It has been hypothesized that MTs, by direct or indirect interactions of the cellulose synthase complexes, are responsible for aligning cellulose MFs. The experimental evidence for this comes from the observed correlated alignment of MTs and MFs (Ledbetter, 1963), and that drug-induced disruption of MTs leads to the subsequent disorganization of MFs (Gardiner *et al.*, 2003; Wightman *et al.*, 2009). The isolation of CesAs and the development of fluorescently-tagged CesAs, has facilitated the study of putative MF-MT interactions through co-localization studies. Using GFP-labelling of AtCesA6 it has been shown that substantial co-localization of MTs and AtCesA6 exists in the primary cell walls of *Arabidopsis* (Paredez *et al.* 2006).

In contrast, reports of MF alignment independent of MTs have been published (Himmelspach *et al.*, 2003). In *Arabidopsis*, cellulose microfibrils were examined in mutant alleles of microtubule associated proteins, such as *microtubule organization 1 (mor1)*, or in plants treated with MT

depolymerizing drugs, such as oryzalin. In the absence of an ordered MT array, newly synthesized MFs were capable of aligning in an ordered fashion (Sugimoto *et al.*, 2001; Himmelspach *et al.*, 2003; Szymanski and Cosgrove, 2009). A hypothetical mechanism by which MTs may play a role cellulose organization is by determining the length and ultrastructure of elementary MFs (Wasteneys 2004; Wasteneys and Fujita 2006). The observations that disruption of MTs resulted in increased CSC velocity, as well as the existence of CSCs in MT free domains, provide support for this hypothesis (Fujita *et al.* 2011). The most recent studies examining CesAs in primary cell walls found that transport of CSCs to the plasma membrane and subsequent secretion is highly coordinated, and requires a complex interaction with the cortical MTs and actin filaments (Sampathkumar *et al.*, 2013). The transport of, and recycling or internalization of CSCs by vesicles in the cortical cytoplasm may be one of the mechanisms mediated by CSC-MT interactions (Crowell *et al.*, 2009; Gutierrez *et al.*, 2009). Until recently, it has been unclear how CSCs and MTs interact, and whether the interactions are direct or mediated via proteins. These questions have recently been partially answered by the identification of *Cellulose synthase interactive protein* 1 (*CSI1*). CSI1 is a cytosolic protein that interacts with primary cell wall CesAs in yeast-two hybrid assays and co-localizes with CSCs at the plasma membrane (Gu *et al.*, 2010; Bringmann *et al.*, 2012b). CSI1 is capable of binding to MT, while simultaneously interacting with cellulose synthase complexes, and so potentially transmitting MT directional information to CSCs embedded in the plasma membrane, providing a mechanism for mediating MT-CesA interactions (Li *et al.*, 2011; Bringmann *et al.*, 2012a). The angle of the MT and subsequent MFA of deposited cellulose, particularly that within the

secondary cell wall, confers structural integrity to individual cells and to the plant as a whole, allowing the plant withstand mechanical forces and stresses acting upon it.

The sessile nature of trees, combined with the dynamic environments in which they grow, places a premium on their ability to respond to various stresses, such as wind, snow or mechanical stress. Trees respond by developing a specialized type of wood, known as reaction wood, which serves to correct the orientation of the stem or branch, or at least to resist mechanical stress. Reaction wood has different properties in gymnosperms and angiosperms (Bamber, 2001). Reaction wood manifests as compression wood in gymnosperms and tension wood (TW) in angiosperms.

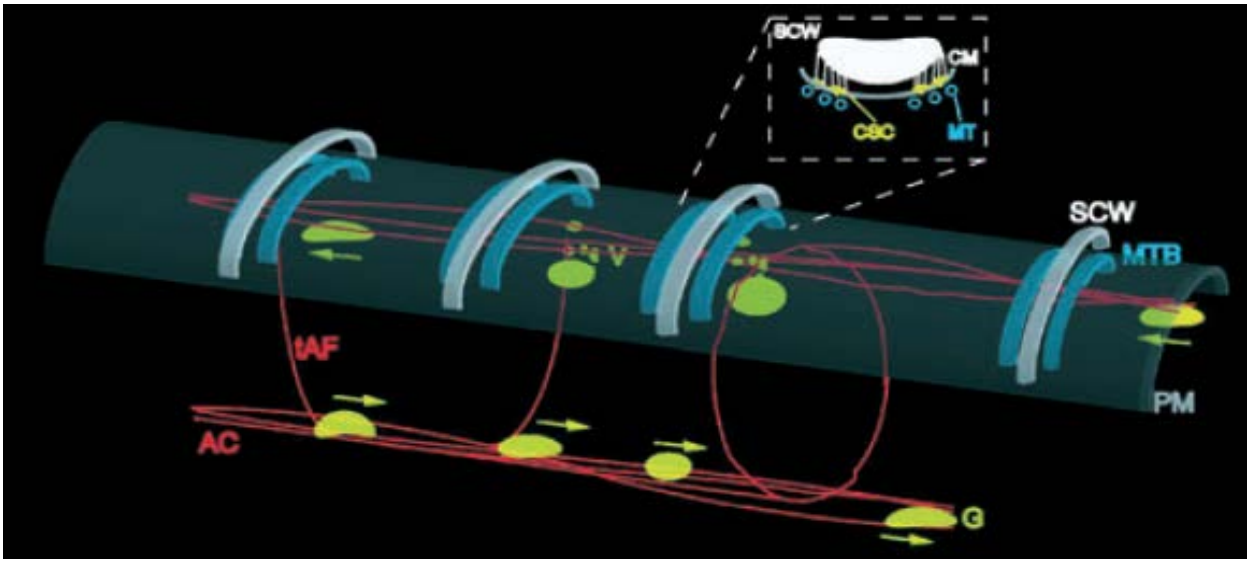

Figure 1.2: A proposed model showing the role of the cytoskeleton in secondary cell wall cellulose synthesis in developing xylem vessel. A longitudinal cross section of an area surrounding a secondary cell wall thickening is shown within the dashed box. AC, actin cable; tAF, transverse actin fibre; G, yellow fluorescent protein-containing Golgi-derived compartment, arrows next to organelles indicate the direction of movement; SCW, secondary cell wall; PM, plasma membrane; V, transport vesicle; MTB, microtubule bundle which is made up of individual microtubules, MT; CSC, cellulose synthase complex; CM, cellulose microfibril which is made up of multiple glucan chains (Wightman and Turner 2008).

Compression wood forms on the underside of the bent stem or branch and differs both physically and chemically from normal wood. In contrast, in angiosperms TW forms on the upper side of a bent stem or branch. TW is characterized as having shorter fibres and increased numbers of fibres, with a decrease in the number of vessel elements. Additionally, there is a large increase in cellulose content, while lignin content remains constant or is only slightly decreased. The replacement of the S3 layer by a "gelatinous layer" (G-layer, Figure 1.1) located inside of the S2 layer of fibres (Joseleau *et al.* 2004; Washusen and Evans 2001) accounts for the increase in cellulose. This G-layer consists almost entirely of pure cellulose that is highly crystalline, and possesses a very small microfibril angle. The lignin chemistry of the G-layer is also altered, displaying an elevated concentration of syringyl moieties compared to normal wood (Joseleau *et al.*, 2004). The S1 and S2 layers are thinner in tension wood in which the G-layer is present, but have normal amounts of lignin and an increased syringyl (S) to guaiacyl (G) lignin ratio. Given the innate reprogramming of cell wall development, and its industrially desirable traits, TW is an ideal model to identify the components of cell wall deposition and further understand cell wall formation. For example, early molecular studies identified secondary cell wall-related candidate genes through expression profiling studies comparing normal wood development profiles to those of TW (Plomion *et al.*, 2003; Paux *et al.*, 2005). Secondary cell wall CesAs were also among the most abundant transcripts in TW, while key lignin biosynthetic genes remained unchanged or were reduced in abundance (Andersson-Gunnerås *et al.* 2006; Paux *et al.* 2005). Tension wood research revealed a member of the *COBRA* gene family, the *AtCOBRA-LIKE4* ortholog in poplar (*PtCOBRA4a*), to be amongst the transcripts showing the largest increase in abundance (Andersson-Gunnerås *et al.* 2006).

1.2 *COBRA* gene family

COBRA genes have been identified as important to cell wall and cellulose biosynthesis in all higher plants investigated to date. To resolve COBRA gene function, it is necessary to understand the protein structure and diversity of COBRA gene families in diverse taxa from an evolutionary context. Establishing the relationship of COBRA with other cell wall biosynthetic components will also further refine our understanding of COBRA function.

1.2.1 Phylogenetic analysis

The *Arabidopsis COBRA* gene family consists of 12 members, the original *AtCOBRA* (*AtCOB*) and *COBRA-LIKE* (*AtCOBL*) 1-11 genes (Roudier *et al.*, 2002). Similarly, 9 family members have been identified in maize (Ching *et al.*, 2006; Brady *et al.*, 2007), 11 in rice (Li *et al.*, 2003a), and 18 in poplar (Ye *et al.*, 2009a). The increased number in poplar had been attributed to a recent genome duplication event (Tuskan *et al.*, 2006). Roudier *et al.* (2002) identified a putative cellulose binding module (CBM) located in the N-terminal region 5 amino acid residues downstream of the predicted N-signal cleavage site (Figure 1.3a), which has subsequently been used to resolve the *AtCOBRA* gene family into two subgroups based on the number of cellulose binding modules. The first group are most similar to *AtCOB* (AtCOBL1-5) and have a single CBM. The second group, *AtCOBL7*-11 are characterized by an additional ~170 N-terminal amino acids downstream of the N-signal peptide cleavage site, containing an additional CBM upstream of the conserved CBM found in all members of the gene family (Figure 1.3b). *AtCOBL6* is a single

outlier belonging to neither group (Roudier, 2002). A similar subgrouping was observed in rice and maize, but with an additional monocot specific subgroup being identified (Brady *et al.* 2007; Li *et al.* 2003).

Figure 1.3: The protein domain structure of subgroup 1 (a) and subgroup 2 (b) COBRA family. Subgroup 2 has an additional 170 amino acids in the N-terminal region of the protein.

The *AtCOBRA* gene family and orthologous poplar family members were found to have varying degrees of overlap in expression in most plant organs (Brady *et al.* 2006; Roudier *et al.* 2002; Schmid *et al.* 2005; Ye *et al.* 2009). Exceptions in *Arabidopsis* are *AtCOBL10* and *AtCOBL12,* which are only expressed in the floral and inflorescence tissues. In maize, only four family members were found to be expressed in the majority of organs (Brady *et al.* 2006). *Arabidopsis* and maize COBRA families were observed to be regulated in a developmental, tissue and cell-specific manner. In summary, *AtCOBRA* and the orthologous gene families display multiple levels of gene expression regulation resulting in a complex spatial-temporal expression pattern, with *PtCOB4a* and *PtCOB4b* being highly up-regulated in woody tissues (Brady *et al.* 2006; Ye *et al.* 2009).

1.2.2 *COBRA*

In *Arabidopsis*, the GPI-anchored protein *COBRA* (*COB*) was first identified as playing a role in conditional root expansion by Benfey *et al* (1993), as *cob* mutants exhibited an abnormal root formation phenotype where the root cells expand radially rather than longitudinally. The resulting aberrant root morphology resembled the hood of a cobra snake, inspiring the name of this protein family. This, and a subsequent study, only observed root defects with aerial organs developing normally (Benfey *et al.* 1993; Schindelman *et al.* 2001). However, the *cob-1* allele was a partial loss-of-function allele, and null alleles (*cob-4* and *cob-5*) were shown to be sterile and lack inflorescence stems, and general abnormal plant growth due to a loss of anisotropic cell growth (Ko *et al.* 2006; Roudier *et al.* 2005). Interestingly, the morphology of root hairs that expand by tip growth are un-altered in *cob* null mutants. This implies that *COB* functions in anisotropic and not tip directed growth in primary cell walls (Brady *et al.* 2007; Roudier *et al.* 2005; Wasteneys and Fujita 2006). The association of *COB* with primary cell wall deposition is further supported by the correlation of gene expression between primary cell wall associated CesAs and COB (Brady *et al.*, 2007). These studies found cellulose levels to be reduced in *cob* lines when compared to WT plants, with the most severe cases showing reduction of 20-30% relative to the wild type. Furthermore, polarized light birefringence was used to demonstrate that cellulose crystallinity was reduced in *cob*-1 mutants (Roudier *et al.* 2005; Schindelman *et al.* 2001).

Although no significant differences in microfibril (MF) angle were detected between wild type and *cobra* null mutants, there was increased variability in the MF angle of cells in the elongation

zone, suggesting a role for COBRA in the processes required to align and orientate MFs (Roudier *et al.* 2005; Wasteneys and Fujita 2006). The on-going debate concerning microtubule-associated orientation of cellulose MFs and the need for COBRA in cellulose MFs alignment lead to the question of COBRA-MT interactions. The use of *ton2-14* and *ton2-13* mutant lines, which exhibit altered cortical MT orientations due to loss-of-function of a phosphatase, were used to test the COBRA-MT relationship (Roudier *et al.* 2005). It was observed that COBRA distribution was increasingly random when MT were disorganized, either due to the *ton* mutation or oryzalin treatment, suggesting potential association or interaction between MT and COBRA (Roudier *et al.*, 2005). From these studies COB scope of function appears to be confined to primary cell wall cellulose biosynthesis during oriented cell expansion. The non-redundant function of COB in primary wall synthesis indicates functional specialization within subgroup 1 of the COBRA gene family, suggesting that other COBRA-like family members might play analogous roles in secondary cell wall formation.

1.2.3 *COBRA-like 4*

The *Arabidopsis AtCOBL4,* the maize homologue *BRITTLE STALK2* (*ZmBK2*), and the rice homologue *BRITTLE CULM 1 (BC1)* are highly expressed in vascular tissue, with expression constrained to cells with thick secondary cell walls, such as tracheary elements and fibres in the xylem (Brady *et al.*, 2006; Dai *et al.*, 2009; Ye *et al.*, 2009a). The *cobra-like4* mutant phenotype was first identified in rice *BRITTLE CULM 1 (BC1)* and *OsBC1*-2 alleles, where the brittle culm phenotype is characterized by a reduction in the amount of mechanical force required to break

the stem (Qian *et al.*, 2001). The *Osbc1-2* mutants had a 30% reduction in cellulose in the culms and corresponding increase in lignin (Table 1.2). The cellulose produced by *bc1* plants has a reduced crystallinity (Liu *et al.*, 2013), which is consistent with the observed reduction in Updegraff cellulose (Li *et al.*, 2003b). Moreover, calcofluor staining of the cellulose in culm cross sections showed a reduction in cellulose in sclerenchyma and vascular tissues (Li *et al.* 2003). Sato *et al.* (2010) further characterized *OsBC1* using a null mutant, *cell wall architecture* 1 (*cwa1*). *cwa1* was characterized by ectopic deposition of phenolic compounds as amorphous masses in cortical fibres and sclerenchyma secondary cell walls, while the overall morphology of the internodes did not differ from wild-type plants. Structural differences in the cortical fibres were only obvious once cell wall thickening was initiated. In rice, arabinose and xylose levels also increased in the *cwa1* mutant, which is likely a compensatory response for the reduced cellulose content (Li *et al.* 2003; Sato *et al.* 2010). *OsBC1* transcripts are most abundant in the culm at heading stage and lowest in young tissues (Dai *et al.* 2009; Li *et al.* 2003).

The role of the cellulose binding module (CBM) in COBL4 genes is controversial, as there is poor similarity of COBL4 CBM2a compared to other characterized CBM2a-types, which bind specifically to crystalline cellulose (Simpson *et al.*, 2000). The specificity of CBM2a for crystalline cellulose is dependent on the spatial arrangement of the surface tryptophan (Trp; Y) residues (Simpson *et al.*, 2010) that hydrogen bond to the planar surfaces of crystalline cellulose in an irreversible manner (McLean *et al.* 2002) (Figure 1.4). To test the functionality of the putative COBL4 CBM in rice, the Trp residues in the cellulose binding module were replaced with valine (Val) residues by Sato *et al.* (2011), showing that specific Trp residues are required

for CBM interaction with cellulose, and more importantly that a CBM is needed for functional BC1. This was confirmed by Liu *et al.* (2013), who observed a reduction in the relative crystalline index of cellulose produced in rice plants expressing *bc1*^{Y46A} or *bc1*^{W72A} alleles, which have mutated CBMs, relative to plants expressing wild-type *BC1*.

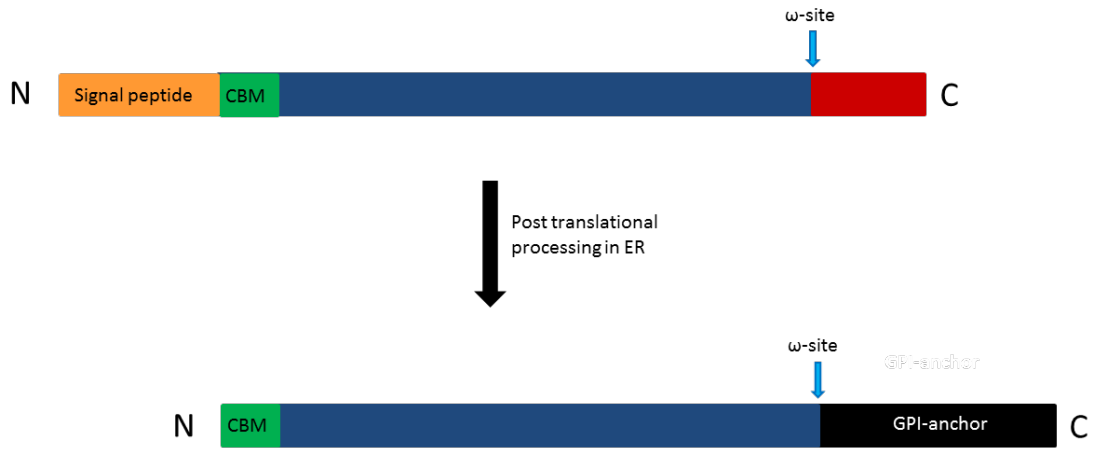

Figure 1.4: Diagrammatic representation of the AtCOBL4 primary transcript and protein structure after post-translational processing in the endoplasmic reticulum (ER).

The maize ortholog of *AtCOBL4* was identified by studies of the *brittle stalk2* (*bk2*) mutant, which arose by a spontaneous mutation (Ching *et al.* 2006). *BK2* transcripts were most abundant in the stalk, specifically in excised vascular bundles (Ching *et al.*, 2006; Brady *et al.*, 2007; Sindhu *et al.*, 2007), and *bk2* mutants had a similar phenotype to the *Osbc1* with increased susceptibility to mechanical stress. The disruption of secondary cell wall formation resulted in altered stem anatomy and cell wall chemistry. There was an absence of secondary vascular bundles and a reduction in density of peripheral vascular bundles (Sindhu *et al.*, 2007). *bk2* stalks also display a 19% reduction in cellulose (Table 1.2), but only a minimal increase in

lignin. Both xylose and mannose content were significantly increased, showing a larger increase than that observed in rice (Ching *et al.*, 2006).

Because *COBL4* orthologs are important in xylem development, *AtCOBL4* orthologs in species with well-developed secondary xylem have been investigated in both poplar and in *Eucalyptus* (Thumma *et al.* 2009; Ye *et al.* 2009; Zhang *et al.* 2009). QTL analysis of *Eucalyptus nitens* identified *EniCOBL4* as a marker for cellulose content (Thumma *et al.*, 2009). In poplar, the COBRA gene family has been studied and transcript abundance patterns determined. *PtCOB3* and *PtCOB5* were identified as putative homologs of *AtCOBL4* (Ye *et al.*, 2009). *PtCOB3* and *PtCOB5* were shown to be expressed in stems and specifically mature xylem (Ye *et al.* 2009; Zhang *et al.* 2009). *AtCOBL4* and its maize orthologs were also found to have expression patterns that correlated with that of secondary cell wall CesAs (Persson *et al.*, 2005; Ching *et al.*, 2006; Brady *et al.*, 2007), and showed increased transcript abundance during TW development in poplar (Andersson-Gunneråas *et al.* 2006). How COBL4 organizes cellulose deposition to promote crystallization of the newly synthesized cellulose as it is extruded from a CSC is unclear.

The COBRA gene family belongs to a class of proteins that have a characteristic C-terminal post-translational modification that acts to direct and anchor the protein in the external leaflet of the plasma membrane. This glycosylphosphatidylinositol (GPI) anchor may impart spatial

localization of COBL4 proteins to the outer leaflet of the cell membrane, thereby in part facilitating COBL4 function.

Table 1.2: Summary of cell wall neutral sugars and lignin composition in *AtCOBL4* homolog mutants relative to wild-type plants.

Experiment	Cellulose	Glucose	Xylose	Arabinose	Galactose	Mannose	Rhamnose	Lignin
Li *et al* 2003^{R} (bc1)	v 30%	v 30%	^ 39%	^ 18%	^ 3%	no change	^ 2%	^ 30%
Sato *et al* 2009^{R} (cwa1)	v 35%	v 11%	^ 14%	^ 16%	NA	NA	NA	^ 17%*
Ching *et al* 2006^{M} (bk2)	v 46%	v 20%	^ 33%	^ 40%	^ 50%	40%	NA	^ 14%
Sindhu *et al* 2007^{M} (bk2)	v 40%	v 25%	^ 15%	^ 2%	^ 30%	NA	NA	NA

^ - increase, v - decrease, ^{R} -rice, ^{M} -maize, $^{()}$- mutant allele * - Total phenolics.

1.3 GPI-anchored proteins

COBRA family members are typical glycosylphosphatidylinositol (GPI)-anchored proteins (GAPs), a class of lipid-anchored proteins that are directed to the cell plasma membrane where they are positioned on the extracellular leaflet (Borner *et al.* 2003; Eisenhaber *et al.* 1999; 2001; Eisenhaber *et al.* 2003). They include arabinogalactan proteins, lipid transfer proteins, and the COBRA family proteins in plants, although the functions of many of these proteins are not well-characterized. GPI-anchors are assembled in the lumen of the ER at the inner leaflet of the ER membrane. The pre-assembled GPI-anchor consists of a carrier lipid, phosphatidylinositol, several sugar residues and an asparagine (Asn) residue that serves as the attachment site for the C-terminus of the GPI-anchored protein (Orlean and Menon, 2007). The classical primary structure of a GPI-anchored protein (Figure 1.4) contains two hydrophobic signal sequences flanking an internal hydrophilic centre (Ye *et al.*, 2009). The first signal sequence is a classical N-

terminal signal sequence, which directs the protein to the endoplasmic reticulum (ER). The second is located at the C-terminus, and is a GPI-signal sequence motif that is sub-divided into four components (Figure 1.5a). The first, an unstructured linker region that is located upstream of the Omega (ω)-cleavage site, is approximately 11 amino acids in length. This is followed by a region of small aa ω-1 to ω+2 including the ω-site where cleavage of the signal sequence occurs and the GPI anchor is attached. Directly downstream is the third component, a spacer region of seven moderately polar amino acids. Finally, there is a hydrophobic tail beginning nine or ten residues downstream of the ω-site continuing to the C-terminus (Eisenhaber *et al.* 1999; 2001; Ye *et al.* 2009).

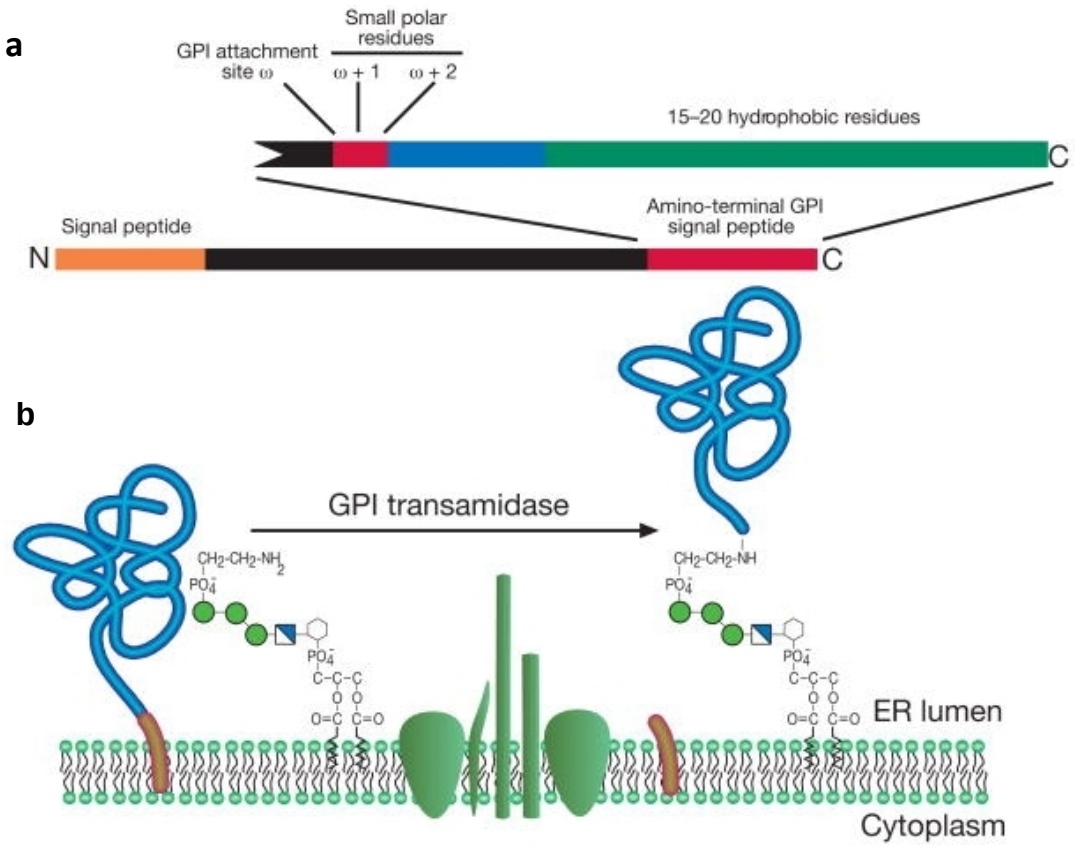

Figure 1.5: (a) diagrammatic representation of the primary structure GAP and (b) attachment of GPI-anchor to a GAP in the ER via GPI transamidase (Ferguson *et al.*, 2009)

Within the ER, the conserved N-terminal signal sequence is cleaved by a signal peptidase. The C-terminal sequence is cleaved at the ω-site, which serves as the attachment site of a pre-assembled GPI-anchor moiety located in the lumen side of the ER membrane (Figure 1.5b) that is facilitated by a GPI-transamidase complex (Paulick and Bertozzi, 2008). A number of Arabidopsis genes involved in GPI-anchor synthesis have been identified including *PEANUT1-5*; *SETH1* and *SETH2*, which have been shown to be integral for pollen tube growth (Lalanne *et al.* 2004, Gillmor *et al.*, 2005). Mutant *Arabidopsis* lines for these genes exhibit multiple cell wall phenotypes including reduced cellulose content, aberrant cell wall morphology and altered chemical composition, including irregular levels of pectin, callose and xyloglucan (Gillmor *et al.*, 2005).

A large number of GPI-anchored proteins have been identified in plants (Borner *et al.*, 2003; Borner *et al.*, 2005). For example, Borner *et al.* (2003) used a combined genomic and proteomics approach to identify a total of 248 putative GAPs in *Arabidopsis*. The identified GAPs encompassed a diverse array of protein families including classical arabinogalactan proteins (AGPs), extensin-related phytocyanins, polygalacturonases, pectate lyases, proteases, receptor-like proteins, fasciclin-like AGPs (FLAs) and the COBRA protein family. The latter two families have members that are associated with primary and secondary cell wall development (Brown *et al.* 2005; Persson *et al.* 2005; Schindelman *et al.* 2001). *AtFLA11* (*irx*13) and *AtCOBL4* (*irx*6) null mutants both result in an *irx* phenotype, as described by Persson *et al.* (2005) and Brown *et al.* (2005).

In the last 10 years it has become apparent that a large proportion of GAPs are associated with detergent resistant membrane (DRM) fractions in plants (Borner *et al.* 2005; Kierszniowska *et al.* 2009; Lefebvre *et al.* 2007; Shahollari *et al.* 2004, Mongrand *et al.* 2004). DRMs are proposed to represent lipid rafts, defined by Lingwood *et al.* (2009) "…as dynamic sterol sphingolipid-enriched nanoscale assemblies that associate and dissociate on a sub-second timescale". The paradigm of these lipid rafts suggests revision of the fluid mosaic model (Singer and Nicolson, 1972), where lipid composition and localization was completely random, freely diffusible and fluid in nature, also defined as the liquid-disorder phase (l_d) (Edidin, 2003). The preferential accumulation and association of longer chained, saturated fatty acids and sterols into lipid rafts or a liquid-ordered phase (l_o) could create thicker regions of plasma membrane at the nano-scale, excluding non-raft lipids through hydrophobic mismatching. These lipid rafts could rapidly coalesce and disassemble in response to intra-cellular or external stimuli through processes thought to require lipid-lipid, lipid-protein and/or protein-protein interactions (Lingwood *et al.* 2009; Lingwood and Simons 2010), through mechanism yet to be fully understood (Brown and London 1998; Edidin 2003).

Lipid rafts have multiple proposed functions, including recruitment and concentration of members of the previously listed protein families, trans-membrane signal transduction, cytoskeleton organization, apoptosis and potentially sites of pathogen entry (Bhat and Panstruga 2005; Nishi and Saigo 2007, Simon-Plas *et al.* 2011). The isolation of several FLAs

(*AtFLA1*, *AtFLA7*, *AtFLA8* and *AtFLA13*) from DRMs in *Arabidopsis* suggests a role for lipid rafts in facilitating plasma membrane-cell wall interactions. A single study in poplar recovered CesAs and SuSy from DRMs (Bessueille *et al.* 2009), however, no other studies to date have isolated CesAs from DRMs.

1.4 Scientific questions and research objectives

The overall goal of this thesis is to understand the role of the GPI-anchored proteins of the COBRA-LIKE4 family, specifically *Arabidopsis AtCOBRA-like4* and poplar *PtCOB4a/b*, in the deposition of cellulose in the secondary cell wall during xylem development. It has been hypothesized that *AtCOBRA* GPI-anchored proteins, located in the outer leaflet of the plasma membrane, may interact with and influence cellulose deposition. COBRA-like proteins could interact directly with cellulose microfibrils via the putative cellulose binding module (CBM) that exists in the native protein, as postulated for the rice gene (*OsBC1)* (Sato *et al* 2010). Alternatively, these membrane-anchored proteins could have an indirect effect on cellulose deposition through interaction(s) with the cellulose synthase complex in the plasma membrane. Either of these hypotheses suggest an integral need for COBRA-like proteins for proper secondary cell wall biosynthesis by facilitating direct or indirect interaction with both PM and cellulose MFs. To elucidate the function of *AtCOBL4*, two model plant systems were used in parallel, hybrid poplar (*Populus alba* × *grandidentata,* clone P39*)* and *Arabidopsis thaliana*.

Based on all relevant literature regarding *AtCOBL4* and its homologs in rice, maize and poplar, the following hypotheses have been generated.

Hypothesis 1: COBL4 mediates the organization of secondary cell wall cellulose deposition at the plasma membrane cell wall interface.

To test this hypothesis, I analyzed both wild-type *Arabidopsis* and *atcobl4* mutants for cell wall composition and organization. I used a comprehensive approach, pairing chemical analyses (cell wall sugar composition, lignin content and cellulose content) with ultrastructural analyses (cellulose crystallinity, MFA and DP). I also used live cell imaging of fluorescently tagged poplar COBL4 to determine spatial localization of the COBRA proteins during secondary cell wall deposition in a model Arabidopsis experimental system. I visualized the cellulose deposition pattern of ectopic protoxylem trans-differentiation using cellulose specific staining and confocal microscopy. Thus, I was able to place the cellulose ultrastructural data in the context of the sub-cellular location of the COBL4 during secondary cell wall biosynthesis.

Hypothesis 2: The poplar orthologs, PtCOB4a and PtCOB4b, are required for cellulose deposition in the secondary cell walls during xylem formation, and this functional role is conserved evolutionarily within angiosperms.

To investigate the conservation of COBL4 function between herbaceous and woody plants the putative poplar COBL4 homologs was isolated and functionally tested in *irx6-2* and *irx6-3,*

atcobl4 mutant lines. To complement this work, *AtCOBL4* was over-expressed in a secondary cell wall specific manner in hybrid poplar, allowing me to enhance COBL4 mediated effects on cellulose biosynthesis and organization. To understand how cellulose deposition is affected by COBL4 in poplar, I employed the suite of chemical and ultrastructural analyses to test hypothesis one.

Chapter 2: Immobile COBL4 facilitates the ordered deposition of cellulose at sites of secondary cell wall deposition

2.1 Introduction

In land plants, the largest sink for carbon sequestered from the atmosphere is the plant secondary cell wall, which is composed of several polysaccharides including hemicelluloses and cellulose, as well as lignin. The cell wall polysaccharide composition is species, tissue, and cell-specific, with cellulose representing the largest single fraction, comprising as much as 45% of the dry mass. Cellulose is a β-1-4 linked glucan chain composed of cellobiose repeating sub-units. It is synthesized by the cellulose synthase complexes (CSCs), which are plasma membrane complexes consisting of associations of individual cellulose synthase proteins (CesAs) (Turner 2006) that extrude cellulose microfibrils of glucan chains into the plant cell wall. Loss-of-function alleles of a single secondary cell wall CesA (*CesA4*, *CesA7*, *CesA8*) cause a dramatic reduction in cellulose production and the canonical irregular xylem (*irx*) phenotype (Turner and Somerville 1997, Brown *et al.* 2005).

Correct organization of newly synthesized cellulose is key to maintaining structural integrity of plant cell walls. Cellulose organization can be separated into three major ultrastructural characteristics: the degree of polymerization (DP), cellulose crystallinity, and cellulose microfibril angle (MFA). DP is the average number of glucose monomers making up a single cellulose glucan chain. Using the terminology of Ding and Himmel (2006), the assembly of chains produced by a CSC is an elementary microfibril; these elementary microfibrils in turn

associate with non-cellulosic polymers to form microfibrils (MF). The spontaneous interaction between newly synthesized glucan chains leads to strong intra- and inter-chain hydrogen bonds, forming crystalline cellulose. Given the heterogeneity of bonding among glucan chains, cellulose produced consists of both amorphous and crystalline regions (Delmer and Amor, 1995), with some authors proposing that DP influences the proportion of cellulose in the crystalline state (Fujita and Wasteneys, 2011). The proteins and processes intricate to cellulose biosynthesis that underpin β-1-4 glucan chain elongation are currently unclear, but likely include proteins that concurrently influence cellulose crystallinity. Microfibril angle (MFA) refers to the angle at which cellulose is deposited relative to the longitudinal axis of the cell. MFA imparts rigidity to the cell, with a smaller MFA conferring a more rigid cell wall (Reiterer and Lichtenegger, 1999).

In primary cell walls, it has been postulated that cellulose crystallinity is determined by several factors: the velocity of the CSCs (Fujita and Wasteneys, 2006), the residence time of the CSC at the plasma membrane (Jacob-Wilk *et al.*, 2006, Paradez *et al.*, 2006), as well as interactions with other cell wall associated proteins including *AtKOR* and *AtCOBRA* (Sato *et al.*, 2001; Li *et al.*, 2003a; Brown *et al.*, 2005; Takahashi *et al.*, 2009). A more crystalline cellulose confers a higher tensile strength to the cell wall (Burgert *et al.*, 2002). The disruption of MF formation via inhibitors (Haigler 1980) or by the use of loss-of-function alleles of genes involved in cellulose biosynthesis (Fujita *et al.*, 2011; Joshi *et al.*, 2011; Harris *et al.*, 2012) results in altered CSC velocity and consequently varying cellulose crystallinities (Bensiman 1980, Fujita *et al.* 2011).

CSC motility through the plasma membrane may be driven by the polymerization of the glucan chains (Paredez *et al.*, 2006; Debolt *et al.*, 2007; Diotallevi and Mulder, 2007; Harris *et al.*, 2010; Fujita *et al.*, 2012), and as such, the emerging cellulose chain propels the CSCs through the plasma membrane. The mechanism that maintains linear CSC trajectories is still unresolved, but is believed to be mediated, in part, by CELLULOSE SYNTHASE-INTERACTIVE PROTIEN 1 (CSI1) that was recently shown to be able to interact simultaneously with primary cell wall CesAs and MT, providing an interface between the cytosolic cortical MT network and CesAs localized in the plasma membrane (Gu *et al.*, 2010b; Li *et al.*, 2011a; Bringmann *et al.*, 2012a; Bringmann *et al.*, 2012b)

Glycosyl phosphatidyl inositol (GPI)-anchored proteins are localized to the outer leaflet of the plasma membrane where they face into the apoplastic space, located precisely at the interface where the CSCs are depositing newly formed cellulose microfibrils into the cell wall. Mutant phenotype analyses have implicated several GPI-anchored proteins in contributing to cellulose deposition and organization. In *Arabidopsis*, two members of the *Fasciclin*-like GPI-anchored protein gene family (*FLA*) were shown to be required for secondary cell wall cellulose deposition: *atfla11/atfla12* double mutant lines had reduced cellulose content, and the cellulose that was deposited had a larger MFA than wild-type *Arabidopsis* (MacMillan *et al.*, 2012). Another GPI-anchored protein gene family, the *COBRA* gene family, has also been identified to play a role in cell wall formation, specifically cellulose deposition in *Arabidopsis* (Benfey *et al.*, 1993; Schindelman *et al.*, 2001; Roudier *et al.*, 2005; Ko *et al.*, 2006). Unlike the

FLAs, the COBRA and COBRA-like (COBL) proteins include a cellulose binding module (Roudier *et al.*, 2002). In *Arabidopsis*, *AtCOB* is required for primary cell wall deposition, and loss-of-function mutants result in dwarfed plants that exhibit impaired anisotropic cell growth and disorganized cellulose (Benfey *et al.* 1993, Schindelman *et al.* 2001; Roudier *et al.* 2005, Wasteneys and Fujita 2006). Similarly, *Arabidopsis COBRA-LIKE4* (*AtCOBL4*) null allele and homologs in other plant taxa have also been characterized by a marked reduction in cellulose production in secondary cell wall deposition (Li *et al.* 2003, Brown *et al.*, 2005, Dai *et al.* 2009, 2011, Sato *et al.*, 2010). Null mutants of *atcobl4* have normal plant growth, but have reduced cellulose content resulting in thinner secondary cell walls. Xylem vessels of *atcobl4* plants are often collapsed, and manifest in the irregular xylem phenotype. Similar phenotypes for *AtCOB* and *AtCOBL4* were observed for orthologs in rice and maize (Li *et al.* 2003, Dai *et al.* 2009, 2011, Sato *et al.* 2010, Liu *et al.* 2013). Immunogold labelling of *BC1*, the rice ortholog of AtCOBL4, showed that BC1 localized not only to the plasma membrane, but was also embedded within the secondary cell wall (Liu *et al.*, 2013). This suggests that BC1 might not remain anchored by its GPI-tail to the plasma membrane, but could be cleaved by a phospholipase and bind via the cellulose binding module to cellulose, to interact directly with wall microfibrils. The dynamics and localization of the COBRA proteins is poorly characterized because of the challenge in tagging a fluorescent protein onto the GPI-anchored protein, where both N- and C-termini are cleaved during biosynthesis. All of the plant systems in which *AtCOBL4* orthologs have been studied only produce limited quantities of secondary cell wall material. The use of a woody plant system, such as the ecologically and economically important *Populus spp.* trees, should aid in resolving the function of *AtCOBL4* orthologs in secondary walls.

In this chapter, I investigated the ultrastructural properties associated with *AtCOBL4* loss-of-function alleles, and show how AtCOBL4 influences cellulose DP and consequently cellulose crystallinity in secondary cell walls. To better understand the function of *AtCOBL4* orthologs, I isolated poplar orthologs *PtCOB4a* and *PtCOB4b*, and use complementation of *Arabidopsis* mutants to demonstrate conservation of function of *AtCOBL4* orthologs between herbaceous and woody plants. Using a novel fluorescent protein; PtCOB4a-cYFP, and live cell imaging, I show that the poplar AtCOBL4 ortholog co-localizes with secondary cell wall thickenings, suggesting a role in the proper organization of cellulose during secondary cell wall deposition.

2.2 Materials and methods

2.2.1 Sequence analysis

Putative *Populus trichocarpa COBRA* gene family member sequences were retrieved from the NCBI database, based on earlier studies by Ye *et al.* (2009) and Zhang *et al.* (2010), and translated to protein sequences. *Arabidopsis COBRA* family members; *AtCOB* (AT5G60920), *AtCOBL4* (AT5G15630) and *AtCOBL6* (AT1G09790) protein sequences (Roudier *et al.* 2002), were included in the data query. These protein sequences were aligned using Muscle and ClustalW was used to generate an un-rooted, neighbour-joining tree with boot-strap values. The neighbour-joining tree was edited using FigTree. Boot strap values represent a 1000 resampling events.

2.2.2 Plant material

Arabidopsis seedlings were germinated on antibiotic selective ½ MS plates lacking sucrose (Murashige and Skoog, 1962) and transferred to soil after 10 days growth. Plants were then grown under controlled 24 hour light (260 µMol/m^2/min) conditions at 22°C (Brown *et al.*, 2005).

2.2.3 Genotyping transgenic lines

The *irx6-1* T-DNA line was kindly provided by Simon Turner, the *irx6-2* and *irx6-3* T-DNA homozygous lines from the GABI-Kat T-DNA library were kindly provided by Drs. Manoj Kumar and Bjorn Sundberg. Homozygous *Arabidopsis irx6-2* and *irx6-3* T-DNA lines were identified by PCR genotyping using the GABI left flanking primer (5′ ATATTGACCATCATACTCATTGC 3′) and respective flanking primers (*irx6-2*: F 5′ GCTGTATCCCAGTTTCAGGTTA 3′, R 5′ ATGGATCCGTAAGGAGAGACT 3′; *irx6-3*: F 5′ TGGAATGTTACCTGCACATAC 3′, R 5′ GTATGAATCTGGTGGAGGTAAC 3′). PCR conditions were as follows: 120 seconds at 95°C ; 30 cycles of 30 s at 95°C, 30s at 56°C, 60 s at 72°C; 120 s at 72°C.

2.2.4 Cloning *PtCOB4a* and *PtCOB4b*

Genomic DNA was isolated from *A. thaliana* (Col) and *P. trichocarpa* (P39). The *AtCOBL4* promoter was cloned into pEntr (Invitrogen) using primers: F5′ CACCTGCAGGAAAACTATGAACAAACTCTA3′, and a reverse primer with a KpnI restriction site R

5′ GGTACCACGACAGATGGCTATACCTAGGTTGAGTAAAGATTTAAGGAAATTG 3′. The *AtCOBL4* promoter was then sub-cloned into pSM3 replacing the *35S* promoter using PstI and KpnI (pSM3-*AtCOBL4*::). *PtCOB4a* and *PtCOB4b* from *P. trichocarpa* were cloned into pEntr using primers: F 5′ CCTAGGATGGAATTCGATAAGTCTGCCAAGGA 3′; R 5′ GGTACC-TCACCCCATTGACAGCAATA 3′; F 5′ CCTAGGATGAAAATGAGATTTCTCTTCTTTATTGTCTTGTTTCTT 3′, R 5′ GGTACCTTACCAGATATACACGAACAGGAAAATCAACGTAGA 3′, respectively. *PtCOB4a* and *PtCOB4b* were then separately sub-cloned into pSM3-*AtCOBL4*:: using AvrII and KpnI, creating pSM3-*AtCOBL4*::*PtCOB4a* and pSM3-*AtCOBL4*::*PtCOB4b*.

2.2.5 PtCOB4a-cYFP fusion construct preparation

Overlapping PCR (Schwab *et al.*, 2006) was used to generate PtCOB4a-YFP, where *PtCOB4a* protein coding sequence CDS was used as template. Three fragments were generated, fragment 1 consisting of *PtCOB4a* CDS lacking a GPI-anchored-anchor (1-417aa), fragment two consisted of the citrine YFP (cYFP) (Griesbeck *et al.*, 2001; Tsien 2001; Debono *et al.*, 2009), and the third fragment consisted of the remaining 36 codons of PtCOB4a. Primers employed were: 1F 5′ CCTAGGATGGAATTCGATAAGTCTGCCAAGGA 3′, 1R 5′ ACCTCCACCTCCAGGAAGCATGCATTCATCACC 3′, 2F 5′ CGGTGATGAATGCATGCTTCCTGGAGGTGGAG 3′, 2R 5′ AGTGTCAGGTGGGGGGGGCGCAGCAGCACCAGCAG 3′, 3F 5′ CTGGTGCTGCTGCGCCCCCCCCACCTGACACTTA 3′, 3R 5′ GGTACCTTGGAGCACCATAACCATGTT 3′. Step-up PCR amplification using IProof taq (Biorad) produced fragments 1-3, and after gel

purification of the fragments, they were used in equal molar concentrations for subsequent overlapping PCR reactions (Schwab *et al.* 2006). *PtCOB4a*-cYFP was then cloned into pZeroblunt (Invitrogen) and sub-cloned into pSM3-*AtCOBL4*:: using AvrII and KpnI.

All constructs were transformed into chemically competent Top10 *E. coli*. Final constructs were transformed into GV3101 *Agrobacterium tumefaciens* and used to transform *Arabidopsis irx6-2 and irx6-3* lines by floral dip (Clough and Bent, 1999). Positive transformants were identified using hygromycin, two positive lines for each construct/plant line combination were subsequently characterized as described below.

2.2.6 Mutant cell (irregular xylem and fibre) phenotype analyses

The bases, approximately 1 cm above the root collar, of *Arabidopsis* primary inflorescence stems were hand sectioned to determine the morphology of the mature vascular system. The cross-sections were then stained with toluidine blue (Turner and Somerville 1997), and five plants per line examined. A Leica light microscope was used to view the cross-sections, and images were captured using a Q-imaging camera and software. Fiber quality analysis was used to determine the length of fiber cells in the *Arabidopsis* stem. In brief, 10mg of the basal 10 cm of primary inflorescence stem was subject to a modified Franklin solution (1 ml 30% H_2O_2 + 1 ml glacial acetic acid + 1 ml ddH_2O) for 6 hours at 72°C, and the fibrous material was recovered and fibres separated in distilled water (H_2O). Fibres were diluted to achieve a flow rate of 20-40

fibres s^{-1} on a Fibre Quality Analyzer (Optest). Five thousand fibres of 5 biological replicates per line were analysed (Park *et al.*, 2008).

2.2.7 Cell wall chemistry

Cell wall monosaccharide composition and lignin content of primary inflorescence stems was determined by a modified Klason method (Coleman *et al.* 2007). In summary, stem tissue isolated from the basal 10 cm section of primary inflorescence stems were pooled for each plant line and Wiley-milled. Extractives were removed from samples with overnight extraction with hot acetone via Soxhlet apparatus . The 100 mg of oven dried stem tissue was incubated in 72% H_2SO_4 for 2 hours with regular stirring. The acid concentration was then diluted to 4% and the samples were treated at high temperature and pressure (autoclave) to completely hydrolyze cell wall polysaccharides. The monosaccharides were quantified by AE-HPLC using an ICS 5000 (Dionex-Thermofisher) fit with a CarboPac PA1 column (Thermofisher) at 0.8 mL/min flow rate, and a pulsed amperometric detector with a gold electrode, and post column supplementation of 100 mM/min NaOH. Acid-soluble lignin content was determined spectrophotometrically at 280 nm, while the acid-insoluble lignin was determined gravimetrically.

2.2.8 Holo-cellulose and α-cellulose content

Holocellulose was determined from 200 mg tissue isolated from the basal 10 cm of primary inflorescence stem, which was pooled for each transgenic and control line. In brief, 3.5 mL buffer (60 mL of glacial acetic acid + 1.3 g NaOH/L) and 1.5 mL of 20% sodium chlorite were added to each sample, and incubated at 50°C with gentle shaking for 16 hours, at which time the reaction was quenched by placing the samples on ice, this reaction was then repeated. The reacted sample was then transferred to a coarse pre-weighed sintered crucible, washed twice with 50 mL of 1% glacial acetic acid, followed by a wash with 10 mL acetone. Finally, the crucibles were dried at 50°C overnight and weighed. The α-cellulose content was then isolated from the recovered holocellulose, by reacting 100 mg holocellulose with 17.5% NaOH for 30 min, diluting the solution to 8.75% NaOH and reacting for a further 30 min. All retentate was filtered through pre-weighed coarse sintered crucibles and washed with distilled water (DI). The retentate was then soaked in 1.0 M acetic acid for 5 min, before being washed with DI water. Crucibles were dried at 50°C overnight and weighed.

2.2.9 Determination of cellulose degree of polymerization

30 mg of α-cellulose was solubilized in 9% LiCl/N,N-Dimethylacetamide (DMAc). Briefly, isolated α-cellulose was swollen in nanopure water with stirring for 48 hours; ddH_2O was then substituted with 100% anhydrous EtOH (Sigma) and stirred for 48 hours, EtOH was substituted with anhydrous DMAc and stirred for 48 hours. Finally, 9% LiCl/DMAc substituted the DMAc, and this solution was stirred for an additional 24 hours. The solubilized cellulose was diluted

and injected on an Agilent 1100 series gel permeation chromatography (GPC) instrument fit with two Styragel columns in series (Waters; 5E, 4E). Cellulose polymer size was determined by multi-angle light scattering and calculated using the program ASTRA (Wyatt Technologies), giving estimates of the average molecular weights.

2.2.10 Measurement of cell wall crystallinity and cellulose MFA

The same basal 5 cm segment of the main stem of each plant, for 5 plants per line, was used to calculate cell wall crystallinity and MFA. Cellulose microfibril angle was determined using X-ray diffraction (Megraw *et al.*, 1998) on a Bruker D8 discover X-ray diffraction unit. Wide-angle diffraction was used in transmission mode with a $CuK_{\alpha}1$ radiation (λ=1.54 Å), and a 0.5 mm collimator, where the scattered photons were collected by a GADDS detector. A theta angle of 0° for both the X-ray source and detector was used for microfibril angle measurement, while for cell wall crystallinity, a detector theta angle of 20° was employed. Crystallinity was determined as described by Vonk (1973), by mathematically fitting the data.

2.2.11 Microscopy

Seedlings from *35S::VND7-GR* (Yamaguchi *et al.* 2010) carrying *AtCOBL4*::*PtCOB4a*-cYFP lines were grown on ½ MS plates lacking sucrose for 7 days under long day conditions at which point 5 ml 10uM dexamethasone (DEX) (Sigma-Aldrich) ½ MS solution was applied to the plate. Seedlings were then placed back under controlled long day conditions for 36-48 hours post-

induction. Whole seedlings were mounted in water and YFP fluorescence detected using a 514 nm laser to excite the YFP on a Perkin Elmer Ultraview VoX Spinning Disk Confocal microscope with a 40X oil objective (NA= 1.26). Images were captured on a Hamamatsu 9100-02 CCD camera. Volocity software (Improvision) was used to operate the spinning-disk confocal/camera platform. Fluorescence Recovery after Photobleaching (FRAP) was performed using an Olympus Multi-photon Laser Scanning Microscope FV1000MPE (Olympus) and Olympus FV10-ASW ver.03.01 (Olympus) software. A 488nm laser, set at 100% power was used to photobleach a single rib of secondary cell wall material in a trans-differentiating protoxylem cell. After the photobleaching for four frames, fluorescent recovery was measured for 60sec. FRAP was performed on 5 separate cells for both *irx6-3/VND7-GR* carrying *AtCOBL4::PtCOB4a*-cYFP and wild-type Columbia transformed with a cytosolic GFP control (Schuetz *et al.*, 2014). Volocity Version 6.1.1 (Improvision) software package was used to analyse the FRAP data.

2.3 Results

2.3.1 Confirming *irx6* phenotype

The strong co-expression correlation of the *Arabidopsis COBRA-like4* (*AtCOBL4*) gene with the secondary cell wall specific Cellulose Synthase (*CesA*) genes led to the hypothesis that *AtCOBL4* could play a role in secondary cell wall biosynthesis (Brown *et al.* 2005). This hypothesis was supported by the identification of the *atcobl4* T-DNA insertional mutant called *irregular xylem6 (irx6-1)* (Brown *et al.*, 2005). *irx6-1* (FLAG_428B03) in the Wassilewskija (Ws) ecotype displayed reduced cellulose content and collapsed xylem vessels. However, no morphological defects

were observed at the whole plant level, although the stems were weak (Brown *et al.*, 2005). In order to study the function of AtCOBL4 and its putative poplar homologs, additional *atcobl4* alleles were identified in the GABI-Kat (GK-329F09, GK-851H06) mutant collection. These mutants have T-DNA insertions in exons four (GK-329F09) and three (GK-851H06) respectively, of *AtCOBL4* coding sequence which manifests in null alleles. In contrast to the Columbia-0 (Col-0) wild-type lines where transcript was detected, *irx6-2* and *irx6-3*, lacked detectable transcript by semi-quantitative PCR, suggesting that they are complete knock-out mutants (Figure 2.1). The characteristic irregular xylem phenotype was again observed in toluidine-blue stained hand sections of the inflorescence stem (Figure 2.2a), consistent with the phenotype of *irx6-1* plants.

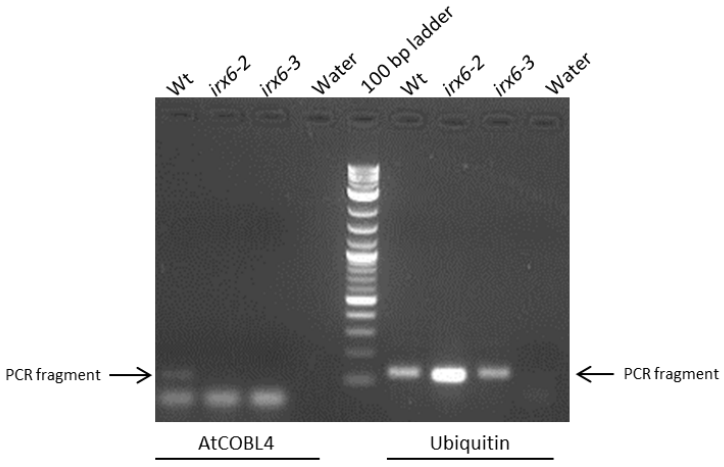

Figure 2.1: Semi-quantitative PCR amplification of *AtCOBL4* and Ubiquitin transcript segments from primary inflorescence stem derived cDNA.

The severely collapsed xylem phenotype raises the question of what effect reduced cellulose content may have on other cell types undergoing secondary cell wall deposition. To answer this, I examined the fibres of *Arabidopsis*, which include the extra-xylary interfascicular as well as xylary fibres.

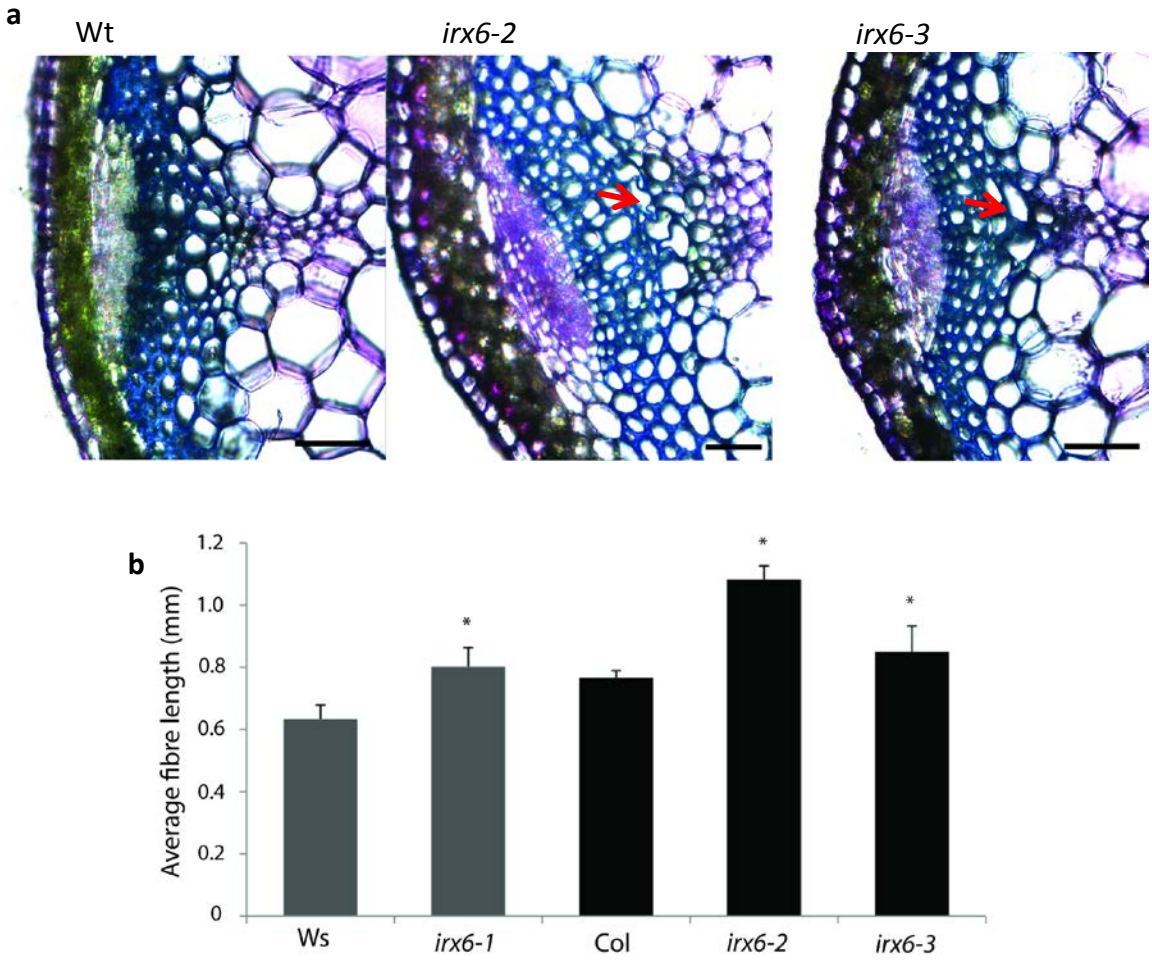

Figure 2.2: Characterization of the cell anatomy defects associated with *irx6-2 and irx6-3* loss-of-function *AtCOBL4* alleles. (a) Toluidine blue-stained *irx6-2 and irx6-3* cross sections of primary inflorescence stems reveal characteristic collapsed xylem phenotype (arrow). (b) Length of fibre cells isolated from primary inflorescence stems, measured with fibre quality analysis, with all *irx6* alleles displaying elongated fibres. Red arrow indicates collapsed xylem. Scale bar: 35µm

Using a fibre quality analyzer (FQA), I quantified the fibre cell lengths of cells isolated from *irx6-2* and *irx6-3* inflorescence stems, which were up to 25% longer than those of wild-type Columbia plants (Figure 2.2b). The increased fibre length was also observed for *irx6*-1 in Ws ecotype (Figure 2.2b) compared to wild-type Wassilewskija. These results demonstrate that

AtCOBL4 is required for secondary cell wall biosynthesis, not only in the metaxylem vessels, but also in fibres. Furthermore, AtCOBL4 contributes to fibre cell elongation, since the overall length of fibre cells in *atcobl4* plants are longer, presumably due to altered secondary cell wall properties.

2.3.2 *AtCOBL4* is required for normal cellulose deposition in cells undergoing secondary cell wall deposition

atcobl4 and orthologous mutants in rice and maize (Brown *et al.*, 2005, Li *et al.*, 2003, Ching *et al.*, 2006) have been shown to display a dramatic reduction in cellulose content. To compare the new *Arabidopsis* mutant alleles, I determined the structural cell wall carbohydrate content of *irx6-2* and *irx6-3* lines, confirming a reduction in cell wall glucose content of 18% and 60%, respectively (Table 2.1). To ascertain if the observed reduction in glucose could be explained by a reduction in cellulose, α-cellulose was isolated and quantified. *irx6-2* and *irx6-3* lines showed a 42% and 52% reduction in α-cellulose content (Table 2.2), respectively; this directly accounts for the overall reduction in cell wall glucose. This raises the question of how a reduction in total secondary cell wall cellulose might be reflected in the ultrastructural properties of the synthesized cellulose. To date, a single study (Liu *et al.* 2013) investigating the rice homolog of *AtCOBL4* (*BC1*) reported on the ability of *BC1* to modify cellulose crystallinity. Here, I characterize all three major cellulose ultrastructural characteristics; cellulose crystallinity, degree of polymerization (DP) and microfibril angle (MFA). The cell wall crystallinity was calculated using x-ray diffraction for *irx6-2*, *irx6-3*, and Col-0 inflorescence stems. Both *irx6*

alleles showed approximately a 50% reduction in cell wall crystallinity compared to the wild-type stems (Table 2.2). It has been hypothesized that cellulose DP may play a role in determining the crystalline state of synthesized cellulose (Fujita and Wasteneys 2011). Our results found that DP was lower in the *irx6* lines relative to that of wild type (Table 2.2), providing strong correlative support for a link between cellulose DP and cellulose to crystallinity. The MFA of *irx6* lines was approximately half of the wild-type stems' MFA. These data suggests that *AtCOBL4* can modulate cellulose crystallinity and that during this process, cellulose DP is also influenced.

Table 2.1: Cell wall chemical composition of primary inflorescence stem wild-type *Arabidopsis* (Col), *irx6-2* and *irx6-3* plant lines.

	% Carbohydrates						% Lignin	
	Ara	**Rha**	**Gal**	**Glu**	**Xyl**	**Man**	**acid soluble**	**acid insoluble**
Wt col	0.8	0.55	1.41	36.1	12.1	1.51	1.98	18.9
irx6-2	0.91	0.52	1.56	29.9	9.30	1.14	2.79	17.6
irx6-3	1.13	0.63	1.71	14.5	10.3	1.4	3.77	18.5

Table 2.2: Characterization of ultrastructural cell wall properties of primary inflorescence stems of Columbia ecotype. n=5, standard deviation ()

Line	**α-cellulose (%)**	**CW crystallinity (%)**	**DP**	**MFA(°)**
Wt	33.98	41	7927	10.29 (0.36)
irx6-2	19.54	21	7470	6.22 (0.64)
irx6-3	16.10	19	6120	5.45 (0.62)

2.3.3 Identification of putative *AtCOBL4* homologs in *P. trichocarpa*

All research examining *AtCOBL4* function has employed herbaceous plants and grass model systems that produce comparatively small amounts of tissue within secondary cell walls. The sheer volume of secondary cell wall produced by trees may place increased importance on AtCOBL4 function and its role in modulating the secondary cell wall cellulose deposition during growth and development. Two studies examining proteins homologous to *Arabidopsis COBRA* genes in poplar have identified a number of putative homologs (Ye *et al.*, 2009, Zhang *et al.*, 2010). From these studies, putative poplar *COBRA-like* sequences were collected from the NCBI database and used to generate a neighbour joining tree (Figure 2.3). The bioinformatics query confirmed that there were two genes encoding proteins with high similarity to AtCOBL4. The use of next generation sequencing data and online transcript abundance tool, BAR (http://bar.utoronto.ca), clearly demonstrated that these proteins are preferentially expressed in the developing xylem of poplar, sites of active secondary cell wall deposition.

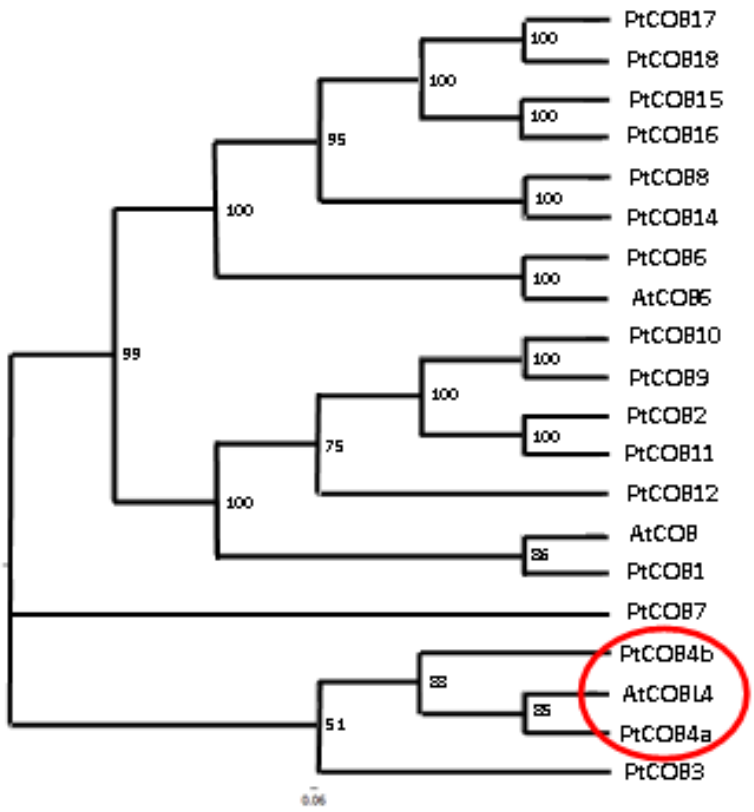

Figure 2.3: The phylogenetic relationships in the poplar COBRA gene family. *AtCOB*, *AtCOBL4* and *AtCOB6* are included. A neighbour joining tree with boot strap values indicated.

To test functional conservation of the secondary cell wall associated COBL4 genes between woody and herbaceous plants, the putative poplar orthologs, *PtCOB4a* and *PtCOB4b*, were isolated from *P. trichocarpa* and introduced into the *Arabidopsis* mutants *irx6-2* and *irx6-3*, driven by the native *AtCOBL4* promoter. *PtCOB4a* and *PtCOB4b* rescued the *irx* phenotype of the *Arabidopsis* mutants, as demonstrated by stem cross-section staining (Figure 2.4a).

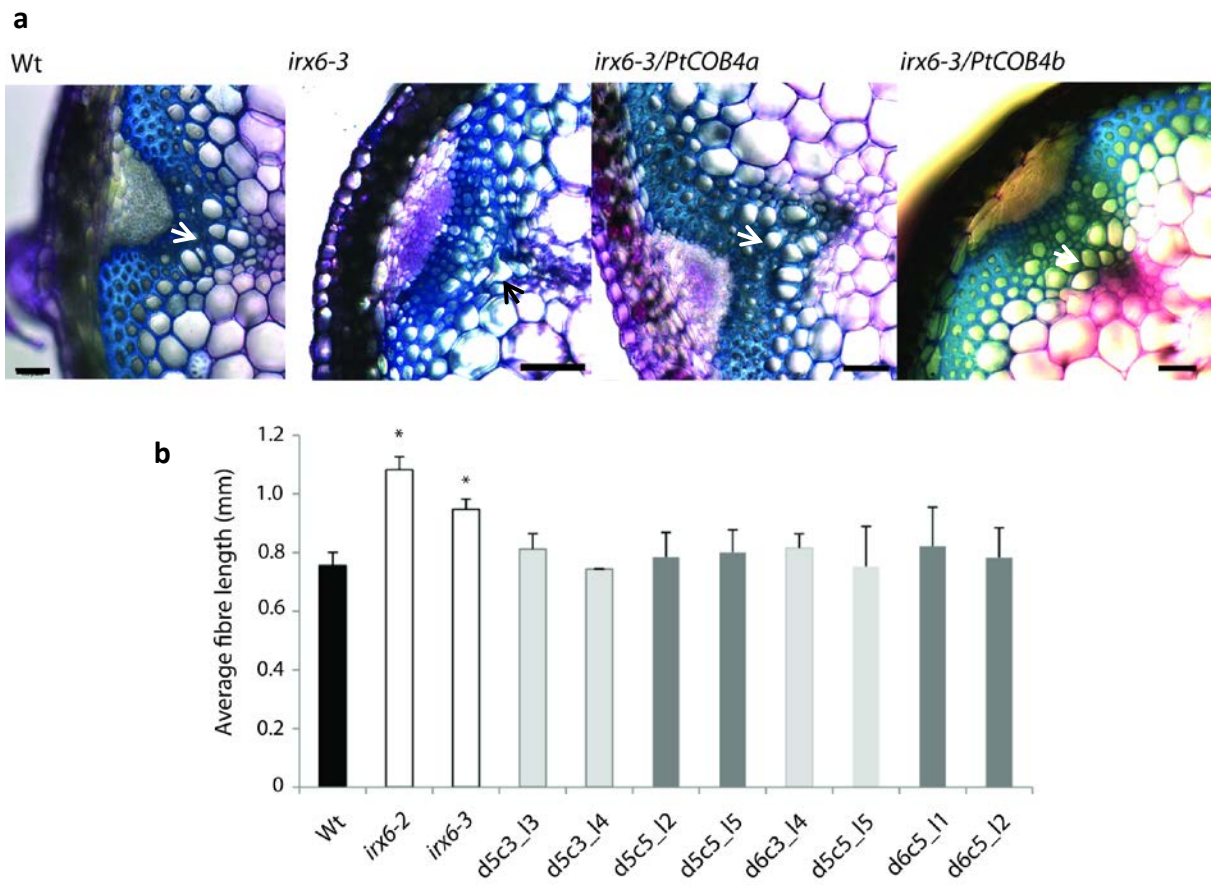

Figure 2.4: *PtCOB4a* and *PtCOB4b* are capable of restoring *irx6* cell morphology phenotypes to that of wild-type *Arabidopsis*. (a) Hand cross-sections of wt, *irx6-3*, *irx6-3*/*AtCOBL4*::*PtCOB4a* and *AtCOBL4*::*PtCOB4a* inflorescence stems stained with Toluidine blue. Scale bar is 35µm. White arrows indicates normal xylem vessels and black arrow shows collapsed xylem (b) Fibre length measurements of fibres recovered from primary inflorescence stems. Wt Col (black bar), *irx6-2* and *irx6-3* (white bar), *irx6-2* or *irx6-3*/*AtCOBL4*::*PtCOB4a* (light grey bars), *irx6-2* or *irx6-3/AtCOBL4::PtCOB4b* (dark grey bars). d5c3 label corresponds to *irx6-2*/*AtCOBL4*::*PtCOB4a*, d5c5 label corresponds to *irx6-2*/*AtCOBL4*::*PtCOB4b*, d6c3 label corresponds to *irx6-3*/*AtCOBL4*::*PtCOB4a*, d6c5 label corresponds to *irx6-3*/*AtCOBL4*::*PtCOB4b.* * Significant difference from Col wild type (p=0.05), n=5, FQA was used to measure fibre length.

Stems from plant lines expressing *PtCOB4a* and *PtCOB4b* had wild type interfascicular fibre lengths as measured by FQA, in contrast to the longer fibers observed in the mutants (Figure 2.4b). Thus, expression of poplar orthologs in *Arabidopsis* restored the altered cell morphology associated with AtCOBL4 deficiency, indicating that *PtCOB4a* and *PtCOB4b* are functionally conserved with *AtCOBL4*.

Table 2.3: Cell wall chemical composition of primary inflorescence stems of wild-type *Arabidopsis* (Col), *irx6-2* and *irx6-3*, and select lines complemented by either *PtCOB4a* or *PtCOB4b*. d5c3 label corresponds to *irx6-2*/*AtCOBL4*::*PtCOB4a*, d5c5 label corresponds to *irx6-2*/*AtCOBL4*::*PtCOB4b*, d6c3 label corresponds to *irx6-3*/*AtCOBL4*::*PtCOB4a*, d6c5 label corresponds to *irx6-3*/*AtCOBL4*::*PtCOB4b*

	% Carbohydrates						% Lignin	
	Ara	**Rha**	**Gal**	**Glu**	**Xyl**	**Man**	**acid soluble**	**acid insoluble**
wt col	0.8	0.55	1.41	36.1	12.1	1.51	1.98	18.9
irx6-2	0.91	0.52	1.56	29.9	9.30	1.14	2.79	17.6
irx6-3	1.13	0.63	1.71	14.5	10.3	1.40	3.77	18.5
d5c3_l3	0.92	0.7	1.56	30.9	12.4	1.53	2.04	16.8
d5c3_l4	0.70	0.51	1.40	31.0	11.8	1.35	2.14	16.8
d5c5_l2	0.94	0.68	1.49	31.1	12.6	1.59	1.78	18.6
d5c5_l5	0.99	0.69	1.35	31.1	15.0	1.80	1.20	16.7
d6c3_l4	1.01	0.62	1.74	28.7	10.3	1.15	2.67	14.7
d6c3_l5	0.92	0.57	1.44	29.2	12.6	1.46	1.81	16.7
d6c5_l1	0.90	0.54	1.5	31.9	12.7	1.50	1.75	17.9
d6c5_l2	0.94	0.58	1.58	31.3	12.8	1.52	1.75	17.9

To confirm that *PtCOB4a* and *PtCOB4b* rescued the cellulose deficient phenotype observed in *irx6* plants, I quantified the amount cell wall derived glucose of the primary inflorescence stems of the complemented lines. *PtCOB4a* and *PtCOB4b* were capable of elevating cell wall glucose levels near to those of wild-type *Arabidopsis* plants (Table 2.3).

To determine if *PtCOB4a* and *PtCOB4b* were also capable of reverting the *irx6* associated cellulose ultrastructural phenotype back to that of wild-type *Arabidopsis*, I measured cell wall MFA and crystallinity (Table 2.4). MFA of the complemented lines was restored to that of wild

type grown under identical conditions, while the crystallinity of the cellulose deposited in *irx6* plants expressing either *PtCOB4a* or *PtCOB4b* was near to that of wild type. The slightly lower levels of crystalline cellulose in the complemented lines, compared to wild type, may due to the slightly lower levels of cellulose deposited in the complemented lines.

Table 2.4: Characterization of cellulose microfibril angle and crystallinity in the primary inflorescence stems of wild-type *Arabidopsis* (Col) and select lines complemented by either *PtCOB4a* or *PtCOB4b*. d5c3 label corresponds to *irx6-2*/*AtCOBL4*::*PtCOB4a*, d5c5 label corresponds to *irx6-2*/*AtCOBL4*::*PtCOB4b*, d6c3 label corresponds to *irx6-3*/*AtCOBL4*::*PtCOB4a*, d6c5 label corresponds to *irx6-3*/*AtCOBL4*::*PtCOB4b*. Standard error ()

	MFA (°)	Crystallinity (%)
Wt	13.5 (0.49)	25.4 (1.48)
d5c3_l3	12.5 (0.87)	25.3 (1.05)
d5c3_l4	14.7 (1.08)	18.7 (1.37)
d5c5_l2	14.7 (0.50)	23.0 (0.53)
d5c5_l5	13.3 (0.57)	24.9 (0.99)
d6c3_l4	13.7 (0.96)	21.8 (4.15)
d6c3_l5	12.2 (0.63)	25.2 (3.67)
d6c5_l1	14.2 (0.50)	23.7 (2.12)
d6c5_l2	13.2 (0.56)	20.1 (2.60)

2.3.4 AtCOBL4 is required for the normal pattern of secondary cell wall cellulose deposition

To examine the role of *AtCOBL4* in cellulose deposition in secondary cell wall domains, an experimental protoxylem tracheary element model was used. *Arabidopsis* lines carrying an inducible master transcriptional regulator (*VND7-VP16-GR*) (Yamaguchi *et al.*, 2010) were crossed with *irx6* lines, and mutants homozygous for *irx6* isolated. Treatment of *VND7-VP16-GR* lines with dexamethasone induces protoxylem differentiation in many cell types of the seedling, including epidermal cells. This unique ectopic expression offers a tool that permits secondary cell wall deposition to be observed directly. In wild-type seedlings carrying *VND7-VP16-GR,* the

cellulose stain Pontamine S4B (Anderson *et al.*, 2010) labelled cell wall domains with the characteristic proto-xylary banding pattern of cellulose (Figure 2.5a). In contrast, in the dexamethasone-induced *irx6-3*/*VND7-VP16-GR* plant lines, cellulose was deposited in a perturbed, disorganized manner with a bifurcated and diffuse cellulose distribution (Figure 2.5b). This phenotype supports the model that *AtCOBL4* is required for organized cellulose deposition in secondary cell walls.

The Pontamine S4B staining of cellulose showed that it had lost its spatial organization in the secondary cell wall thickenings in protoxylem elements (Figure 2.5).

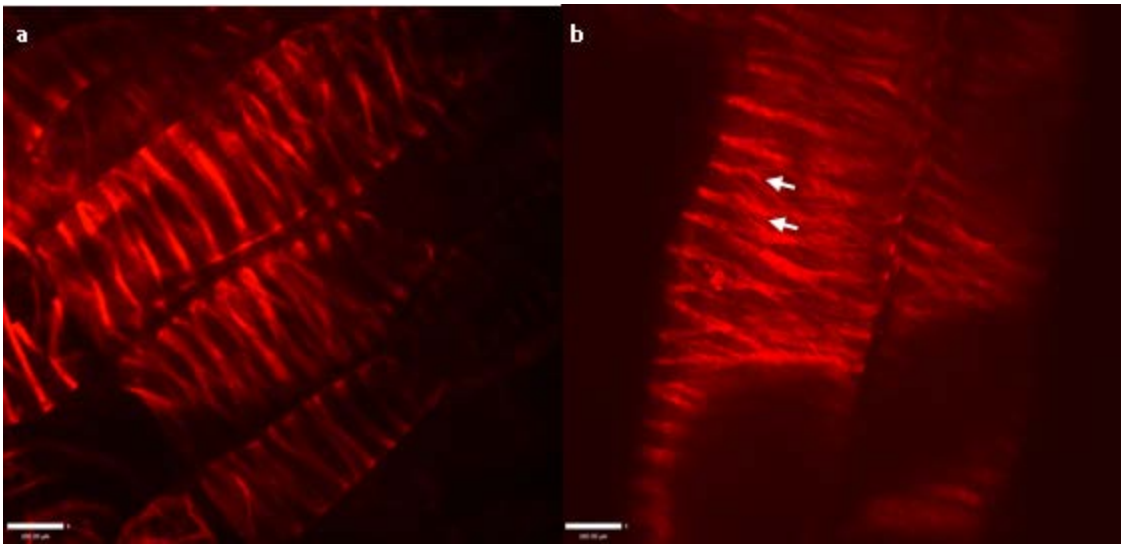

Figure 2.5: Cellulose organization in *VND7* and *VND7*/*irx6-3* trans-differentiating protoxylem cells. (a) Wild-type VND7-directed ectopic protoxylem cells with a discrete, highly organized cellulose, stained with Pontamine S4B. (b) *VND7*/*irx6-3* ectopic protoxylem cells with a bifurcated, loosely organized pattern of cellulose deposition. Arrows indicated bifurcated cellulose deposition. Scale bar is 10 µm.

To determine if AtCOBL4 has the correct temporal and spatial localization to influence the cellulose synthase complex or the organization of newly synthesized cellulose in the secondary cell wall, a fluorescently labelled poplar PtCOB4a fusion construct (*AtCOBL4::PtCOB4a-cYFP*) was designed. The cYFP was inserted just upstream of the omega-site (Figure 2.6a) in a variable region characterized by several small amino acids to prevent cYFP from blocking the cellulose binding module (CBM) at the N-terminus or either of the signal sequences at both the N- and C-termini. The PtCOB4a-cYFP was expressed in *Arabidopsis VND7-VP16-GR* lines under the control of the native *Arabidopsis AtCOBL4* promoter.

When *VND7-VP16-GR* lines were treated with dexamethasone, ectopic protoxylem trans-differentiation was induced in 7-day old seedlings. The functional capacity of the construct was confirmed by examining the secondary cell wall deposited in seedlings stained with Pontamine S4B. In plants expressing *PtCOB4a*-cYFP in the *irx6* background, tight, discrete bands of secondary cell wall cellulose deposition typical of protoxylem in wild-type *Arabidopsis* were observed (Figure 2.7a, c). In contrast, the *irx6-3*/ *VND7-VP16-GR* seedlings displayed disrupted, diffuse cellulose deposition during ectopic protoxylem differentiation (Figure 2.7b). These observations suggest that the fluorescently-tagged construct was functional.

Live cell imaging of *AtCOBL4::PtCOB4a-cYFP* in *irx6-3*/*VND7-VP16-GR* lines revealed fluorescent signal localized to the cell periphery, in a banding pattern characteristic of secondary cell wall thickenings (Figure 2.6b). Interestingly, PtCOB4a-cYFP was not only observed at the periphery of secondary cell wall thickenings, *i.e.* at the plasma membrane or cell wall interface, but throughout the secondary cell wall thickenings (Figure 2.6b inset).

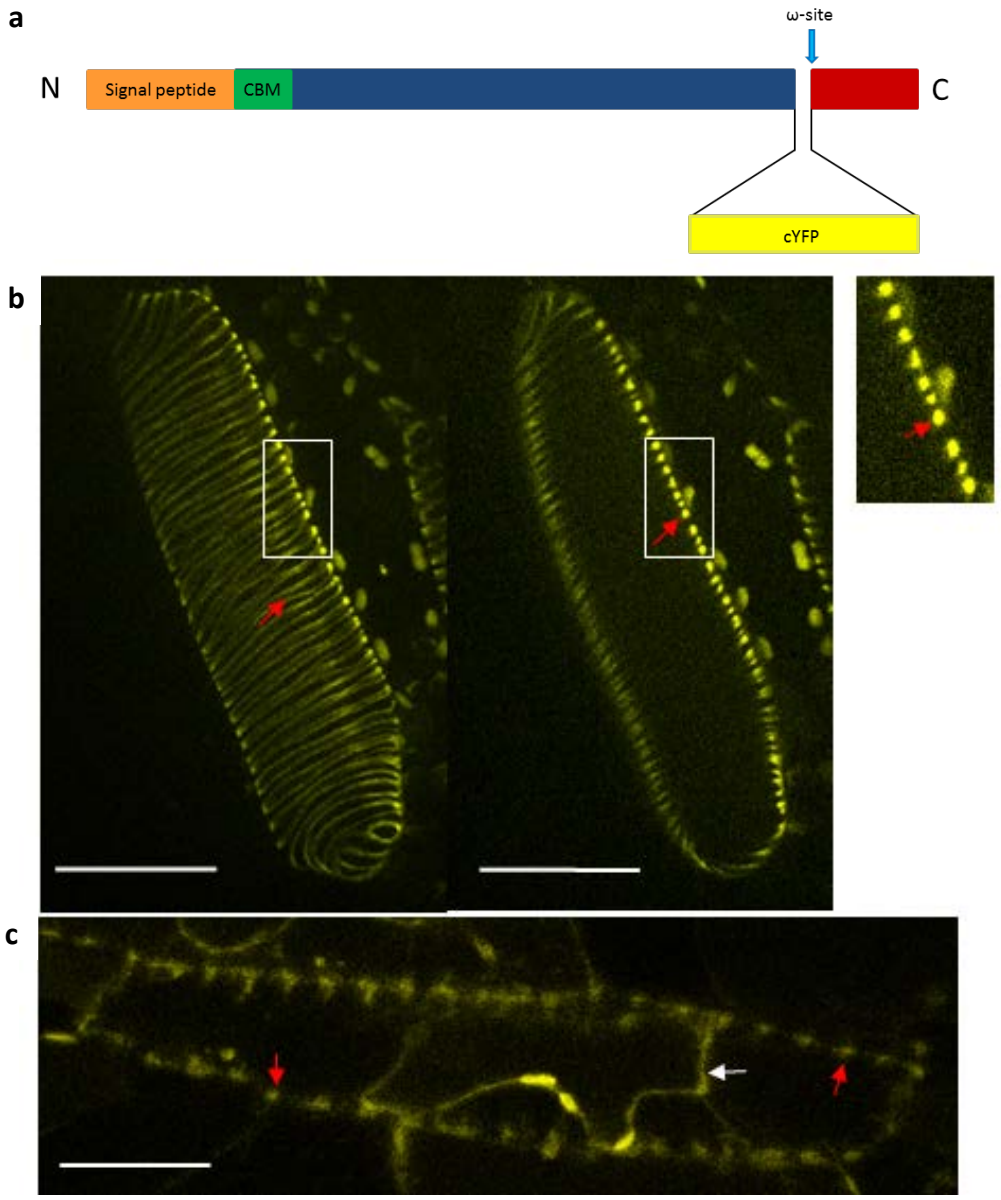

Figure 2.6: Localization of PtCOB4a-YFP in trans-differentiating protoxylem cells of *Arabidopsis*. (a) A diagrammatic representation of the PtCOB4a-YFP fusion protein showing the site of YFP insertion. (b) A maximum projection of PtCOB4a-YFP localization to secondary cell wall thickenings (left panel), and a single optical section (right panel), inset shows PtCOB4a-YFP distributed throughout the secondary cell wall thickenings. (c) A maximum projection showing plasmolysis of trans-differentiating protoxylem cells shows PtCOB4a localization to both the plasma membrane and secondary cell wall thickenings. Red arrows indicate secondary cell wall thickenings, white arrow indicates plasma membrane. Scale bar is 40µm.

This suggests that a proportion of the PtCOB4a protein population is bound to cellulose in these secondary cell wall thickenings. Immuno-gold labelling of BC1 in rice revealed a similar distribution of BC1 throughout secondary cell wall thickenings (Liu *et al.*, 2013).Plasmolysis of VND7-induced *irx6-3*/*VND7* + PtCOB4a-cYFP seedlings demonstrated that when the plasma membrane retracted from the cell wall, PtCOB4a-cYFP signal was maintained at the secondary cell wall thickenings as well as at the plasma membrane (Figure 2.6c).

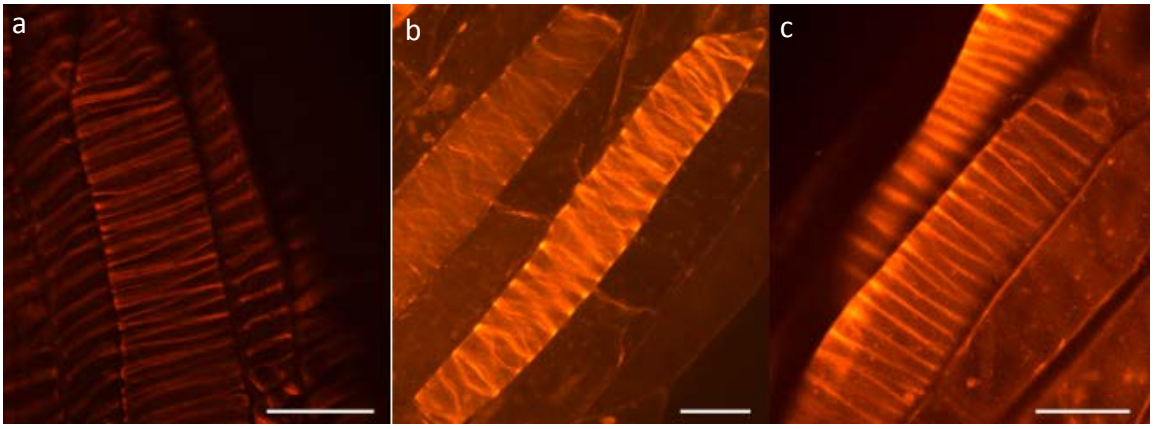

Figure 2.7: PtCOB4a-cYFP complementation of organized cellulose deposition in ectopic protoxylem cells stained with Pontamine S4B. (a) Wild-type VND7-directed ectopic protoxylem cells with a discrete, highly organized secondary wall thickenings. (b) VND7-directed ectopic protoxylem cells in the *irx6-3* mutant, with a bifurcated, loosely organized pattern of secondary cell wall thickenings. (c) In the *irx6-3* mutant lines carrying PtCOB4a-cYFP, discrete, highly organized wall thickenings are observed, similar to wild type. Scale bar = 20µm

This raises the question of whether PtCOB4a is mobile once it is inserted into the plasma membrane. Fluorescence recovery after photobleaching (FRAP) analysis of PtCOB4a-cYFP at the plasma membrane was used to address this question. FRAP revealed that PtCOB4a-cYFP was immobile at the plasma membrane once it was localized to the secondary cell wall thickenings

(Figure 2.8). Preforming FRAP on cells of Wt control seedlings expressing cytoplasmic GFP, confirmed rapid recovery of more than 80% of the initial GFP signal within 60 seconds. These data are consistent with the cell plasmolysis data, which demonstrated that a portion of PtCOB4a-cYFP remained bound to the secondary cell wall thickenings.

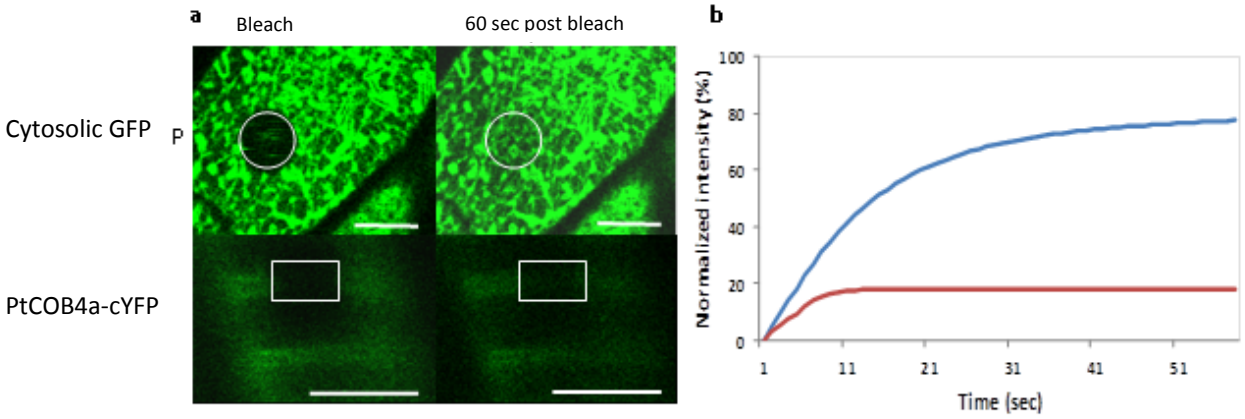

Figure 2.8: Mobility of PtCOB4a-cYFP at the plasma membrane cell wall interface. (a) FRAP examples for control cytosolic GFP and PtCOB4a-cYFP. (b) A representative fluorescence recovery curve of cytosolic GFP (blue) control and of PtCOB4a-cYFP (red). White circle and box indicate regions that were photobleached. Scale bar : 10µm

To determine if PtCOB4a-cYFP co-localized with microtubules, I introduced RFP labelled Tubulin-5α (RFP-Tubulin) into the VND7/*irx6-3*/PtCOB4a-cYFP lines. PtCOB4a-cYFP was observed to align with bundles of MT at the secondary cell wall thickenings (Figure 2.9). Roudier *et al.* (2005) report that the primary cell wall AtCOB distribution at the plasma membrane closely mirrored cortical MT patterning just below the plasma membrane. Wightman *et al.* (2008) demonstrated that YFP-CesA7 co-localized with microtubules in the protoxylem tracheary elements of *Arabidopsis* seedlings. This suggests that PtCOB4a most likely co-localizes with the secondary cell wall CesAs.

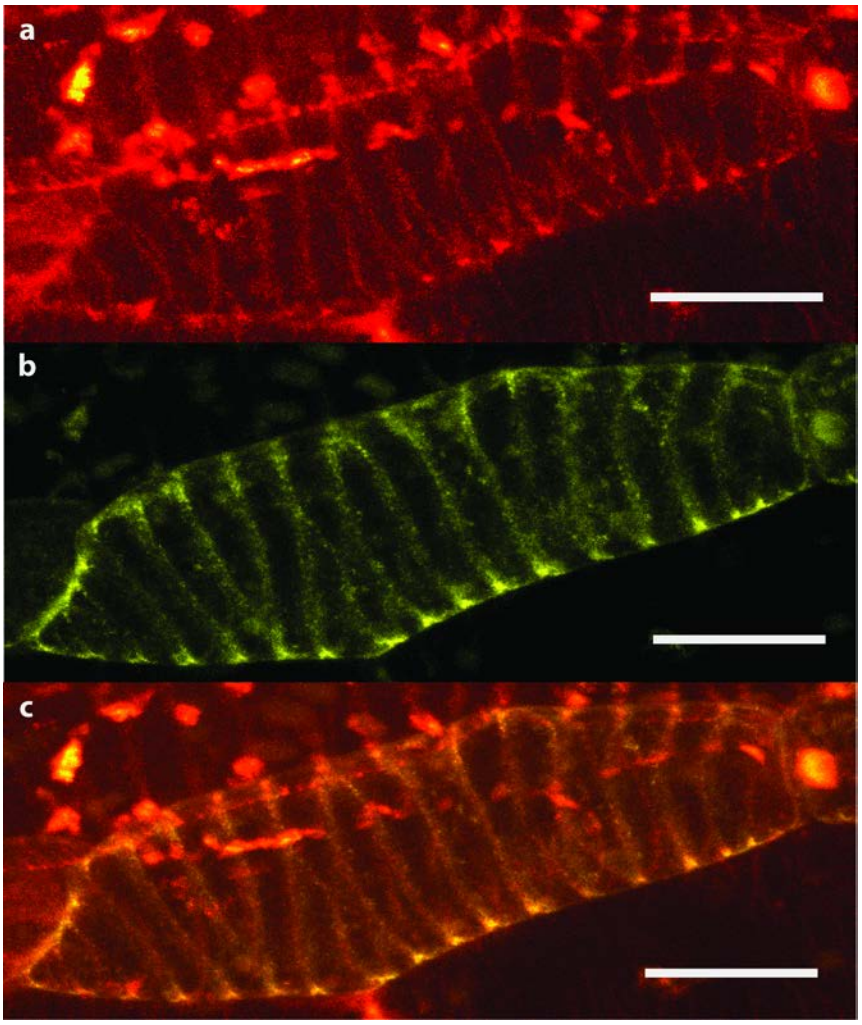

Figure 2.9: Co-localization of PtCOB4a-YFP with microtubules in trans-differentiating protoxylem cells. (a) RFP-tubulin6α labelled microtubules. (b) PtCOB4a-YFP localization to secondary cell wall thickenings, (c) image a and b merged to show co-localization. Scale bar = 20µm

At the whole plant level, the *AtCOBL4*::*PtCOB4a*-cYFP construct failed to rescue the *irx6* phenotype of mature plants as indicated by the unrestored cell wall derived glucose levels (Table 2.5) of primary inflorescence stems. As the YFP C-terminal tag does not block the CBM located at the N-terminus of the protein, the reason for PtCOB4a-YFP not restoring the wild-type metaxylem vessel phenotype, while apparently complementing the protoxylem tracheary

element phenotype, is not clear. The cellulose content of *irx6-2*/PtCOB4a-cYFP lines was similar to that of *irx6-2* plants, which also suggests that the fluorescent protein construct was not functional in the fibres, which make up the bulk of the secondary cell wall material in stems. In these cell types, the cYFP may prevent proper protein folding or interfere with interactions with proteins localized to the plasma membrane.

Table 2.5: Cell wall neutral sugar composition of primary inflorescence stems of un-induced VND7 *Arabidopsis,* and select VND7/*irx6-3* lines expressing *AtCOBL4*::*PtCOB4a*-cYFP.

	Ara	Rha	Gal	Glu	Xyl	Man
VND7	0.57	0.66	1.16	25.78	10.05	1.45
VND7/*irx6-3* + PtCOB4a-cYFP_L1	0.69	0.98	0.98	10.28	10.53	1.43
VND7/*irx6-3* + PtCOB4a-cYFP_L3	0.76	1.03	1.55	10.39	11.47	1.52
VND7/*irx6-3* + PtCOB4a-cYFP_L4	0.75	0.75	1.38	10.22	10.22	1.41

2.4 Discussion

This study aims to unravel the mechanisms that underpin the ordered arrangement of cellulose within secondary cell walls. More specifically, I focused on how *AtCOBRA-LIKE4* mediates the ordering of cellulose at sites of active secondary cell wall deposition. To achieve this, I performed an in depth analysis of the cell wall composition of the basal section of *Arabidopsis* primary inflorescence stem (the section of the stem with the highest proportion of secondary cell wall material) from wild type and two T-DNA insertion lines (*irx6-2* and *irx6-3*). Sugar analysis confirmed that glucose levels were reduced by up to 50% in *irx6-2* and *irx6-3* plants when compared to wild-type *Arabidopsis*. By isolating the α-cellulose from wild type and the *irx6* mutant lines, I was able to confirm that the observed reduction in cell wall glucose was due

to diminished cellulose content within secondary cell wall material. These findings point to *AtCOBL4* playing a direct role in cellulose production in the secondary cell wall.

I was then interested in how the loss of *AtCOBL4* function influenced the ultrastructural properties of the cellulose that was produced in the *irx6-2* and *irx6-3* lines. The ultrastructural properties of cellulose of primary importance are microfibril angle (MFA), cellulose crystallinity and degree of polymerization (DP). These are the properties of cellulose that confer mechanical and structural strength, and more importantly, the cell wall (Burgert 2006, MacMillan *et al.* 2013). The MFA of the cellulose deposited was substantially reduced to an angle of between 5.5-6.2° relative to the longitudinal axis of the cell. In contrast, double mutants in the *FASCICLIN*-LIKE-*ARABANOGALACTAN* (*FLA*) proteins, *atfla11* and *atfla12,* (MacMillan *et al.* 2010), which had a large reduction (30%) in cellulose content, had an increased MFA. This suggests that these two classes of GPI-anchored proteins, *AtCOBL4* and *AtFLA11*/*AtFLA12* function independently to influence the MFA of cellulose deposited within the cell wall.

The increased fibre length associated with the *irx6* mutation is likely due to a failure in secondary cell wall deposition that limits fibre cell intrusive growth (Gritsch and Murphy 2005). The thinner, weaker secondary cell walls may not be able to withstand the turgor pressure within the expanding fibre cells, resulting in the increase of fibre length and a decreased MFA as the cellulose MFs reorient such that they are more aligned to the longitudinal axis of the fibre cell. This resembles the observed reorientation of cellulose during anisotropic root cell

expansion (Roland and Vian, 1979; Anderson *et al.*, 2010). Our finding that perturbed cellulose is produced in *irx6* plants, with a lower crystallinity that is primarily due to the large decrease in the length of the glucan chains synthesized by secondary cell wall CesAs, is consistent with the model for cellulose synthesis put forward by Fujita and Wasteneys (2011). Longer glucan chains provide uninterrupted polymers that are available for inter-molecular non-covalent bonding between adjacent glucan chains, and thus promote crystallization of the ensuing cellulose. This demonstrates not only the need for sufficient cellulose production to maintain the cellular form and integrity, but the need for the individual glucan chains to be of sufficient length. This also suggests that a large reduction in secondary cell wall cellulose does not predict the change in MFA, but rather reflects the properties that the functional proteins confer to the deposited cellulose.

I next addressed the question of functional conservation of the *AtCOBL4* between herbaceous and woody plants using *Arabidopsis* and poplar as model systems. Based on next generation sequencing data and published phylogenies of the poplar *COBRA* gene family (Zhang *et al.*, 2009; Ye *et al.*, 2009b), two potential orthologs of *AtCOBL4*, *PtCOB4a* and *PtCOB4b,* were selected. Evolutionarily, the recent partial genome duplication in poplar (Tuskan *et al.* 2006) is the most likely explanation for PtCOB4a and PtCOB4b both having a high similarity to AtCOBL4 at the amino acid level. Transformation with the native *AtCOBL4* promoter driving expression of *PtCOB4a* or *PtCOB4b* in the *irx6-2* and *irx6-3 Arabidopsis* lines, led to reversion of the *irx6 Arabidopsis* mutant lines to a wild-type phenotype, demonstrating a conservation of *COBL4*

function during secondary cell wall deposition across taxa. The recovery of fibre cell length supports the functional conservation finding, suggesting that a secondary effect of *AtCOBL4* is determining the final cell geometry of tip growing fibre cells in *Arabidopsis*.

Using confocal microscopy, in combination with fluorescent cellulose stains and fluorescent labelling of PtCOB4a, I was able to provide a snapshot of secondary cell wall cellulose deposition in the inducible *VND7* system developed by Yamaguchi *et al.* (2010). This experimental system permits observations of real-time, secondary cell wall deposition during ectopic protoxylem differentiation in wild-type and *irx6 Arabidopsis* backgrounds. Staining ectopically differentiating seedlings with the cellulose-specific Pontamine S4B dye showed that cellulose synthesis, in the presence of AtCOBL4, results in tightly packaged, discrete domains of secondary cell wall deposition. In contrast, when induced, *irx6* seedlings produce cellulose that partially loses its spatial constraint to discrete domains of secondary cell wall deposition. The disorganized and bifurcated pattern of deposited cellulose suggests that AtCOBL4 functions in organizing cellulose, likely by providing an environment amenable to efficient cellulose biosynthesis and crystallization. Cellulose crystallization is known to be reduced when plants are exposed to calcofluor white, which binds to the cellulose, hindering intermolecular cellulose interactions (Benziman *et al.* 1980, Haigler *et al.* 1980, Anderson *et al.* 2010). Liu *et al.* (2013) showed that seedling roots of rice *bc1* mutants are insensitive to calcofluor white treatment at all but the highest concentrations suggesting that *bc1* is required for optimal cellulose crystallization. By fluorescently labelling PtCOB4a with cYFP, I was able to show that PtCOB4a-

YFP localizes to the sites of secondary cell wall deposition in trans-differentiating protoxylary cells, and that the PtCOB4a-YFP co-aligns with RFP-labelled cortical microtubule bundles situated directly below sites of secondary cell wall deposition. Wightman and Turner (2008) demonstrated that YFP-AtCesA7 co-localizes with fluorescently labelled cortical MT in the spiral secondary cell wall thickenings of *Arabidopsis* root treachery elements. This knowledge allows us to place AtCOBL4 and orthologs spatially and temporally in position to facilitate a maximum efficiency in cellulose elongation and crystallization. This does not appear to require direct interaction between CesAs and AtCOBL4, as yeast-two-hybrid and pull-down assays have not detected any interactions between CesAs and AtCOBL4 (Taylor *et al.*, 2003; Desprez *et al.*, 2007; Gu *et al.*, 2010b; Liu *et al.*, 2013). Instead, it is likely that AtCOBL4 binds to newly synthesized cellulose as it is being extruded from the CSCs, providing stability to the emerging cellulose chain, ultimately facilitating maximal inter-chain crystallization. Alternately, AtCOBL4 may bind to previously deposited cellulose, and as such contribute to organizing the plasma membrane to provide "tracks" along which CSCs move depositing cellulose.

When taken in the context of the cell wall chemistry, these findings reveal how AtCOBL4 plays a central role in determining CSCs efficiency, organizing newly synthesized cellulose at sites of secondary cell wall deposition, and ultimately influencing the anisotropic growth of fibre cells.

Chapter 3: AtCOBL4-directed organization of cellulose during secondary cell wall deposition in hybrid poplar

3.1 Introduction

The woody tissues of trees, are dominated by cells that are rich in secondary cell walls that provide strength and durability to the tissues and the tree as a whole. The secondary cell wall is composed primarily of three major components; lignin (~22%), hemicelluloses (~26%) and cellulose (~45%) (Coleman *et al.* 2007, Coleman *et al.* 2009). The most abundant biopolymer, cellulose, confers structural strength to the secondary cell wall allowing the cell to not only resist extracellular forces, but also internal forces such as turgor pressure. Despite intensive research for more than 50 years, there are many unanswered questions regarding both the synthesis and regulation of cellulose production *in planta*. At sites of secondary cell wall deposition, cellulose is synthesized by secondary cell wall specific *Cellulose Synthases* (*CesA4*, *CesA7*, *CesA8*), which are thought to be arranged in an ordered fashion into a cellulose synthase complex (CSC). Active CSCs are localized to the plasma membrane and extrude cellulose chains into the apoplastic space where the cellulose is rapidly incorporated into the secondary cell wall (Turner and Somerville, 1997b; Somerville, 2006; Carpita, 2011). In the bacteria *Rhodobacter sphaeroides*, a single CesA is capable of synthesizing a β-1,4-glucan chain of cellulose, and the structure of this CesA was recently solved (Morgan *et al.*, 2013). It is likely that plant CesAs have retained the ability to produce cellulose with a similar mechanism. This implies that if the rosette arrangement of CesAs holds true, that between 18-36 glucan chains make up an elementary microfibril, a number which has been supported by atomic force microscopy imaging of maize primary cell wall cellulose organization (Ding, 2007). As the individual

cellulose chains are extruded into the apoplastic space, they spontaneously crystallize, a consequence of strong intra- and inter-molecular hydrogen bonding (Kudlicka *et al.* 1995).

The degree of crystallization along the length of cellulose microfibrils is not uniformly maintained, but is rather a combination of crystallized cellulose interspersed with regions of para-crystalline (amorphous) cellulose (Saxena and Brown, 2005; Ruel *et al.*, 2012). The crystalline nature of cellulose precludes other cell wall components, such as hemicelluloses, from interacting with anything but glucan residues at the MF surface or with internally localized glucan chain native to the amorphous regions (Ding *et al.* 2006, Ding *et al.* 2013). The molecular mechanisms underpinning cellulose crystallinity are unclear. Recent advances in live cell imaging have suggested that the velocity at which CSCs move through the plasma membrane is correlated somewhat with the crystalline state of the ensuing cellulose (Fujita *et al.* 2011; Harris *et al.* 2012; Fujita *et al.* 2013). In primary cell walls, cellulose deposited at a higher polymerization rate or increased CSC velocity results in a decrease in cellulose crystallinity (Benziman *et al.*, 1980; Haigler *et al.*, 1980; Harris *et al.*, 2012).

Cortical microtubules (MT) arrange in bundles in the cytosol beneath the plasma membrane that are aligned in the same orientation as deposited cellulose MFs (Ledbetter and Porter 1963). Consequently, it has been hypothesized that MT play a role(s) in determining the orientation of deposited cellulose. However, the extent of, and requirement of MT for correct MF orientation has long been debated (Mueller and Brown 1982, Emons *et al.* 1992,

Himmelspach *et al.* 2003, Sugimoto *et al.* 2003). Using live cell imaging, Paredez *et al.* (2006) demonstrated the co-alignment of MT and CSCs during primary cellulose biosynthesis and that MT were required during cellulose deposition. MT bundles localize to sites in the cytosol below sites of active primary cell wall deposition and are thought to spatially direct the insertion of CesAs into the plasma membrane. Once the initial pattern of cellulose deposition is set, microtubules could continue to influence the CSC trajectories, recycling of CesAs from the plasma membrane and pattern of cellulose deposition (Wasteneys and Fujita, 2006; Crowell *et al.*, 2009; Gutierrez *et al.*, 2009). Building on these findings, Fujita *et al.* (2011), elegantly showed that MTs influence the crystalline ultrastructure of cellulose deposited in the primary cell wall. The authors showed that when MTs were disrupted, cellulose crystallinity did not decline in rapidly elongating plants, while when ROP-INTERACTIVE CRIB MOTIF-CONTAINING PROTEIN 1 (*RIC1)* is over-expressed, MTs stably bundle and cellulose crystallinity decreases (Fujita *et al.* 2011). Moreover, when plants were undergoing rapid stem elongation at 29°C, cellulose crystallinity was higher in *mor1*-1 plants relative to wild-type plants. CSC velocity is greater in the *mor1-1* plants at 29°C than wild type, and it appears that a positive correlation exists between CSC velocity and increasing cellulose crystallinity (Fujita *et al.* 2013).

In plant biology, the study of secondary cell wall biosynthesis has lagged behind that of primary cell wall. The depth at which the plant vasculature is situated within the overall plant architecture has limited the resolution of live cell imaging. Moreover, to understand chemical changes requires the degradation of the entire wall to elucidate the fundamental changes that occur during gene disruption. As such, to date, studies have been limited to anatomical,

physiological and somewhat crude chemical phenotypes associated with defective alleles of genes required for secondary cell wall biosynthesis. A series of studies in *Arabidopsis* employing YFP-labelled secondary cell wall *AtCesA7*, revealed that AtCesA7 localized to the spiral secondary cell wall thickenings in root tracheary elements and co-localized with MT bundles (Wightman and Turner, 2008b). This suggests that similar mechanisms may underlie primary and secondary cell wall deposition.

The *COBRA* gene family of GPI-anchored proteins have been shown to be required for correct cellulose deposition in the primary cell wall (Benfey *et al.*, 1993; Roudier *et al.*, 2002; Li *et al.*, 2003a; Brown *et al.*, 2005; Roudier *et al.*, 2005b). Similarly, *COBRA-LIKE4* (*AtCOBL4*) was shown to be required for secondary cell wall cellulose deposition (Brown *et al.*, 2005). Loss-of-function *atcobl4* mutants do not display an altered primary growth phenotype, despite a 50% reduction in cellulose content in the stem. In fibres and tracheary elements of these mutants, the reduced cellulose content is correlated with dramatically thinner secondary cell walls, and manifests in an irregular (*irx*) xylem phenotype as the vessels are unable to withstand the negative pressures associated with transpiration (Brown *et al.*, 2005). In rice, the *AtCOBL4* ortholog *BC1* was discovered, with the *bc1* mutant having reduced cellulose content in secondary cell walls. In addition, the *cell wall architecture1* (*cwa1*) allele accumulates phenolic compounds in the sclerenchyma cells (Li *et al.*, 2003a; Sato *et al.*, 2010). Sato *et al.* (2011) went on to show that a cellulose binding module (CBM) located at the N-terminus of COBRA proteins is required for proper *BC1* function. *BC1* has recently been shown to play a role in determining the crystalline

state of cellulose within the secondary cell wall (Liu *et al.*, 2013). The underlying mechanism influencing cellulose crystallinity remains unclear.

All studies aiming to elucidate the function of *AtCOBL4* and its homologs have utilized model herbaceous systems that produce stems with limited secondary cell wall-containing tissues. The use of a woody model system, such as poplar, with a secondary cell wall-rich architecture may provide further, finer insights into the mechanism of *AtCOBL4* function. In chapter 2 of this thesis, I clearly demonstrated the conservation of function between herbaceous *Arabidopsis* (*AtCOBL4*) and *P. trichocarpa* orthologs *PtCOB4a* and *PtCOB4b*. In this chapter, I over-expressed *AtCOBL4* in a secondary cell wall specific manner using the endogenous *PtCesA8* promoter in hybrid poplar (*P. alba x P. grandidentata*, P39). Detailed analysis of the cell walls deposited in poplar plants over expressing *AtCOBL4* confirmed a cellulose specific function for *AtCOBL4*. The data supports a model where AtCOBL4 functions at a point soon after cellulose synthesis, likely as the glucan chains are extruded into the apoplastic space and are incorporated into the cell wall. Furthermore, I show that *AtCOBL4* function has a positive feedback on cellulose biosynthesis, increasing the length of individual glucan chains. By examining cell morphology, I confirmed a secondary effect altering the DP and cellulose crystallinity during the intrusive growth of fibre cells identified in chapter 2.

3.2 Materials and methods

3.2.1 Cloning of *AtCOBL4*

The *AtCOBL4* (At5G15630) coding sequence was cloned from *Arabidopsis thaliana* (Columbia ecotype) using cDNA (iScript, Biorad), synthesized from RNA isolated from the primary inflorescence stems of six-week-old plants (Primers: F 5' CAAGGTACCATGAGGCTCCTCTTCAG 3'; R 5' CAAGAGCTCTCACCATATTGAGATGAAT 3'). The *AtCOBL4* CDS was cloned into pZeroBlunt (Invitrogen) and then sub-cloned in pSM3-*PtCesA8*::His, that consisted of a 2.8kb *PtCesA8* promoter sequence linked to a His-Tag, using KpnI and SacI restriction sites, producing pSM3-*PtCesA8*::His-*AtCOBL4*.

3.2.2 Generation of transgenic hybrid poplar

The binary vector pSM3-*PtCesA8*::His-*AtCOBL4*, was first transformed into *Agrobacterium tumefaciens* EHA105 (Hood *et al.* 1993) by the standard freeze thaw method (Holsters *et al.*, 1978). Leaf discs tissue culture plantlets from hybrid poplar P39 were prepared using a #4 cork borer. The sterile leaf discs were then used in a leaf disc inoculation procedure, as described by Coleman *et al.* (2008).

Putative transgenic plants were first identified by hygromycin antibiotic selection. Subsequently, surviving plants were genotyped by isolating genomic DNA using a modified CTAB protocol, based on Rogers and Benedich (1994). In brief, 100 mg of ground leaf tissue in a

microcentrifuge tube was re-suspended in 1 ml CTAB extraction buffer (2% [w/v] hexadecyltrimethylammonium bromide [CTAB; Sigma], 100 mM Tris- HCl, pH 8.0, 1.4 M NaCl, 20 mM EDTA, 1% [w/v] polyvinylprylidone, and 0.2% [v/v] 2-mercaptoethanol), incubated at 65°C for one hour, after which cell debris were pelleted by centrifugation. One volume of phenol:chloroform:isoamyl alcohol (Sigma) was then added to the CTAB-plant extract and centrifuged. DNA was precipitated from the recovered aqueous phase by addition of half a volume of isopropanol followed by centrifugation. Precipitated DNA was washed by centrifugation in 75% ethanol and re-suspended in 100 µl Nanopure H_2O. Primers amplifying the *AtCOBL4* CDS were used in a genotyping PCR to confirm the presence of pSM3-*PtCesA8*::His-*AtCOBL4* in the putative transgenic P39 poplar lines.

Plants of each positive transgenic event were then multiplied by clonal propagation, and ultimately 10 plants were transferred to pots and grown under controlled greenhouse conditions for 4 months. At which point 4 plants per transgenic line was destructively sampled.

3.2.3 RNA isolation and Transcript abundance

Total RNA was isolated from 100 mg of frozen, ground developing xylem using Plant RNA reagent (Ambion) according to manufacturer's instructions. RNA yields were quantified using a NanoDrop Lite instrument (Thermo Scientific). 10 µg of total RNA was treated with DNase (TurboDNase, Ambion) for 30 min at 37°C, after which the DNAse was inactivated using DNase

inactivation Reagent (Ambion). 1 µg of DNAse treated RNA was used in a 20 µl first-strand cDNA synthesis reaction using iScript reverse transcriptase (Biorad).

Real-time PCR was used to quantify *AtCOBL4* transcript abundance on a C1000 Thermal Cycler Bio-Rad CFX96 Real-Time PCR System (Bio-Rad). 20 µl RT-qPCR reactions were set up using Ssofast Evagreen qPCR master mix (Biorad) and 1 µl template. Primers used to quantify *AtCOBL4* transcript were forward (5' GAGCTGCGTCAAGGCTGAT 3') and reverse primers (5' GTGGACTCTAACAGGGCACAT 3'). A house keeping gene, *Transcription-Initiation Factor5α,* was used to calculation relative transcript abundance, using the forward (5′ GACGGTATTTTAGCTATGGAATTG 3′) and reverse primers (5′ CTGATAACACAAGTTCCCTGC 3′). The RT-qPCR conditions were as follows: 95°C for 30 s, followed by 40 cycle of 95°C for 30 s, 66°C for 10s, and 72°C for 10 s. Relative transcript abundances for *AtCOBL4* were determined by expressing *AtCOBL4* Ct-values relative to *Transcription-Initiation Factor5α* Ct-values (Ralph *et al.*, 2006).

3.2.4 Microscopy

The first basal internodes above the root collar of stems collected for destructive sampling were rehydrated in dH_2O overnight prior to use. 40 µm thick cross-sections were made using a sliding bench-top microtome (American optical, Model # 860). The sections were then stained with Toluidine blue and viewed using a Leica DMR light microscope (Leica Microsystems Inc.). Images

were captured with a QImaging Qicam camera (QImaging) using OpenLab software (PerkinElmer Inc.).

3.2.5 Analysis of cell wall chemistry

The xylogenic tissue was separated from the pith and ground using a Wiley-mill to pass a 40-mesh screen. Extractives were removed from the ground woody material by over-night hot acetone extraction in Soxhlet apparatus, after which extractive free samples were dried over night at 50°C in an oven. A modified Klason method (Coleman *et al.*, 2008) was used to quantify the carbohydrate and lignin content of 200 mg of extractive-free dried wood tissue by incubating in 72% H_2SO_4 for 2 hours with regular stirring. The acid concentration was then diluted to 4% and the samples were treated at high temperature and pressure (autoclave) to completely hydrolyze cell wall polysaccharides. The monosaccharides were quantified by AE-HPLC using an ICS 5000 (Dionex-Thermofisher) fit with a CarboPac PA1 column (Thermofisher) at 0.8 mL/min flow rate, and a pulsed amperometric detector with a gold electrode, and post column supplementation of 100 mM NaOH. Acid-soluble lignin content was determined spectrophotometrically at 280 nm, while the acid-insoluble lignin was determined gravimetrically.

3.2.6 Holo- and α-cellulose isolation

200 mg of ground, extract free wood was mixed with 3.5 mL buffer (60 mL of glacial acetic acid + 1.3 g NaOH/L) and 1.5 mL of 20% sodium chlorite, and incubated at 50°C with gentle shaking for 16 hours, at which time the reaction was quenched by placing the samples on ice and this reaction was repeated. The reacted sample was transferred to a coarse pre-weighed sintered crucible, washed twice with 50 mL of 1% glacial acetic acid, followed by a wash with 10 mL acetone. Finally, the crucibles were dried at 50°C overnight and weighed. α-cellulose content was then isolated from the recovered holocellulose by reacting 100 mg holocellulose with 17.5% NaOH for 30 min, the solution was then diluted to 8.75% NaOH and reacted for a further 30 min. All retentate was filtered through pre-weighed coarse sintered crucibles and washed with distilled (DI) water. The retentate was then soaked in 1.0 M acetic acid for 5 min, before being washed with DI water. Crucibles were dried at 50°C overnight and weighed (Yokoyama *et al.*, 2002).

3.2.7 Cellulose degree of polymerization

30 mg of α-cellulose were solubilized in 9% LiCl/N,N-Dimethylacetamide (DMAc). Briefly, isolated α-cellulose was swollen in ddH_2O with stirring for 48 hours; ddH_2O was substituted for 100% anhydrous EtOH (Sigma) and stirred for 48 hours, EtOH was substituted for anhydrous DMAc and stirred for 48 hours. Finally, 9% LiCl/DMAc substituted the DMAc, and this solution was stirred for an additional 24 hours. The solubilized cellulose was diluted and injected on an Agilent 1100 series GPC instrument fit with two Styragel columns in series (Waters; 5E, 4E).

Cellulose polymer size was determined by multi-angle light scattering and calculated using the program ASTRA (Wyatt Technologies), giving estimates of the average molecular weights.

3.2.8 Cell wall crystallinity and cellulose MFA

To investigate the hypothesized link between cellulose DP and cellulose crystallinity (Fujita *et al.* 2011), the second internode above root collar was longitudinally sectioned, yielding a 3.2 mm thick section that was used to calculate cell wall crystallinity and MFA. This was done for four plants per transgenic line. Cellulose microfibril angle was determined using X-ray diffraction (Megraw *et al.*, 1998) on a Bruker D8 discover X-ray diffraction unit. Wide-angle diffraction was used in transmission mode with a $CuK_{\alpha}1$ radiation (λ=1.54 Å), and a 0.5 mm collimator, where the scattered photons were collected by a GADDS detector. A theta angle of 0° for both the X-ray source and detector was used for microfibril angle measurement, while for cell wall crystallinity a detector theta angle of 20° was employed. Crystallinity was determined as described by Vonk (1973), by mathematically fitting the data.

3.2.9 Fibre cell length

Fibre cell length was estimated on specimens isolated from the third internode above the root collar, approximately 10 cm above the soil. The xylem tissue was separated from the pithy tissue, and reacted with Franklin solution (1:1 30% peroxide and glacial acetic) at 70°C for 48 hours. The reaction solution was removed and the samples gently washed with tap water. The

individual fibres were separated by briefly stirring in tap water, and the resulting fibre suspension was assessed on a fibre quality analyzer to measure 5000 fibres per sample at a flow rate of 20-40 fibres per second.

3.2.10 Biomechanics

Tensile test were performed on 200 µm thick sections one internode in length, approximately 4 cm in length, created on a bench-top microtome (American optical, Model # 860). A custom made dog-bone template was used to produce specimens with a neck width of 3.21 mm. Tensile tests were performed using an Instron tensometer (Instron, model 5565) with a 500 Newton load cell. Three point bending was performed using the same tensometer. A custom made three point bending apparatus was used to break 1.68 mm x 1.68 mm samples of approximately 4 cm in length. A constant cross-head extension rate of 20 mm/min was used. BlueHill software was used to capture and calculate the modulus of elasticity (MOE) for each sample.

3.3 Results

3.3.1 Secondary cell wall-specific over expression of *AtCOBL4*

atcobl4 mutants are known to have a significant reduction in cellulose content. However, the reduced cellulose does not result in a primary cell wall defect, but instead in collapsed xylem vessels, consistent with the previously described irregular xylem (*irx*) phenotype, pointing to a

secondary cell wall-specific function (Chapter 2). Quantitative trait loci (QTL) analysis in *Eucalyptus nitens* identified a *cis*-acting polymorphism, SNP7, in *EniCOBL4A* as a marker for cellulose content, which also influences the allelic expression of *EniCOBL4A* (Thumma *et al.*, 2009). These findings indicate that *AtCOBL4* function, like that of its homologs in other species, is influencing cellulose deposition in plants. To better understand the role of the closely related poplar *AtCOBL4* homologs in wood formation in poplar, I isolated the *AtCOBL4* coding sequence (CDS) and placed it under the control of the *PtCesA8* promoter (*PtCesA8::AtCOBL4)*. This permitted me to over-express *AtCOBL4* in a secondary cell wall-specific manner in poplar, avoiding any potential side effects of incorrect spatial expression in tissues producing solely primary cell walls. The *Arabidopsis* rather than poplar gene was used to avoid silencing. *PtCesA8::AtCOBL4* was introduced into a hybrid poplar clone (*P. alba* x *P.grandidentata*; P39) via agrobacterium-mediated transformation, which resulted in nine positive transformed lines. The resulting transgenic plant lines were multiplied in tissue culture and then transferred to a controlled greenhouse conditions for four months of growth.

3.3.2 *AtCOBL4* transcript abundance and wood anatomy

AtCOBL4 transcript abundance in developing xylem of each transgenic line and the corresponding control was determined using RT-qPCR. Transgenic lines five and six (designated OE5 and OE6) showed the highest levels of *AtCOBL4* expression (Figure 3.1), while line nine (OE9) showed very little *AtCOBL4* expression (Figure 3.1) offering an individual to serve as a transformed control for which to compare highly expressing *AtCOBL4* lines. An assessment of

AtCOBL4 over expressing stem cross-sections by light microscopy of histochemically stained specimens did not reveal any alteration to the arrangement of cells within the stem or cell morphology (Figure 3.2). This suggests that increased *AtCOBL4* transcript abundance above the native levels does not result in altered cell wall architecture.

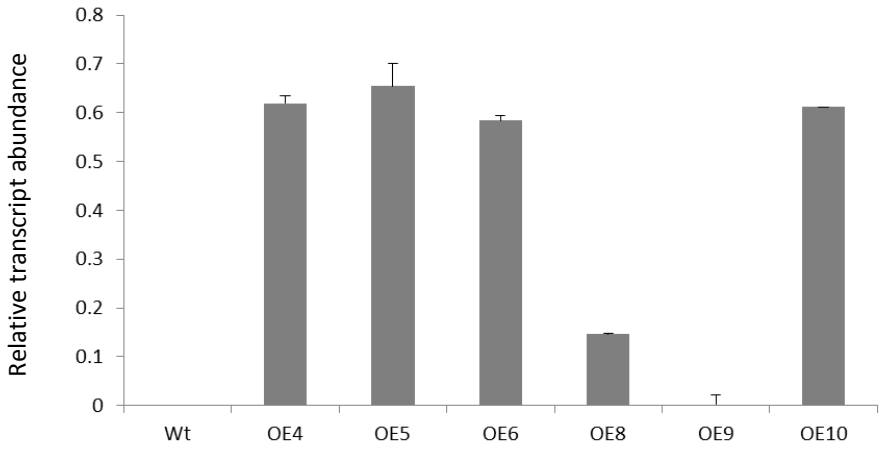

Figure 3.1: Relative transcript abundance of *AtCOBL4* in developing xylem in the transgenic poplar lines. *AtCOBL4* transcript levels were quantified relative to Elongation Factor 5α transcript abundance.

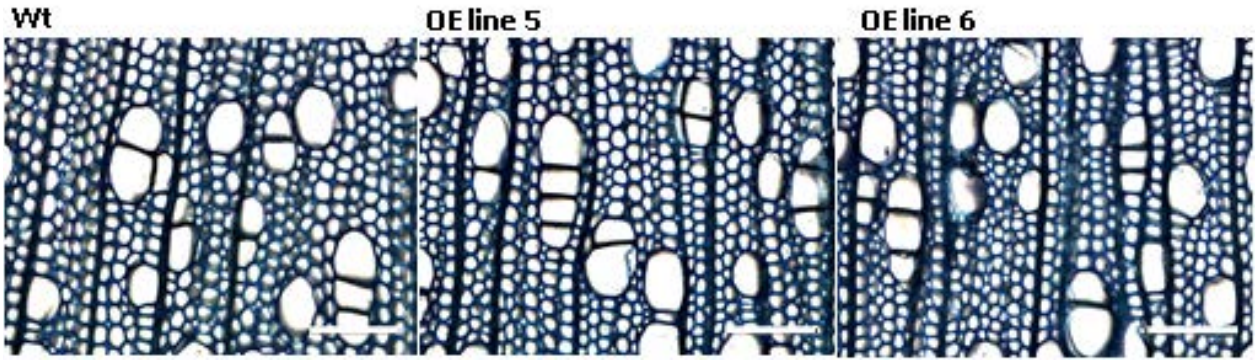

Figure 3.2: Stem cross sections of hybrid poplar over expressing *AtCOBL4* stained with toluidine blue. No difference in the stems was observed. AtCOBL4 over expression lines 5 and 6 represent typical OE line stem sections showing xylem fibres and vessels. Scale bar: 50µm

3.3.3 Cell wall chemistry

The xylem tissue of the over expression and control hybrid poplar lines, were next characterized chemically. Total lignin content did not differ significantly from that of wild-type trees, which is consistent with *AtCOBL4* not functioning in lignin biosynthesis. No significant increases in cell wall derived glucose were observed for the over expression lines (Table 3.1), with few other changes in hemicellulose or pectic derived carbohydrates. Cellulose content for the over expression lines were also determined, with OE4 and OE6 (Table 3.2) found to have a significantly increased cellulose content.

Table 3.1: Cell wall sugar and lignin composition of hybrid poplar lines over expressing AtCOBL4 (pSM3-PtCesA8::AtCOBL4). N= 4

	% Carbohydrates						% Lignin	
	Ara	**Rha**	**Gal**	**Glu**	**Xyl**	**Man**	**Acid soluble**	**Acid in-soluble**
Wt	0.28 (0.02)	0.41 (0.02)	0.94 (0.13)	43.3 (0.62)	15.8 (0.39)	1.58 (0.06)	3.2 (0.17)	19.0 (0.97)
OE4	0.27 (0.02)	0.45 (0.01)	0.78 (0.15)	43.1 (0.54)	15.1 (0.22)	1.88 (0.12)	3.4 (0.39)	20.3 (0.59)
OE5	0.31 (0.05)	0.46 (0.02)	1.07 (0.20)	42.2 (0.50)	15.3 (0.70)	1.72 (0.07)	3.2 (0.41)	19.9 (1.22)
OE6	0.27 (0.02)	0.45 (0.01)	0.82 (0.20)	42.9 (1.82)	15.5 (1.24)	1.90 (0.34)	3.0 (0.23)	19.2 (0.71)
OE8	0.32 (0.01)	0.47 (0.04)	1.28 (0.20)	43.6 (0.77)	15.5 (0.70)	1.9 (0.18)	3.2 (0.21)	19.8 (0.91)
OE9	0.27 (0.08)	0.46 (0.02)	0.75 (0.09)	36.4 (1.67)	13.8 (0.61)	1.56 (0.24)	3.1 (0.17)	19.9 (0.42)
OE10	0.23 (0.02)	0.41 (0.02)	1.27 (0.50)	41.2 (0.38)	13.3 (0.74)	1.51 (0.06)	3.3 (0.18)	19.3 (0.91)

Table 3.2: Holocellulose, α-Cellulose, cellulose crystallinity and microfibril angle (MFA) analysis of hybrid poplar lines over expressing AtCOBL4 (pSM3-PtCesA8::AtCOBL4). N=4, bold lettering indicates significant difference from Wt (P=0.05)

	% Holo-cellulose	% α-cellulose	Crystallinity (%)	MFA(°)
Wt	64.9 (0.43)	34.4 (0.42)	37.9 (0.85)	15.2 (0.61)
OE4	64.9 (0.19)	**38.1** (0.70)	**41.4** (1.71)	15.6 (0.49)
OE5	64.2 (0.81)	34.7(0.36)	39.1 (0.91)	14.9 (0.78)
OE6	64.8 (0.40)	**37.7** (1.52)	**40.**2 (0,70)	15.6 (1.31)
OE8	62.8 (0.20)	36.7 (1.74)	38.9 (1.91)	14.1 (1.28)
OE9	63.5 (0.87)	33.5 (0.75)	39.7 (2.50)	13.1 (0.77)
OE10	63.3 (0.80)	35.7 (1.85)	41.8 (2.17)	13.6 (0.55)

3.3.4 Cell wall ultrastructural properties

Recently *BC1* in rice was shown to influence cellulose crystallinity (Liu *et al.*, 2013) stimulating the question of the possibility of other *COBL4* homologs altering the ultratructural arrangement of cellulose produced in secondary cell walls. Here, we show that all lines over expressing *AtCOBL4* had an increase in cell wall crystallinity, on average 3% higher relative to wild-type hybrid poplar (Table 3.2), which is consistent with the increased levels of α-cellulose deposited in *AtCOBL4* lines, and its involvement in post-polymerization organization of cellulose biosynthesis.

Next, I measured the microfibril angle of cellulose deposited in wild-type and *AtCOBL4* over expressing lines by X-ray diffraction, which indicated that there was no significant difference from the MFA between the transgenic lines and wild-type plants (Table 3.2). This finding suggests that AtCOBL4 does not play a role in orientating the cellulose that is deposited in secondary cell walls. As such, we concluded that *AtCOBL4* function is specialized and restricted the organization of newly synthesized cellulose, be it into elementary MF or MF bundles, rather than arranging the orientation of cellulose within the cell wall.

The mechanism by which *AtCOBL4* influences the packaging of newly synthesized cellulose into a highly crystalline structure is unclear. It has been observed that an increase in the length of the individual glucan chains making up cellulose MFs in wood with a higher cellulose

crystallinity (Fujita *et al.*, 2011b, Foston *et al.* 2011). To test this hypothesis, we calculated the degree of polymerization of the cellulose chains for wild-type poplar and *AtCOBL4* expressing lines with increased cellulose crystallinity. The measurement of DP revealed that there was an increase in cellulose crystallinity when cellulose polymer molecular increased. Transgenic lines four, five, six, eight and 10 all had an increased DP relative that of wild type (Figure 3.3). Combining these data, a putative role for AtCOBL4 is to organize newly synthesized cellulose as it is extruded into the apoplastic space by facilitating the efficient crystallization of newly synthesized cellulose in a cellulose DP dependent manner.

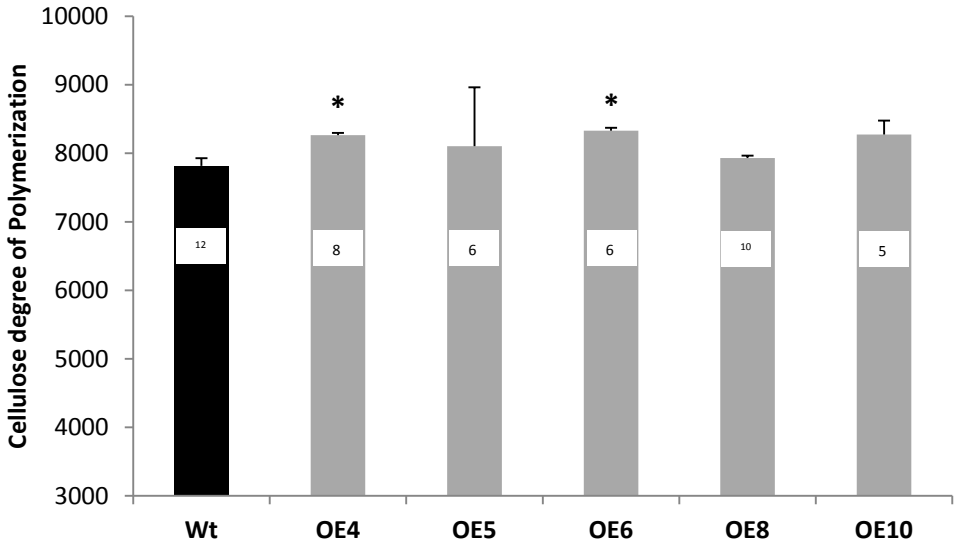

Figure 3.3: Cellulose DP of wild-type and hybrid poplar over expression AtCOBL4. Wild-type (black column) and OE lines (grey columns) n=4 plants per line, star indicates statistically significant difference from Wt (P= 0.05), number inset into columns is the average polydispersity of the cellulose (as a percentage).

3.3.5 Impact of cellulose ultrastructure on tip growing fibre cells

Secondary cell wall deposition typically commences with the cessation of primary cell wall expansion once the final cell dimensions are achieved (Wardrop and Harada, 1965). Intrusive

tip-growth, characteristic of interfasicular fibre cells in *Arabidopsis* and xylem fibre cells are an exception to the typical progression of cell growth and expansion followed by secondary cell wall deposition. Intrusive growth occurs at both tips of a fibre cell and is concurrent with secondary cell wall deposition that initiates at the centre of the cell and extends outwards towards the cell tips (Gritsch and Murphy, 2005). Gritsch *et al.* (2008) hypothesized that the deposition of the secondary cell wall serves to limit and finally inhibit tip growth, determining the final length of the fibre cell. In *Arabidopsis,* plants lacking functional AtCOBL4 protein have altered interfasicular cell length phenotype. Specifically, *irx6* plants have longer interfasicular fibres than wild-type *Arabidopsis* plants. *irx6* plants also have a reduced cellulose content, that could be argued to be the primary cause of the observed aberrant fibre growth phenotype. The modest increase in cellulose content in the *AtCOBL4* transgenic poplar lines allowed me to test this hypothesis. If secondary cell wall cellulose content is the primary determinant limiting intrusive growth then I predicted little to no change in fibre length in the poplar *AtCOBL4* over expression lines. As such, I measured xylem fibre cell lengths in the *AtCOBL4* over expression lines and wild-type poplar, and found that xylary fibre length was shorter in the over expression lines by up to 8% (Figure 3.4), relative to the control trees. When comparing the fibre length to *AtCOBL4* expression levels in poplar, the reduction in fibre length is negatively correlated with *AtCOBL4* over expression. These results allow us to exclude secondary cell wall cellulose content as the primary determinant of intrusively growing fibre cell length. Rather, pointing to cellulose organization as a key determinant of intrusive growth of fibre cells in poplar.

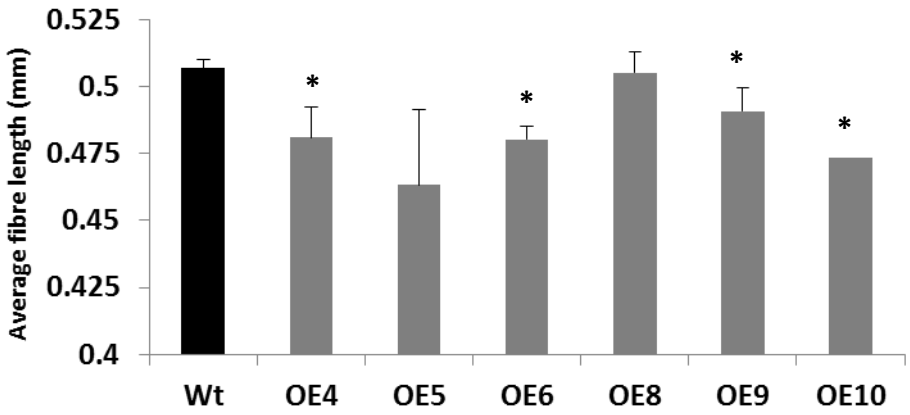

Figure 3.4: Xylem fibre cell length for wild-type and *AtCOBL4* over expression lines. AtCOBL4 OE lines have reduced fibre length. n= 4 plants per line, 5000 fibres per plant. A star indicates statistically significant difference from Wt (P= 0.05)

3.3.6 Wood biomechanical properties

Cellulose provides structural strength to the cell wall, and ultimately the tree. The ultrastructural properties of the cellulose deposited within secondary cell walls underlie the biomechanical properties ascribed to the cell wall. Hence, the biomechanical properties of the woody tissues are dependent on cellulose ultrastructure (Burgert, 2006; Geitmann and Ortega, 2009). To ascertain if altering cellulose DP and crystallinity of the secondary cell wall are sufficient to alter the biomechanical properties of wood, I performed both uni-axial tensile tests and three-point flexural tests on wood specimens from both control and transgenic lines. For the three-point flexural tests, I capitalized on the invariant MFA between wild-type and transgenic poplar lines to ascribe changes in the biomechanical properties of the wood sample to altered DP/cellulose crystallinity. Tensile tests perform on 200 µm thick stem sections, one internode in length, showed that lines four and six have slightly, but not significantly increased

tensile strength when compared to wild-type trees (Figure 3.5a). The remaining lines displayed tensile strengths that did not differ significantly from that of wild-type poplar.

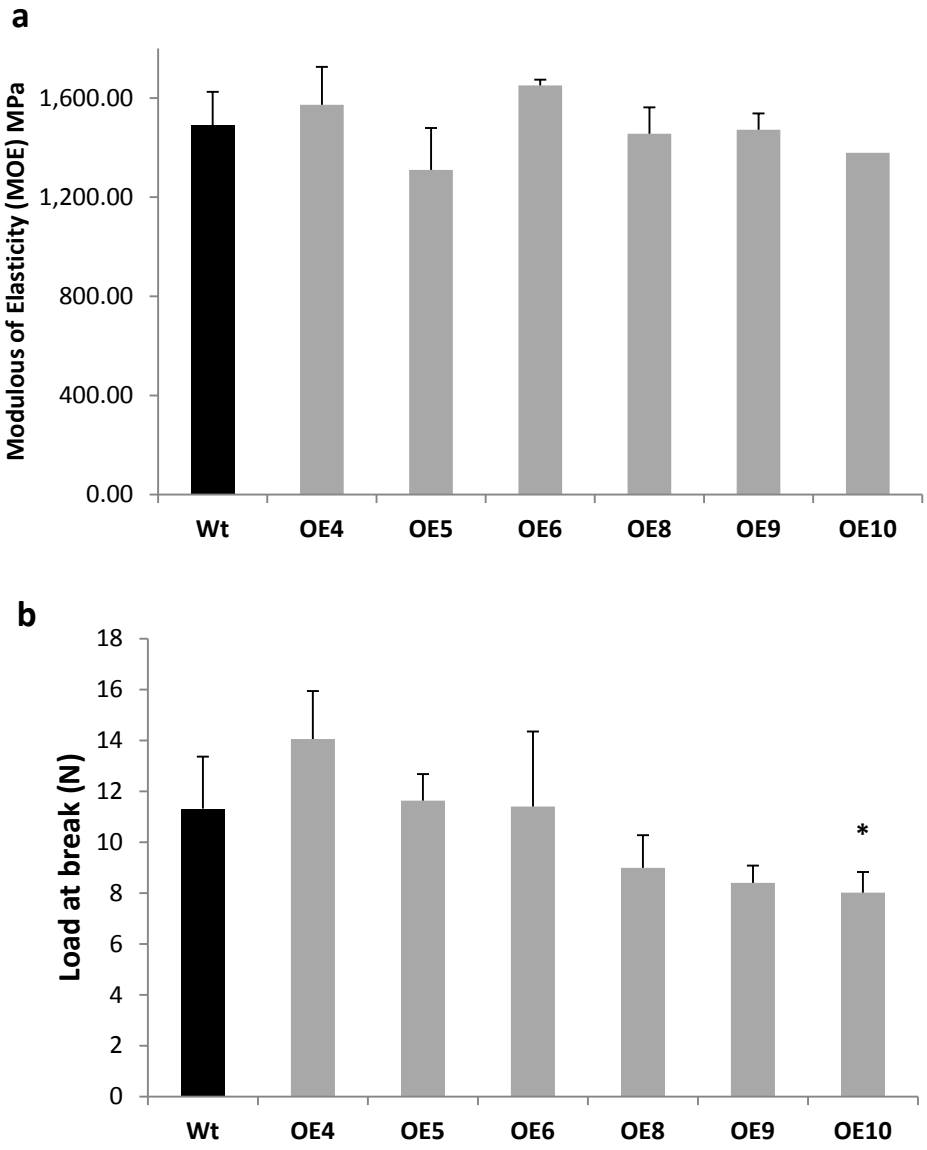

Figure 3.5: Tensile properties of wood produced in *AtCOBL4* over expressing lines. (a) Modulus of elasticity of xylem samples. (b) Maximum load capacity of xylem samples. n= 4 plants per line, with a minimum of 5 breaks per plants. * indicates significantly different from wild-type at P= 0.05

When the maximum load capacity was examined, OE4 had the highest load bearing capacity (Figure 3.5b), but not significantly when a t-test was applied. Interestingly, a t-test (P= 0.05) indicated that OE10 had a significantly lower load capacity when compared to wild type. This was unexpected, as OE10 had an increased cellulose DP and crystallinity when compared to wild-type poplar, and an increase in cellulose crystallinity and DP are thought to increase the strength and load capacity of cellulose in the cell wall. Thus, it is likely that the shorted fibres contributed more to the change in this biomechanical trait than the ultrastructural modifications. In contrast to the tensile tests, the flexural properties of poplar trees over expressing *AtCOBL4,* did not show any significant change (P= 0.05) when compared with the wild-type trees (Figure 3.6a). When the area under the curve for the tensile tests were calculated, the results followed the same trend as the flexural MOE results, and were also not significantly different from wild-type poplar (Figure 3.6b). A trend, although not statistically significant, was that OE4 and OE6 had a MOE greater than wild type in the tensile tests.

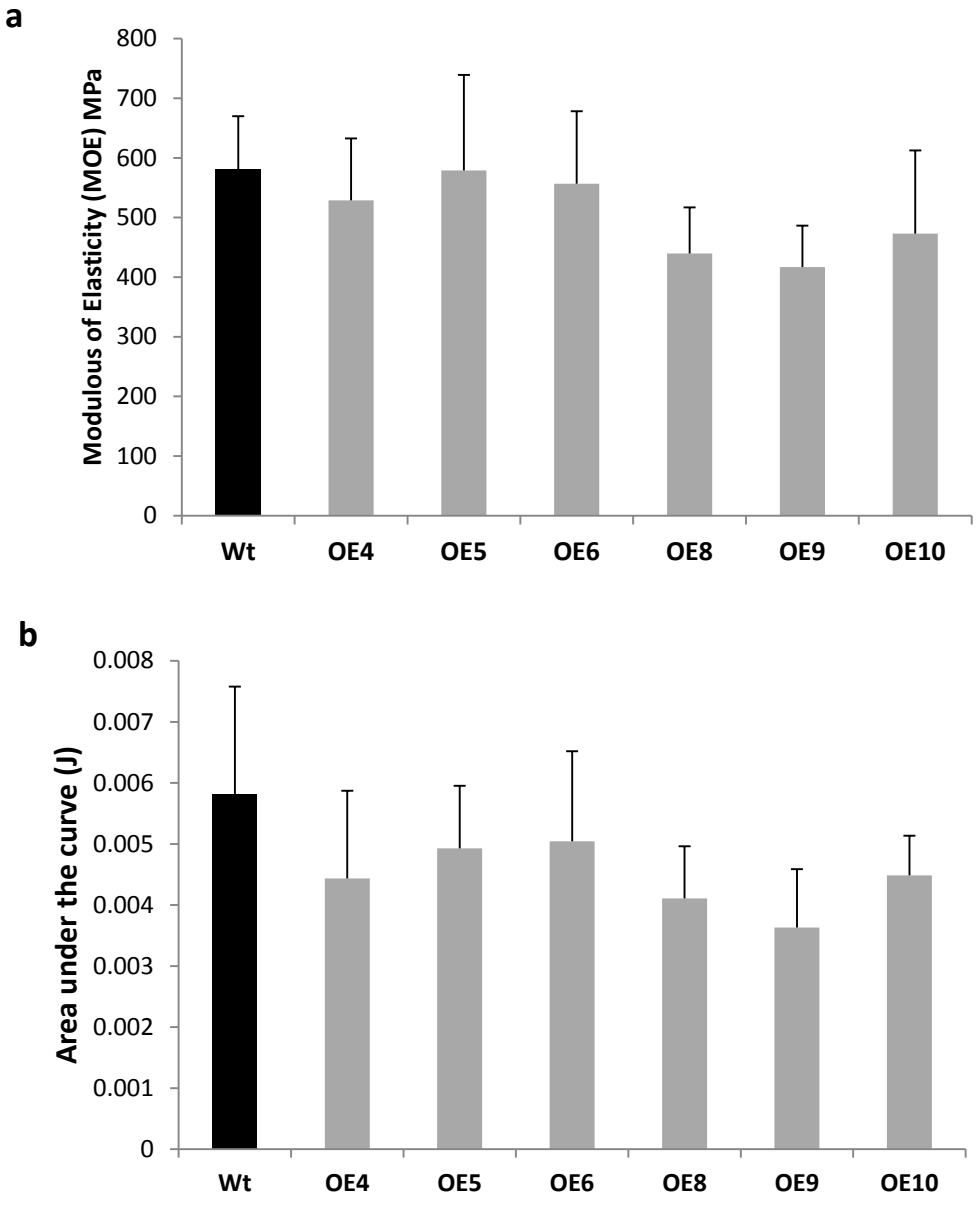

Figure 3.6: Three-point bending of poplar trees over expressing *AtCOBL4*. (a) Modulus of elasticity of xylem. (b) Area under the stress-strain curve. n= 4 plants per line, with a minimum of 5 breaks per plants.

3.4 Discussion

Cellulose is the primary structural component of the plant cell wall, conferring rigidity to the wall, while remaining sufficiently dynamic to accommodate and withstand internal and external biomechanical stress and plant growth. Resolving AtCOBL4's place in the bio-machinery of

cellulose synthesis should help delineate how cellulose biosynthesis is reflected in cellulose structure. Preceding studies of *AtCOBL4* function have concentrated on how loss-of-function alleles of *AtCOBL4* impinge on cellulose biosynthesis. The dramatic reduction in cellulose content is likely to cause several secondary effects that may mask the subtleties of *AtCOBL4* function. A common secondary effect of disrupting primary or secondary cell wall cellulose deposition is the activation of defence related pathways in response to impaired cell wall integrity (Cano-Delgado *et al.* 2003, Ko *et al.* 2006, Hernandez-Blanco *et al.* 2007). To refine our understanding of the mechanism(s) underlying *AtCOBL4* function, we employed the model tree system, poplar, with its rapid and abundant xylogenic tissue. This inherent substantive ratio of secondary cell wall material to primary cell wall could enhance any effects of altered *AtCOBL4* abundance on secondary cell wall and cellulose biosynthesis. To this end, we over-expressed *AtCOBL4* in a secondary cell wall specific manner using the *PtCesA8* promoter, thus, regulating the expression of *AtCOBL4* in a spatially appropriate manner.

3.4.1 AtCOBL4 enhances cellulose biosynthesis

Several independent positive transformed lines were identified; RT-qPCR confirmed the presence of *AtCOBL4* transcripts, and showed non-uniform *AtCOBL4* expression among the transgenic lines. This gradient of *AtCOBL4* expression enabled us to determine if an over-abundance of *AtCOBL4* is sufficient to influence cellulose deposition. Over expression of *AtCOBL4* resulted in small increases in α-cellulose content. Similarly, over expression of sucrose synthase (SuSy), which is involved in supplying precursor to the cellulose synthase complex,

also increased cellulose production (Coleman *et al.* 2008, Coleman *et al.* 2009). These findings demonstrate the plastic nature of cellulose biosynthesis. *AtCOBL4* does not appear to have a catalytic domain and is localized to the external leaflet of the plasma membrane, implying that *AtCOBL4* functions downstream of UDP-glucose incorporation into the growing cellulose chains. This does not exclude the possibility of *AtCOBL4* mediating feedback on cellulose synthesis, which is evident in loss-of function *AtCOBL4* and homologs in rice and maize (Li *et al.* 2003, Brown *et al.* 2005, Ching *et al.* 2006). In chapter 2, I identified the loss-of-function *atcobl4* phenotype, indicating that AtCOBL4 directly affects cellulose ultrastructure, reducing cellulose organization. Here, I expand on this research, determining the effect of *AtCOBL4* over-abundance on cellulose ultrastructure in poplar trees.

3.4.2 *AtCOBL4* sub-functional specialization in determining cellulose ultrastructural properties

The presence of a CBM at the N-terminus of *AtCOBL4* suggested that *AtCOBL4* interacts directly with cellulose (Roudier *et al.* 2002). Sato *et al.* (2011) tested this hypothesis using a series of point mutation in the CBM that replaced the Trp residues with Val residues. These substitutions caused in loss of *BC1* function that lead to a reduction in cellulose content. The GPI-anchor at the C-terminus of AtCOBL4 likely anchors it in the plasma membrane, which inherently places AtCOBL4 in a position to impart stability to cellulose chains by directly interacting with cellulose chains as they are synthesized. This spatial stability creates an opportunity for AtCOBL4 to influence the ultrastructural properties of cellulose deposited in the secondary cell wall. In *Arabidopsis*, an unrelated GPI-anchored protein family, Fasciclin-like Arabinogalactan (FLAs)

have also been shown to play a role in cellulose biosynthesis. *AtFLA11* and *AtFLA12* are required for normal secondary cell wall cellulose deposition and may influence the MFA of deposited cellulose (MacMillan *et al.* 2010). Using X-ray diffraction, I determined the cellulose MFA in AtCOBL4 over expression lines, and found that it was not significantly different from that of wild-type trees. This suggests a sub-functionalization of these GPI-anchored proteins, underpinning the various characteristics of cellulose ultrastructure. Whether these components interact or are dependent on each other is an avenue of ongoing research. Our data indicates that *AtCOBL4* does not play a role in orientating cellulose as it is incorporated into existing cell wall matrix. Rather, *AtCOBL4* functions to organizes cellulose as it is being extruded from the CSCs, ensuring optimal cellulose packaging and assembly in elementary MFs.

The cell wall crystallinity of the transgenic poplar lines was increased in lines over expressing *AtCOBL4* by up to ~4 %. In rice, *BC1* was also shown to modulate the crystallite size of cellulose (Liu *et al.* 2013). The manner in which *AtCOBL4* achieves cellulose crystal organization is still unclear, but is may be dependent to some degree on cellulose polymerization.

3.4.3 AtCOBL4 abundance modulates cellulose degree of polymerization: cellulose DP as a determining factor in cellulose biosynthesis and ultrastructural properties

It is hypothesized that cellulose crystallinity is, in part, dependent on the length of the glucan chains composing cellulose MF deposited in the cell wall (Fujita *et al.* 2011). To resolve how *AtCOBL4* influences cellulose crystallinity, I investigated the correlation between cellulose DP

and cellulose crystallinity, revealing that, apart from line nine, plant lines over expressing *AtCOBL4* tended to produced cellulose with a longer DP relative to control trees, with OE5 being significantly longer. Moreover, an increase in the length of cellulose DP is linked to elevated *AtCOBL4* transcript abundance. It was observed that cellulose with higher crystallinity was generally associated with a longer DP. This finding provides direct evidence for *AtCOBL4* influencing cellulose DP, and implies that cellulose DP underlies and predicts the proportion of cellulose in a crystalline state within the secondary cell wall. Cellulose DP, the most fundamental property of cellulose, is likely to be influenced by CSC velocity (Fujita *et al.* 2011, Fujita *et al.* 2013). It is thought that the active process of cellulose synthesis and expulsion of newly linked glucan units from the CesAs composing a CSC propels the CSC through the plasma membrane (Heath, 1974; Herth and Schnepf, 1980). The rapid, spontaneous self-assembly of the glucan chains into highly crystalline elementary fibres likely concentrates the propulsive forces generated by the polymerization process. Furthermore, these elementary fibres are the most likely binding target of *AtCOBL4*s CBM. Could AtCOBL4 direct these propulsive forces? Analysis of VND7/*irx6 Arabidopsis* lines described in chapter 2 suggests that this may be the case.

Cortical microtubules are thought to be responsible for determining the initial pattern of cellulose deposition within a cell wall, be it a primary or secondary cell wall. After the pattern of cellulose deposition is established in a cell, it is maintained, by as yet unidentified MT independent processes. Once the cell wall pattern is established, MTs continue to function as a

targeted delivery system for components required for cellulose and cell wall maturation, promoting organized cellulose deposition (reviewed by Wasteneys 2004, Szymanski and Cosgrove 2009). In contrast, *AtCOBL4* is perfectly positioned to maintain and promote the organization of newly synthesized cellulose as it is extruded from CSCs. Anchoring of *AtCOBL4* in the plasma membrane would permit and promote linear CSC trajectories. The resistance, positional stability of *AtCOBL4* anchored in the plasma membrane in combination with CBM directed binding to newly synthesized cellulose would also provide a means to focus and direct the propulsive energy of cellulose polymerization.

3.4.4 Coincident cell intrusive growth and secondary cell wall deposition in fibres cells influence maximum attainable cell length

In chapter 2, I showed that *irx6* plants have elongated interfasicular fibre cells, and it is well known that these cells play a supportive role, permitting plants to maintaining an erect upright orientation. Concurrently, I have shown that by over expressing *AtCOBL4* in a secondary cell wall specific manner in hybrid poplar produces an opposite phenotype, *i.e.* shorter fibres. The xylary fibre length of transgenic lines with differing *AtCOBL4* abundance showed a significant reduction in xylary fibre length. Lines with higher *AtCOBL4* transcripts abundance generally had shorter fibres than those with low levels of *AtCOBL4* transcript. The small increase in cellulose is unlikely to account for this change in cell morphology. More likely is that the significant increase in ultrastructural organization: increased cellulose DP and indirectly crystallinity are likely responsible for limiting the xylem fibre cell elongation. The increased structural strength

conferred by higher cell wall crystallinity and cellulose with longer DP provides greater resistance against intrusive cell growth. It has been shown that the orientation of the cellulose MFs provides additional mechanical force capable of resisting turgor pressure and reducing cell wall plasticity (Gietman and Ortega 2009, Kierzkowski *et al.* 2012).

Anderson *et al.* (2010) showed, using a combination of cellulose specific dyes and live cell imaging of cell expansion in *Arabidopsis* roots, that cellulose MFs reoriented from a transverse to longitudinal orientation during anisotropic epidermal cell growth. In primary cell walls, α-expansins act to loosen the cell wall by acting on the polymers cross-linking load-bearing cellulose MFs, facilitating cell wall creep (Marga *et al.*, 2005). Interestingly, over expression of α-expansin, *PttEXPA1,* in hybrid poplar resulted in increased fibre diameter, but not fibre length. This suggests that if expansins are required for intrusive tip growth in poplar, this requires expansins other than *PttEXPA1* (Gray-Mitsuda *et al.*, 2008). Moreover, this places the concomitant deposition of a secondary cell wall during tip growth in fibres in a position to influence the maximum potential longitudinal growth of fibre cells. Building on this, altering secondary cell wall cellulose organization and ultrastructure would likely have a direct impact on fibre cell tip growth. A review of the mechanics of cell expansion by Hamant and Traas (2010) raises the question of the role of cell wall components, specifically cellulose in cell growth. This is especially critical in orientated cell wall growth. This work, in part, answers the question raised by Hamant and Traas, and lays the foundation for further fine-tuning of our understanding of orientated cell growth. I was able to show how cellulose ultrastructure,

specifically, cellulose crystallinity and DP, serve to limit cell expansion during intrusive tip growth. This is likely due to the cellulose of a longer DP and higher crystallinity, which confers increased strength to the cell wall, and such, is capable of resisting tip growth-derived cell expansion.

3.4.5 Wood biomechanics

Plant secondary cell walls, deposited to the inside of the primary cell wall, provide physical support, maintaining cell shape and structural integrity to woody tissues. Central to the strength of the secondary cell wall is the deposition of highly organized cellulose. Cellulose ultrastructure dictates many cell wall properties, including stiffness and strength (Burgert 2006). Microfibril angle determines the flexural stiffness of a cell wall, with a smaller MFA resulting in a stiffer cell wall. Cellulose crystallinity also influences the biomechanical properties of the cell wall, with higher cellulose crystallinity increasing the strength of the cellulose biopolymer (Gassan and Bladzki, 1998). AtCOBL4-directed modification of the cellulose ultrastructure in the secondary cell wall, without large changes in cellulose content, provides a tool to investigate the impact of cellulose ultrastructure on the biomechanical properties of the wood. Tensile test experiments did not reveal significant changes to the biomechanical properties of the over expression lines. It was predicted that the increase in cellulose crystallinity and DP in poplar trees over expressing *AtCOBL4* might increase the stiffness of the wood produced in the absence of altered MFA. In rice, plants with cellulose deficiencies have weakened culms, and the reduction in crystalline cellulose in *bc1* plants results in a 50%

reduction in culm load bearing capacity in three point bending tests (Li *et al.* 2003). In my experiments, the altered fibre cell morphology (shorter xylem fibres), associated with *AtCOBL4* over expression may have obscured the effect of the increased cellulose DP and crystallinity by reducing the surface area that was available to adjacent fibres to bind to each other. The small increases in MOE detected for OE4 and OE6 are likely due to these lines having among the largest increases in cellulose crystallinity and DP. A possible means of separating the effects of cellulose ultrastructure and cell morphology on biomechanics properties of wood, would be to separate and isolate intact fibre cells. This would enable the characterization of the biomechanical implications of altered cellulose ultrastructure on fibre cells. The lack of significant differences in MOE in between over expression line and wild-type poplar in the three point bending experiments may be the result of the similar MFA measured in Wt and *AtCOBL4* over expression lines, as MFA is a major determined of flexural stiffness (Gassan and Bladzki, 1998).

Chapter 4: Summary and future directions

4.1 Major findings of this work

The primary objective of this research was to resolve how *COBRA-Like4* contributes to secondary cell wall cellulose deposition. In chapter 1, I reviewed the status of current research pertaining to cellulose biosynthesis and the role of the COBRA gene family on cellulose biosynthesis and deposition. Through this review, I developed the hypothesis that *AtCOBL4* binds to newly synthesized cellulose in the apoplastic space to produce highly ordered cellulose, and therefore ultimately increasing cellulose biosynthesis efficiency. To test this hypothesis, several key questions were raised and addressed in chapters 2 and 3. First, I examined the impact of loss-of-function *atcobl4* alleles on cellulose ultrastructure and the implications of these perturbations on cell growth and morphology. During the course of my research, Liu *et al.* (2013), showed that *BC1*, the rice ortholog of *AtCOBL4,* influenced the crystalline state of newly deposited cellulose. These findings in rice concur with my results in the model plant *Arabidopsis*. Next, I investigated the conservation of *AtCOBL4* function between herbaceous plants and a woody angiosperm species using *Arabidopsis thaliana* and *Populus trichocarpa,* respectively. Third, I tested whether the over expression of *AtCOBL4* in hybrid poplar could alter cellulose deposition in a favourable manner. Finally, I determined the localization of *PtCOB4a* in cells undergoing active secondary cell wall deposition to spatially and temporally link *AtCOBL4* to cellulose biosynthesis and deposition. By answering these questions, I have expanded our understanding of *AtCOBL4* function and its role in cell wall synthesis.

4.1.1 Characterization of *AtCOBL4* in *Arabidopsis*

Initially, *atcobl4* was identified as a cellulose deficient mutant in *Arabidopsis* and rice, where cellulose depletion was restricted to cells synthesizing secondary cell walls (Li *et al.* 2003, Brown *et al.* 2005). Subsequently, only marginal progress was made in our understanding of the molecular mechanism of *AtCOBL4* or how its function related to the specialized and complex bio-machinery responsible for secondary cell wall biosynthesis. Sato *et al.* (2010) confirmed the presence of a cellulose binding module and its requirement for *BC1* function in rice. Recently, Liu *et al.* (2013) showed that BC1 influences the crystallite size of cellulose synthesized. In chapter 2, I characterized two novel *atcobl4* mutant alleles; *irx6-2* and *irx6-3*. The first step was to characterize the cell wall polysaccharide composition. My studies demonstrated a substantial decrease in cell wall-derived glucose. By isolating the α-cellulose from *irx6-2* and *irx6-3* inflorescence stems, I was able to attribute the altered glucose content to a reduction in cellulose content (Figure 4.1). Cross-sections of inflorescence stems stained with toluidine blue indicated that the reduced cellulose affected the secondary cell walls, manifesting in thin secondary cell walls. Moreover, this resulted in xylem vessels characteristic of the irregular xylem phenotype described by Somerville *et al.* (2003).

With the *irx6* phenotype confirmed, I proceeded to characterize the cellulose deposited within *irx6-2* and *irx6-3* plants by first determining the microfibril angle (MFA). Another family of GPI-anchored proteins, *AtFLA11* and *AtFLA12,* are hypothesized to play a role in contributing to the MFA of cellulose being deposited during secondary cell wall formation (Brown *et al.* 2005,

MacMillan *et al.* 2010). *atfla11*/*atfla12* double mutants are characterized by reduced cellulose content and an increase in MFA (Figure 4.1). Here, I observed that the MFA was reduced in *irx6* plants when compared to wild-type *Arabidopsis* grown under identical conditions; this is the first report of cellulose MFA being associated with an *irx6* phenotype.

I proceeded to measure the cell wall crystallinity, which was drastically reduced in the *irx6* plants (Figure 4.1), agreeing with Liu *et al.* (2013) who reported reduced cellulose crystallinity in *bc1* rice plants. These findings suggest a role for *AtCOBL4* as a facilitator in organizing newly synthesized cellulose. It has been hypothesized that cellulose crystallinity is, in part, determined by the length of the cellulose chains that make up the elementary microfibrils (Fujita *et al.* 2011). To test this, the degree of cellulose polymerization was assessed, and indeed shown to be significantly shorter in the *irx6* plants. This is the first report of altered cellulose DP for any cellulose deficient plants not resulting from defective Cellulose Synthases and implies, as suggested by Fujita *et al.* (2011), that DP can act as a determinant of cellulose crystallinity. *AtCOBL4* likely interacts with newly synthesized cellulose chains via the cellulose binding modules to assemble the cellulose chains into closely packed aggregates to permit hydrogen bonding of associated chains to form ordered crystalline matrices. *AtCOBL4* achieves this, in part, by ensuring that the cellulose being extruded from the CSC is of sufficient DP.

The severity of the deficiency of the irregular xylem phenotype, which is particularly evident in the metaxylem elements, raised the next question that I addressed: do other cell types

producing secondary cell walls in *irx6* plants have altered cell morphology? To answer this, I used interfasicular fibres as a model. These cells are characterized by intrusive tip growth that occurs concomitantly with the initiation of secondary cell wall deposition (Lev-Yudan 2001, Gritsch *et al.* 2008)..

	irx6-2	*irx6-3*	d5c3_l3	d5c3_l4	d5c5_l2	d5c5_l5	d6c3_l4	d6c3_l5	d6c5_l1	d6c5_l2
Glucose	0.83	0.40	0.86	0.86	0.86	1.00	0.80	0.81	0.88	0.87
α-Cellulose	0.57	0.54	1.11	0.94	1.00	1.14	0.95	0.82	0.71	0.73
Crystallinty	0.51	0.46	1.00	0.74	0.91	0.98	0.86	0.99	0.93	0.79
AI Lignin	0.93	0.98	0.89	0.89	0.98	0.90	0.78	0.88	0.95	0.95
AS Lignin	1.41	1.90	1.03	1.08	0.90	0.67	1.35	0.91	0.88	0.88
Hemicellulose	0.79	0.70	1.08	1.02	1.05	1.00	1.25	1.09	0.93	0.96
Arabinose	1.14	1.41	1.15	0.88	1.18	1.05	1.26	1.15	1.13	1.18
Rhamnose	0.95	1.15	1.27	0.93	1.24	1.01	1.13	1.04	0.98	1.05
Galactose	1.11	1.21	1.11	0.99	1.06	0.91	1.23	1.02	1.06	1.12
Xylose	0.77	0.85	1.02	0.98	1.04	1.19	0.85	1.04	1.05	1.06
Mannose	0.75	0.93	1.01	0.89	1.05	1.13	0.76	0.97	0.99	1.01
Fibre length	1.43	1.25	1.08	0.99	1.04	1.02	1.08	1.00	1.09	1.04
MFA	0.60	0.53	0.93	1.09	1.09	0.99	1.01	0.90	1.05	0.98

Figure 4.1: Summary of the chemical and ultrastructural properties of wild-type *Arabidopsis*, *irx6-2*, *irx6-3,* and *irx6-2* or *irx6-3* complemented *Arabidopsis* lines grown under 24 hours light conditions. Values represent the fraction percentage compared to wild-type plants (e.g.: 0.66 glucose corresponds to 66% of the wild-type level), such that values above and below 1.0 represent an increase and decrease compared to wild type, respectively. Red colours indicate a large decrease, green colours a large increase. Orange and yellow colours represent a range of moderate decreases, no change, to moderate increases. MFA – microfibril angle, AS – acid soluble lignin, AI – acid insoluble lignin. d5c3 label corresponds to *irx6-2*/*AtCOBL4*::*PtCOB4a*, d5c5 label corresponds to *irx6-2*/*AtCOBL4*::*PtCOB4b*, d6c3 label corresponds to *irx6-3*/*AtCOBL4*::*PtCOB4a*, d6c5 label corresponds to *irx6-3*/*AtCOBL4*::*PtCOB4b*

I measured the length of fibre cells in wild-type *Arabidopsis* and three different *irx6* alleles; *irx6-1*, *irx6-2* and *irx6-3*, respectively. The fibre cells in the *irx6* mutant lines are as much as 25% longer than those of wild-type plants (Figure 4.1). This provides important supporting evidence for the hypothesis that the deposition of the secondary cell wall occurs concurrently with

intrusive growth in fibre cells and, importantly, that *AtCOBL4* plays a crucial role in determining the maximal longitudinal tip growth of fibre cells. Together, the morphological and ultrastructural implications of altered cellulose deposition due to defective *AtCOBL4* alleles raised the next questions: how does *AtCOBL4* achieve a highly ordered cellulose deposition and maintain cellulose DP? By making use of the VND7 inducible system developed in the Demura lab (Yamaguchi et al 2011), I overcame the difficulties of live cell imaging of vascular tissues deep within the plant. The VND7 system directs ectopic trans-differentiation of seedling epidermal cells into protoxylem tracheary elements. Employing this system in the *irx6-2* plant background, Dr. Mathias Schuetz and I investigated the organization of the cellulose deposited within the protoxylem secondary cell wall thickenings of wild-type/VND7 and *irx6-2*/VND7 plants. We observed that the secondary cell wall cellulose in wild-type plants was organized into tight bundles, while the cellulose deposited in the *irx6-2* plants was less organized and diffuse, and often bifurcated. This provided additional confirmation that *AtCOBL4* plays a role in the organization of the cellulose deposited at sites of secondary cell wall biosynthesis. To further investigate this organization, I created a PtCOBL4a-YFP fusion protein and introduced it into *irx6-2 Arabidopsis* carrying the inducible VND7. By driving ectopic protoxylem trans-differentiation of seedling epidermal cells, Yoshi Watanabe and I showed that PtCOB4a localizes to the discrete domains where active secondary cell walls are being deposited. Moreover, this conclusion was strengthened when we determined that PtCOB4a-cYFP co-localized with RFP-tubulin labelled cortical microtubule bundles situated directly below sites of secondary cell wall deposition. Collectively, this provides compelling evidence that PtCOB4a has the correct spatial and temporal regulation to act on newly synthesized cellulose.

It had previously been shown that a putative rice ortholog of *AtCOB*, *BCL4*, localized to the primary cell wall as well as the plasma membrane when ectopically expressed in onion epithelial cells (Dai *et al.* 2010). In an attempt to determine if PtCOB4a localized to the plasma membrane and the secondary cell wall, we plasmolyzed VND7-induced differentiating seedlings by application of mannitol. This showed that PtCOB4a-cYFP was contained within the plasma membrane and the secondary cell wall thickenings of epidermal cells trans-differentiating into protoxylary elements, consistent with the findings of Dai *et al.* (2010). Liu *et al.* (2013) demonstrated that *BC1* could be cleaved from its GPI-anchor by Phospholipase C, providing a possible mechanism for the release of *BC1* from the plasma membrane. The observation that a portion of PtCOB4a-cYFP population remains bound to cellulose suggested that the PtCOB4a is irreversibly bound to cellulose via its CBM.

Primary cell wall CesAs have been shown to be highly mobile, moving in linear trajectories at the surface of the plasma membrane (Paradez *et al.* 2007). I was interested whether PtCOB4a-cYFP was mobile within the plasma membrane. Using FRAP (fluorescence recovery after photobleaching), I was able to quantify the recovery of cYFP signal within the zone that was photobleached. As predicted by the presence of the cellulose binding module, PtCOB4a-cYFP was immobile, as demonstrated by the lack of cYFP fluorescence recovery of the bleached area. The immobile nature of the plasma membrane-PtCOB4a-cellulose interaction confers the ability of PtCOBL4a to impart stability, organizing cellulose deposition at the secondary cell wall.

Using this data we provide the following hypothesis for the mechanism of *AtCOBL4* function: plasma membrane anchored *AtCOBL4* binds to newly synthesized cellulose as it is being extruded into the apoplastic space. This aids in stabilizing the linear trajectories of the CSCs through the plasma membrane ensuring proper cellulose polymerization and therefore maximizing cellulose crystallization.

4.1.2 Characterizing *AtCOBL4* through over expression in hybrid polar

In chapter 3, I refine our understanding of *AtCOBL4* function using the established knowledge of *AtCOBL4* functional conservation between a herbaceous (*Arabidopsis*) and woody plant (P. *trichocarpa*). The sheer volume of secondary cell wall material produced by trees makes them a better system to tease out the finer details or components of secondary cell wall biosynthesis. Capitalizing on this, I over-expressed *AtCOBL4* in hybrid poplar in a secondary cell wall specific manner using the poplar *CesA8* promoter. This avoided potential silencing effects that arise when using native genes and minimized the risk of incorrect spatial and temporal expression of *AtCOBL4*.

I compared the cell wall composition of several over expression lines with wild-type poplar, and found no significant increase in cell wall glucose. By isolating α-cellulose from these lines I was, however, able to detect increased cellulose content in two over expression lines. The significant changes to cellulose ultrastructure of *Arabidopsis irx6* mutants prompted me to investigate the ultrastructural properties of the cellulose in the over expression lines of hybrid poplar. I first

determined the microfibril angle of the cellulose in the cell walls and found no significant change. Next, I calculated cell wall crystallinity and cellulose DP. I was able to detect small, but significant changes in both cell wall crystallinity and cellulose DP, both increasing in the over expression lines. The observed increases were positively correlated with the levels of *AtCOBL4* transcript abundance. These findings further strengthen the idea that cellulose DP is a crucial determinant of cellulose crystallinity.

Next, I investigated whether over expression of *AtCOBL4* had an impact on the intrusive growth of xylary fibres in rapidly growing hybrid poplar. Using a fibre quality analyzer, I measured the xylem fibres of wild-type and transgenic lines overexpressing *AtCOBL4,* and found that there was indeed a significant reduction in fibre length in the overexpression lines. This reduction was generally correlated with levels of *AtCOBL4* transcript abundance. These findings again reinforce the hypothesis that *AtCOBL4* organizes newly synthesized cellulose in fibre cells. Primary cell wall Cellulose Synthases are estimated to spend approximately 7-30 min at the plasma membrane synthesizing cellulose (Paradez *et al.* 2006, Sampathkumar *et al.* 2013) before being recycled back into the cytosol by SmaCCs and MASCs (Crowell *et al.* 2009, Gutierrez *et al.* 2009). This implies that under normal growth conditions CesAs should consistently synthesize cellulose chains of similar DP. Assuming that secondary cell wall CesAs also have a conserved life span at the plasma membrane, the increased cellulose DP observed in the over expression lines implies that *AtCOBL4* plays a role in modulating the efficiency of cellulose biosynthesis in a secondary cell wall-specific manner. This modulation of cellulose

biosynthesis has direct and indirect implications on the cellulose ultrastructure, cellulose content and cell wall strength, which ultimately affect cell growth and development.

The use of two model plant systems has allowed me to refine our understanding of the potential mechanism underlying *AtCOBL4* function. The idea that AtCOBL4 could directly influence cellulose biosynthesis, at the point of glucan chain polymerization, influencing rates of polymerization, has implications on several facets of plant growth and development.

I put forward two possible mechanisms by which AtCOBL4 acts. Model A predicts that AtCOBL4 binds directly to newly synthesized cellulose as it is being extruded into the apoplastic space. In so doing, it directs the propelling force of cellulose polymerization to maintain linear CSC trajectories (Figure 4.2). Model B predicts that AtCOBL4 binds to previously deposited cellulose in the cell wall. In this way, it organizes the plasma membrane in such a manner that it promotes linear CSC trajectories, channelling the propelling energy of cellulose polymerization (Figure 4.2).

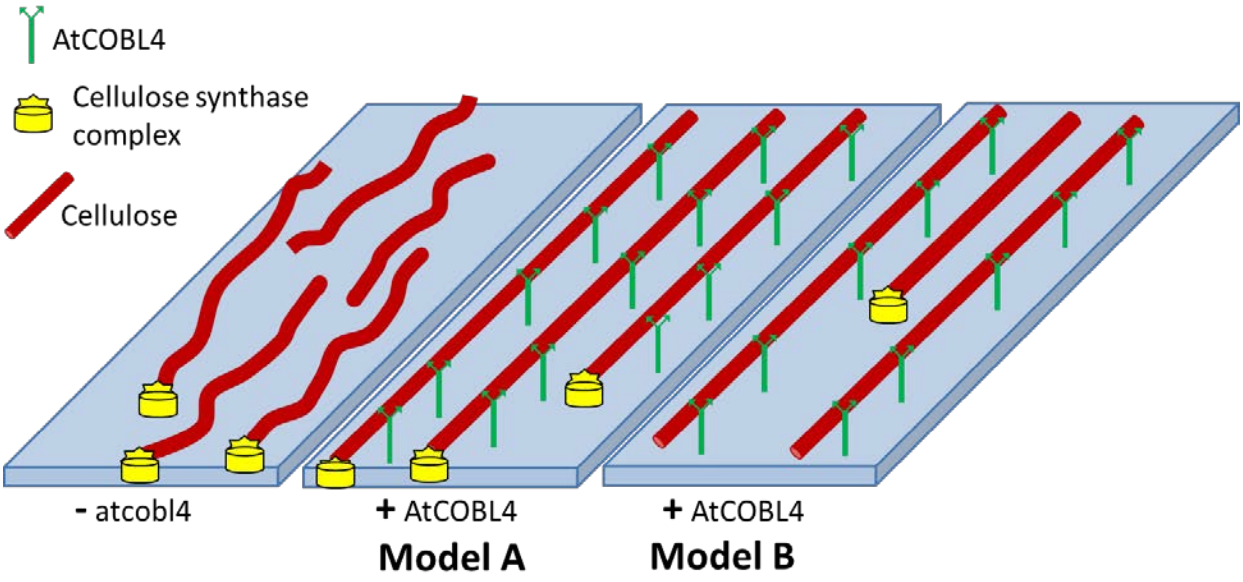

Figure 4.2: A diagrammatic representation of the hypothesized models for AtCOBL4 function. In the absence of functional AtCOBL4, disorganized cellulose of a shorter DP is deposited within the secondary cell wall. Model A predicts that AtCOBL4 binds to newly synthesized cellulose as it is being extruded into the apoplastic space, providing the stability to maintain linear CSC trajectories. In Model B AtCOBL4 binds to previously deposited cellulose, organizing the plasma membrane, providing channels along which subsequent CSCs travel in a linear, organized fashion.

4.2 Outstanding questions and future directions

4.2.1 Investigating the sub-functional specialization within the *COBRA* gene family

The *Arabidopsis* COBRA gene family consists of 12 members that can be divided into two sub-groups using the number of cellulose binding modules (CBMs) as the defining criteria; sub-group one has a single CBM, while sub-group two has two CBMs (Roudier et al 2002). Moreover, there is specialization between and within the COBRA family sub-groups. Sub-group one appears to function in primary and secondary cellulose deposition of all plant cells (Benfey et al 1993, Brown *et al.* 2005), while sub-group two members are required for tip growth and each has a specialized function in specific cell types, such as root hair and/or pollen tubes

(Hochholdinger *et al.*, 2008; Li *et al.*, 2013). Within sub-group one, *AtCOB* functions in primary cell wall cellulose deposition, while *AtCOBL4* functions in secondary cell wall cellulose deposition. The structural similarities between these two proteins raises the question as to whether their cell wall specialization is purely due to spatial regulation, or due to subtle changes in amino acid composition that may confer different functions. One possible approach to answering this question is to alter the spatial regulation of *AtCOB* and *AtCOBL4*. This could be achieved by placing *AtCOB* expression under the control of the *AtCOBL4* promoter and introducing the construct into an *irx6 Arabidopsis* line, and the reciprocal process where the *AtCOBL4* gene is driven by the primary *AtCOB* promoter and introduced into an *atcob Arabidopsis* line. If *AtCOB* and *AtCOBL4* possess functional overlap, a thorough analysis of the cellulose produced in these complementary plant lines would reveal if, for example, *AtCOBL4* conferred secondary cell wall cellulose characteristics (longer DP) to cellulose produced by primary cell wall CesAs and vice versa. From an evolutionary perspective, it would be interesting to determine if the divergence of AtCOB and AtCOBL4 function coincides with the appearance of secondary cell walls, and if this divergence of function appears at the same time as secondary cell wall specific CesAs.

4.2.2 Investigating the effect of various cellulose deficient and defective cell wall mutants on cellulose DP

The evidence presented in this thesis points to cellulose DP being an important underlying determinant of not only cellulose organization, but anisotropic cell expansion. Research in the

Mansfield lab undertaken by L. McDonnell (unpublished) investigated the ultrastructural properties of cellulose associated with defective alleles of each of the secondary cell wall cellulose synthases, and showed that under short day growth conditions *atcesa4, atcesa7 and atcesa8* mutant plants produced cellulose with a DP 50% shorter than that of wild-type *Arabidopsis*. Long day growth conditions are associated with increased plant biomass (Mitchell and Lucanus, 1962) and, under such conditions, *atcesa4* and *atcesa7* mutant lines showed a reduction in cellulose DP of approximately 60% and 30% of that of wild-type *Arabidopsis*, respectively. Interestingly, *atcesa8* mutant plants had a longer DP than wild-type plants. These findings imply that cellulose DP is highly plastic and responds to both genetic and environmental factors. In order to gain a complete understanding of cellulose organization and how cellulose biosynthesis influences final cellulose organization within the plant cell wall, it will be necessary to characterize several cellulose and cell wall mutants for cellulose DP. Given that cellulose DP and crystallinity underpin many key characteristics of secondary cell walls, including matrix polysaccharide and lignin integration into the cell wall, research linking these two processes is warranted. To determine if cellulose DP and crystallinity can influence the tethering of matrix polysaccharides to cellulose, two approaches could be used. Firstly, one could quantify the proportion of hemicellulose released when cell wall material is treated with endoglucanases relative to the amount of xylose released by strong alkali treatment after endoglucanase treatment (Guillén *et al.*, 1995; Pauly *et al.*, 1999; Verbelen *et al.*, 2010). This would show the proportions of un-tethered, endoglucanase accessible hemicellulose, and tethered hemicellulose that is only recovered by strong alkali treatment. Second, an indirect measure of hemicellulose tethering might be to quantify the amount of cell wall creep across

Arabidopsis lines of varying DP and crystallinity when treated with β-expansin (McQueen-Mason and Cosgrove, 1995; Tabuchi *et al.*, 2011).

4.2.3 AtCOBL4 as an organizer of the plasma membrane at sites of secondary cell wall deposition

The close proximity of the cell wall to the plasma membrane has raised the question of how cell wall attributes influence the movement of the protein components of the plasma membrane (Feraru *et al.* 2011). An elegant study by Martiniere *et al.* (2012), demonstrated that the cell wall restricts the movement of proteins that are either exposed to the apoplastic space or localized to the outer leaflet of the plasma membrane. Furthermore, Feraru *et al.* (2011) observed that cell wall interactions with the transmembrane protein PIN2, an auxin transporter, restricted the mobility and localization of PIN2 in the plasma membrane. The nature of cell wall-PIN2 interaction was further refined, and was found to be cellulose dependent (Feraru *et al.* 2011). The highly organized pattern of cellulose deposited within the secondary cell wall could provide a stable scaffold with which proteins could interact to help order the plasma membrane lipid bilayer. It is well established that protein-protein interactions, cytoskeleton-plasma membrane, and nano-scale lipid organization (lipid rafts) influence the organization and fluid dynamics of the plasma membrane (Kusumi *et al.*, 2005; Lenne *et al.*, 2006; Lingwood and Simons, 2010). The ability of GPI-anchored COBRA proteins to bind to cellulose while being anchored in the outer leaflet of the plasma membrane places them in a position to participate in ordering the plasma membrane at sites of secondary cell

wall biosynthesis. I hypothesize that the COBRA protein family, by interacting simultaneously with the plasma membrane and cell wall, could provide a means to influence the dynamic movement of proteins anchored in the plasma membrane. To test this hypothesis, AtCOBL4-cYFP could be used as a marker of sites of secondary cell wall deposition in combination with either the VND7 or VND6 systems. Making use of the established and characterized suite of "minimal" fluorescently labelled plasma membrane proteins developed by Martiniere *et al.* (2012), one could determine the mobility of the GFP-labelled minimal membrane proteins in the presence or absence of AtCOBL4 using FRAP. Building on this, one could compare the mobility of the suite of proteins at sites within a cell containing or lacking secondary cell wall deposition. If AtCOBL4 does indeed influence protein mobility, it would be of interest to determine if the simultaneous interaction between cell wall AtCOBL4 and the plasma membrane is required to influence protein mobility in plasma membrane. This could be addressed by using an AtCOBL4 modified to have a non-functional CBM.

4.2.4 Post Golgi trafficking of secondary cell wall associated proteins to sites of active secondary cell wall deposition, a free ride?

It is thought that CSCs can pre-assemble prior to arrival at the plasma membrane, and that upon inserting into the plasma membrane, the CSCs commence cellulose biosynthesis (Guerriero *et al.*, 2010; Carpita, 2011a). This would require that proteins forming part of the cellulose biosynthesis machinery are present at sites of secondary cell wall deposition concurrent with CSC delivery to the plasma membrane. The reported co-transport of primary

cell wall CesAs and CSI in the same Golgi-derived compartments to the plasma membranes (Gu *et al.*, 2010a; Li *et al.*, 2011; Bringmann *et al.*, 2012b) begs the question: are secondary cell wall associated proteins, such as AtCOBL4 and AtFLA12/AtFLA11 co-transported with CesAs? Alternatively, are secondary cell wall associated proteins transported together, independently of CesAs? One could also investigate if cell wall associated proteins localized at the plasma membrane are transported with, or independently of, secreted cell wall proteins. *AtCOBL4* would be an ideal candidate to address these questions, as AtCOBL4 is required at the time of active cellulose polymerization. The use of the *VND7* system developed by Yamaguchi *et al.* (2010) would provide a suitable system to visualize and quantify the trafficking of fluorescently labelled proteins required for secondary cell wall biosynthesis. By using different fluorophores to label select proteins (*i.e.* RFP and cYFP), it would permit the visualization of the transport of different labelled fusion proteins using live cell imaging. Introducing two different fluorescently labelled proteins into the same plant should make it possible to quantify any co-localization of the proteins during trafficking, if it occurs.

4.2.5 Laying to rest the debate of MT vs MF orientation determination: a secondary cell wall answer

For over half a century it has been known that cortical microtubules align with cellulose microfibrils of the cell wall (Ledbetter and Porter 1963). During this period, several contentious issues have been debated, including (1) do MTs determine the initial pattern of MFs deposited in the cell wall, and (2) are MTs required to maintain the pattern of cellulose MF deposition

once the initial pattern has been established? Early studies appeared to indicate that MTs were required for establishing the initial pattern and maintaining the pattern of cellulose deposition. The predominant model, the cellulose-synthase constraint model, predicted that cortical MTs provided tracks that direct subsequent CSC trajectories to maintain the pattern of cellulose deposition (Giddings and Staehelin, 1988). However, more recently, new models for ordered cellulose deposition are gaining popularity. For example, Baskin (2001) suggested a template-incorporation model, that implies that initial pattern of cellulose serves as a template for subsequent MFs deposition and, as such is independent of MTs. Support for the template incorporation model was provided using MT mutant *Arabidopsis* lines and MT disrupting chemicals to evaluate the role of MTs in organizing cellulose deposition after the initial primary wall had been synthesized. It was determined that MFs were correctly ordered and aligned in the absence of MT. In addition, double mutants of *mor1-1* and *rsw1-1* had an additive effect (Baskin, 2001; Sugimoto *et al.*, 2003). This model has since been called into question. The use of 2,6-dichlorobenzonitrile (DCB), a cellulose synthesis inhibitor, to disrupt primary cell wall biosynthesis in microtubule mutant *mor1-1* plants showed that once DCB was removed cellulose deposition occurred in an ordered fashion, even in the presence of a disordered cellulose template (Himmelspach *et al.*, 2003; Wasteneys, 2004).

Advances in live cell imaging facilitate the simultaneous visualization and tracking of fluorescently labelled primary cell wall CSCs in the presence of fluorescently labelled MTs (Paredez *et al.* 2006), confirming the spatial proximity of MTs on the cytosolic face of the

plasma membrane in relation to CSCs. A physical link was found between CSCs and MT in the form of the protein *CSI1* that is capable of interacting with MTs and CesAs simultaneously in primary cell walls (Gu *et al.* 2010, Li *et al.* 2011, Bringmann *et al.* 2012). This provides support for continued MT-directed CSC trajectories after the initial pattern of cellulose deposition is established and challenging the template incorporation model at the plasma membrane.

Interestingly, *CSI1* does not appear to be expressed in plant vasculature, at least in seedlings (Gu *et al.* 2010). This raises the question as to whether there are other mechanisms required to maintain linear CSC trajectories in secondary cell wall producing cells or whether MTs are sufficient. If the second hypothesis is true, it also raises another question: are MTs required for establishing MF patterning and/or maintaining MF patterning? The massive cellular reprogramming and absence of machinery required for secondary cell wall biosynthesis in VND7 inducible plants lines provide a suitable model system to answer these questions. Naive un-induced cells would not have the secondary wall cellulose or MT organizing components to provide a template for the first cellulose elementary fibres. By using chemical agents capable of MT depolymerization or stabilization such as oryzalin or paclitaxel in time trial experiments of plants containing fluorescently labelled MT and CSCs, we could reveal at what points MT are required.

4.3 Final conclusions

In summary, the overall aim of this research was to resolve the function of *AtCOBL4* in secondary cell wall biosynthesis. To this end, I characterized two novel *AtCOBL4* mutant alleles; *irx6-2* and *irx6-3*, provided evidence for COBL4 in organizing cellulose deposited during secondary cell wall deposition. I proceeded to refine the role of COBL4 in secondary cell wall cellulose deposition, utilizing both *Arabidopsis* and poplar model systems to demonstrate that COBL4, through the appropriate spatial distribution determines the crystalline state of deposited cellulose, likely via controlling cellulose DP. In addition, I identified COBL4 as a determinant of elongative growth in fibre cells, which may influence intrusive growth by modulating the ultrastructural properties of secondary cell wall cellulose. This provides the first direct evidence for the role of secondary cell wall deposition in determining anisotropic cell expansion of fibre cells.

References

Anderson C, Carroll A, Akhmetova L (2010a) Real-time imaging of cellulose reorientation during cell wall expansion in *Arabidopsis* roots. Plant p **152**: 787–796

Anderson CT, Carroll A, Akhmetova L, Somerville C (2010b) Real-time imaging of cellulose reorientation during cell wall expansion in *Arabidopsis* roots. Plant Physiol **152**: 787–796

Andersson-Gunneråsa S, Mellerowicz EJ, Love J, Segerman B, Ohmiya Y, Coutinho PM, Nilsson P, Henrissat B, Moritz T, Sundberg B (2006) Biosynthesis of cellulose-enriched tension wood in Populus: global analysis of transcripts and metabolites identifies biochemical and developmental regulators in secondary wall biosynthesis. Plant J **45**: 144–165

Bamber RK (2001) A general theory for the origin of growth stresses in reaction wood: how trees stay upright. **22**: 205–212

Barnett J, Bonham VA (2004) Cellulose microfibril angle in the cell wall of wood fibres. Biol Rev **79**: 461–472

Baskin TI (2001) On the alignment of cellulose microfibrils by cortical microtubules: a review and a model. Protoplasma **215**: 150–171

Benfey PN, Linstead PJ, Roberts K, Schiefelbein JW, Hauser MT, Aeschbacher R a (1993) Root development in *Arabidopsis*: four mutants with dramatically altered root morphogenesis. Development **119**: 57–70

Benziman M, Haigler CH, Brown RM, White AR, Cooper KAYM (1980) Cellulose biogenesis : Polymerization and crystallization are coupled processes in Acetobacter xylinum. Proc Natl Acad Sci **77**: 6678–6682

Bessueille L, Bulone V (2008) A survey of cellulose biosynthesis in higher plants. Plant Biotechnol J **25**: 315–322

Bessueille L, Sindt N, Guichardant M, Djerbi S, Teeri TT, Bulone V (2009) Plasma membrane microdomains from hybrid aspen cells are involved in cell wall polysaccharide biosynthesis. Biochem J **420**: 93–103

Bhat R a, Panstruga R (2005) Lipid rafts in plants. Planta **223**: 5–19

Boerjan W, Ralph J, Baucher M (2003) Lignin biosynthesis. Annu Rev Plant Biol **54**: 519–546

Borner GHH, Lilley KS, Stevens TJ, Dupree P (2003) Identification of glycosylphosphatidylinositol-anchored proteins in *Arabidopsis*. A proteomic and genomic analysis. Plant Physiol **132**: 568-579

Borner GHH, Sherrier DJ, Weimar T, Michaelson LV, Hawkins ND, MacAskill A, Napier JA, Beale MH, Lilley KS, Dupree P (2005) Analysis of detergent-resistant membranes in *Arabidopsis*. Evidence for plasma membrane lipid rafts. Plant Physiol **137**: 104

Brady SM, Long T a, Benfey PN (2006) Unraveling the dynamic transcriptome. Plant Cell **18**: 2101–2111

Brady SM, Song S, Dhugga KS, Rafalski JA, Benfey PN (2007) Combining expression and comparative evolutionary analysis. The COBRA gene family. Plant Physiol **143**: 172–187

Bringmann M, Landrein B, Schudoma C, Hamant O, Hauser M, Persson S (2012a) Cracking the elusive alignment hypothesis : the microtubule – cellulose synthase nexus unraveled. Trends Plant Sci **17**: 666–674

Bringmann M, Li E, Sampathkumar A, Kocabek T, Hauser M, Persson S (2012b) POM-POM2 / CELLULOSE SYNTHASE INTERACTING1 Is Essential for the Functional Association of Cellulose Synthase and Microtubules in *Arabidopsis*. Plant Cell **1**: 1–16

Brown D a, London E (1998) Functions of lipid rafts in biological membranes. Annu Rev Cell Dev Biol **14**: 111–136

Brown D, Wightman R, Zhang Z, Gomez Ivan Atanassov LD, Bukowski J-P, Tryfona T, McQueen-Mason SJ, Dupree P, Turner S (2011) *Arabidopsis* genes IRREGULAR XYLEM (IRX15) and IRX15L encode DUF579 containing proteins that are essential for normal xylan deposition in the secondary cell wall. Plant J **66**: 401–413

Brown DM, Zeef LAH, Ellis J, Goodacre R, Turner SR (2005) Identification of novel genes in *Arabidopsis* involved in secondary cell wall formation using expression profiling and reverse genetics. Plant Cell Online **17**: 2281-2292

Burgert I (2006) Exploring the micromechanical design of plant cell walls. Am J Bot **93**: 1391–1401

Burgert I, Keckes J, Frühmann K, Fratzl P, Tschegg SE (2002) A Comparison of Two Techniques for Wood Fibre Isolation ± Evaluation by Tensile Tests on Single Fibres with Different. For Prod J **4**: 9–12

Caffall KH, Mohnen D (2009) The structure, function, and biosynthesis of plant cell wall pectic polysaccharides. Carbohydr Res **344**: 1879–1900

Carpita NC (2011a) Update on mechanisms of plant cell wall biosynthesis: how plants make cellulose and other (1->4)-β-D-glycans. Plant Physiol **155**: 171–184

Carpita NC (2011b) Update on Mechanisms of Plant Cell Wall Biosynthesis How Plants Make Cellulose and Other (1→4)-β-D-Glycans1.pdf. Plant Physiol **155**: 171–184

Chaffey N, Barlow P, Sundberg B (2002) Understanding the role of the cytoskeleton in wood formation in angiosperm trees: hybrid aspen (Populus tremula x P. tremuloides) as the model species. Tree Physiol **22**: 239–249

Chen F, Dixon RA (2007) Lignin modification improves fermentable sugar yields for biofuel production. Nat Biotechnol **25**: 759–761

Ching A, Dhugga KS, Appenzeller L, Meeley R, Bourett TM, Howard RJ, Rafalski A (2006) Brittle stalk 2 encodes a putative glycosylphosphatidylinositol-anchored protein that affects mechanical strength of maize tissues by altering the composition and structure of secondary cell walls. Planta **224**: 1174–1184

Clough SJ, Bent AF (1999) Floral dip : a simplified method for Agrobacterium-mediated transformation of *Arabidopsis* thaliana. Science (80-) **16**: 735–743

Coleman HD, Park J-Y, Nair R, Chapple C, Mansfield SD (2008) RNAi-mediated suppression of p-coumaroyl-CoA 3'-hydroxylase in hybrid poplar impacts lignin deposition and soluble secondary metabolism. Proc Natl Acad Sci U S A **105**: 4501–4506

Cosgrove DJ (2000) Expansive growth of plant cell walls. Plant Physiol Biochem **38**: 109–124

Cosgrove DJ (2005) Growth of the plant cell wall. Nat Rev Mol Cell Biol **6**: 850–861

Crowell EF, Bischoff V, Desprez T, Rolland A, Stierhof Y-D, Schumacher K, Gonneau M, Höfte H, Vernhettes S (2009) Pausing of Golgi bodies on microtubules regulates secretion of cellulose synthase complexes in *Arabidopsis*. Plant Cell **21**: 1141–1154

Dai X, You C, Wang L, Chen G, Zhang Q, Wu C (2009) Molecular characterization, expression pattern, and function analysis of the OsBC1L family in rice. Plant Mol Biol **71**: 469–481

Debolt S, Gutierrez R, Ehrhardt DW, Somerville C (2007) Nonmotile Cellulose Synthase Subunits Repeatedly Accumulate within Localized Regions at the Plasma Membrane in *Arabidopsis* Hypocotyl Cells following. Structure **145**: 334–338

Delmer DP, Amor Y (1995) Cellulose biosynthesis. Plant Cell **7**: 987–1000

Derba-Maceluch M, Awano T, Takahashi J, Lucenius J, Ratke C, Kontro I, Busse-Wicher M, Kosik O, Tanaka R, Winzéll A, Kallas A, Leśniewska J, Berthold F, Immerzeel P, Teeri TT, Ezcurra I, Dupree P, Serimaa R and Mellerowicz EJ (2014) Suppression of xylan endotransglycosylase *PtxtXyn10A* affects cellulose microfibril angle in secondary wall in aspen wood. New Phyt doi: 10.1111/nph.13099

Desprez T, Juraniec M, Crowell EF, Jouy H, Pochylova Z, Parcy F, Höfte H, Gonneau M, Vernhettes S (2007) Organization of cellulose synthase complexes involved in primary cell wall synthesis in *Arabidopsis* thaliana. Proc Natl Acad Sci U S A **104**: 15572–15577

Ding S (2007) Nanoscale Characterization of Plant Cell Wall Microfibril Structure. Biotechnol. Bioeng.

Ding S-Y, Himmel ME (2006) The maize primary cell wall microfibril: a new model derived from direct visualization. J Agric Food Chem **54**: 597–606

Diotallevi F, Mulder B (2007) The Cellulose Synthase Complex : A Polymerization Driven Supramolecular Motor. Biophys J **92**: 2666–2673

Edidin M (2003) The state of lipid rafts: from model membranes to cells. Annu Rev Biophys Biomol Struct **32**: 257–283

Eisenhaber B, Bork P, Eisenhaber F (1999) Prediction of potential GPI-modification sites in proprotein sequences. J Mol Biol **292**: 741–758

Eisenhaber B, Bork P, Eisenhaber F (2001) Post-translational GPI lipid anchor modification of proteins in kingdoms of life: analysis of protein sequence data from complete genomes. Protein Eng **14**: 17–25

Eisenhaber B, Wildpaner M, Schultz CJ, Borner GHH, Dupree P, Eisenhaber F (2003) Glycosylphosphatidylinositol lipid anchoring of plant proteins. Sensitive prediction from sequence-and genome-wide studies for *Arabidopsis* and rice. Plant Physiol **133**: 1691-1702

Fagard M, Desnos T, Desprez T, Goubet F, Refregier G, Mouille G, McCann M, Rayon C, Vernhettes S, Höfte H (2000) PROCUSTE1 encodes a cellulose synthase required for normal cell elongation specifically in roots and dark-grown hypocotyls of *Arabidopsis*. Plant Cell **12**: 2409–2424

Feraru E, Feraru ML, Kleine-Vehn J, Martiniere A, Mouille G, Vanneste S, Vernhettes S, Runions, Frimi J (2011) PIN Polarity Maintenance by the Cell Wall in *Arabidopsis.* Curr Biol **21**: 338-343

Ferguson MA, Kinoshita T, Hart GW (2009) Essentials of Glycobiology. Cold Spring Harb Cold Spring Harb Lab Press Chapter 11 Fig 11.6 Chapter 11

Franke R, Humphreys JM, Hemm MR, Denault JW, Ruegger MO, Cusumano JC, Chapple C (2002) The *Arabidopsis* REF8 gene encodes the 3-hydroxylase of phenylpropanoid metabolism. Plant J **30**: 33–45

Fujita M, Himmelspach R, Hocart CH, Williamson RE, Mansfield SD, Wasteneys GO (2011) Cortical microtubules optimize cell-wall crystallinity to drive unidirectional growth in *Arabidopsis*. Plant J **66**: 915–928

Fujita M, Lechner B, Barton D a, Overall RL, Wasteneys GO (2012) The missing link: do cortical microtubules define plasma membrane nanodomains that modulate cellulose biosynthesis? Protoplasma **249**: 59–67

Fujita M, Himmelspach R, Ward J, Whittington A, Hasenbein N, Liu C, Truong TT, Galway ME, Mansfield SD, Hocart CH, Wasteneys GO (2013) The anisotropy1 D604N Mutation in the *Arabidopsis* Cellulose Synthase1 Catalytic Domain Reduces Cell Wall Crystallinity and the Velocity of Cellulose Synthase Complexes. Plant Phys **162**: 74-85

Funada R, Miura H, Shibagaki M, Furusawa O, Miura T, Fukatsu E, Kitin P (2001) Involvement of Localized Cortical Microtubules in the Formation of a Modified Structure of Wood. J Plant Res **114**: 491–497

Gardiner JC, Taylor NG, Turner SR (2003) Control of Cellulose Synthase Complex Localization in Developing Xylem. Society **15**: 1740–1748

Geitmann A, Ortega JKE (2009) Mechanics and modeling of plant cell growth. Trends Plant Sci **14**: 467–478

Giddings TH, Staehelin LA (1988) Planta Spatial relationship between mierotubules and plasma-membrane rosettes during the deposition of primary wall microfibrils in Closterium sp . Planta **173**: 22–30

Gillmor CS, Lukowitz W, Brininstool G, Sedbrook JC, Hamann T, Poindexter P, Somerville C (2005) Glycosylphosphatidylinositol-anchored proteins are required for cell wall synthesis and morphogenesis in *Arabidopsis*. Plant Cell **17**: 1128-1139

Gray-mitsumune M (2004) Expansins Abundant in Secondary Xylem Belong to Subgroup A of the α-Expansin Gene Family. Plant Physiol **135**: 1552–1564

Gritsch CS, Murphy RJ (2005) Ultrastructure of fibre and parenchyma cell walls during early stages of culm development in Dendrocalamus asper. Ann Bot **95**: 619–629

Gu Y, Kaplinsky N, Bringmann M, Cobb A, Carroll A, Sampathkumar A, Baskin TI (2010a) Identi fi cation of a cellulose synthase-associated protein required for cellulose biosynthesis. Proc Natl Acad Sci **107**: 12866–12871

Guerriero G, Fugelstad J, Bulone V (2010) What do we really know about cellulose biosynthesis in higher plants? J Integr Plant Biol **52**: 161–175

Guillén R, York WS, Pauly M, An J, Impallomeni G, Albersheim P, Darvill a G (1995) Metabolism of xyloglucan generates xylose-deficient oligosaccharide subunits of this polysaccharide in etiolated peas. Carbohydr Res **277**: 291–311

Gutierrez R, Lindeboom JJ, Paredez AR, Emons AMC, Ehrhardt DW (2009) *Arabidopsis* cortical microtubules position cellulose synthase delivery to the plasma membrane and interact with cellulose synthase trafficking compartments. Nat Cell Biol **11**: 797–806

Haigler CH, Brown RM, Benziman M (1980) Calcofluor white ST Alters the in vivo assembly of cellulose microfibrils. Science (80-) **210**: 903–906

Harris D, Bulone V, Ding S-Y, DeBolt S (2010) Tools for cellulose analysis in plant cell walls. Plant Physiol **153**: 420–426

Harris DM, Corbin K, Wang T, Gutierrez R, Bertolo AL, Petti C, Smilgies D (2012) Cellulose microfibril crystallinity is reduced by mutating C-terminal transmembrane region residues. Proc Natl Acad Sci **109**: 4098-4103**Heath I** (1974) A unified hypothesis for the role of membrane bound enzyme complexes and microtubules in plant cell wall synthesis. J Theor Biol **48**: 445–449

Herth W, Schnepf E (1980) The fluorochrome, calcofluor white, binds oriented to structural polysaccharide fibrils. Protoplasma **105**: 129–133

Himmelspach R, Williamson RE, Wasteneys GO (2003) Cellulose microfibril alignment recovers from DCB-induced disruption despite microtubule disorganization. Plant J **36**: 565–575

Hochholdinger F, Wen T-J, Zimmermann R, Chimot-Marolle P, da Costa e Silva O, Bruce W, Lamkey KR, Wienand U, Schnable PS (2008) The maize (Zea mays L.) roothairless 3 gene encodes a putative GPI-anchored, monocot-specific, COBRA-like protein that significantly affects grain yield. Plant J **54**: 888–898

Holsters M, Waele D De, Depicker A, Messens E, Montagu M Van, Schell J (1978) Transfection and transformation ofAgrobacterium tumefaciens. Mol Gen Genet **163**: 181–187

Jacob-wilk D, Kurek I, Hogan P, Delmer DP (2006) The cotton fiber zinc-binding domain of cellulose synthase A1 from Gossypium hirsutum displays rapid turnover in vitro and in vivo. Proc Natl Acad Sci **103**: 12191–12196

Jeffries TW (1990) Biodegradation of lignin-carbohydrate complexes. Biodegradation **1**: 163–176

Jensen JK, Kim H, Cocuron J-C, Orler R, Ralph J, Wilkerson CG (2010) The DUF579 domain containing proteins IRX15 and IRX15-L affect xylan synthesis in *Arabidopsis*. Plant J **66**: 387–400

Jones L, Ennos a R, Turner SR (2001) Cloning and characterization of irregular xylem4 (irx4): a severely lignin-deficient mutant of *Arabidopsis*. Plant J **26**: 205–216

Joseleau J-P, Imai T, Kuroda K, Ruel K (2004) Detection in situ and characterization of lignin in the G-layer of tension wood fibres of Populus deltoides. Planta **219**: 338–345

Joshi CP, Thammannagowda S, Fujino T, Gou J, Avci U (2011) Perturbation of Wood Cellulose Synthesis Causes Pleiotropic Effects in Transgenic Aspen. Molec plant **4**: 331–345

Journal I (2001) Anatomical characteristics of tension wood and opposite wood in young inclined stems of poplar (Populus Eupamericana cv Ghoy).IAWA Journal **22**: 133–157

Ko J-H, Kim JH, Jayanty SS, Howe G A, Han K-H (2006) Loss of function of COBRA, a determinant of oriented cell expansion, invokes cellular defence responses in *Arabidopsis* thaliana. J Exp Bot **57**: 2923–2936

Kusumi A, Nakada C, Ritchie K, Murase K, Suzuki K, Murakoshi H, Kasai RS, Kondo J, Fujiwara T (2005) Paradigm shift of the plasma membrane concept from the two-dimensional continuum fluid to the partitioned fluid: high-speed single-molecule tracking of membrane molecules. Annu Rev Biophys Biomol Struct **34**: 351–378

Lalanne E, Honys D, Johnson A, Borner GHH, Lilley KS, Dupree P, Grossniklaus U, Twell D (2004) SETH1 and SETH2, two components of the glycosylphosphatidylinositol anchor biosynthetic pathway, are required for pollen germination and tube growth in *Arabidopsis*. Plant Cell Online **16**: 229-240

Ledbetter MC (1963) a “Microtubule” in Plant Cell Fine Structure. J Cell Biol **19**: 239–250

Lei L, Zhang T, Strasser R, Leed CM, Gonneaue M, Mach L, Vernhettes S, Kim SH, Cosgrove DJ, Li S and Gu Y (2014) The jiaoyao1 Mutant Is an Allele of korrigan1 That Abolishes Endoglucanase Activity and Affects the Organization of Both Cellulose Microfibrils and Microtubules in *Arabidopsis*. Plant Cell **26**: 2601-2616

Lenne P-F, Wawrezinieck L, Conchonaud F, Wurtz O, Boned A, Guo X-J, Rigneault H, He H-T, Marguet D (2006) Dynamic molecular confinement in the plasma membrane by microdomains and the cytoskeleton meshwork. EMBO J **25**: 3245–3256

Lev-Yudan S (1997) Fibres and Fibre-sclereids in Wild-type *Arabidopsis* thaliana. Ann Bot **80**: 125–129

Li S, Ge F-R, Xu M, Zhao X-Y, Huang G-Q, Zhou L-Z, Wang J-G, Kombrink A, McCormick S, Zhang XS, Zhang Y (2013) *Arabidopsis* COBRA-LIKE 10, a GPI-anchored protein, mediates directional growth of pollen tubes : Plant J **74**: 486–497

Li S, Lei L, Somerville CR, Gu Y (2011) Cellulose synthase interactive protein 1 (CSI1) links microtubules and cellulose synthase complexes. Proc Natl Acad Sci **109**: 185–190

Li Y, Qian Q, Zhou Y, Yan M, Sun L, Zhang M, Fu Z, Wang Y, Han B, Pang X, et al (2003a) BRITTLE CULM1, which encodes a COBRA-like protein, affects the mechanical properties of rice plants. Plant Cell **15**: 2020–2031

Lingwood D, Kaiser H-J, Levental I, Simons K (2009) Lipid rafts as functional heterogeneity in cell membranes. Biochem Soc Trans **37**: 955–960

Lingwood D, Simons K (2010) Lipid rafts as a membrane-organizing principle. Science **327**: 46–50

Liu L, Shang-guan K, Zhang B, Liu X, Yan M, Zhang L (2013) Brittle Culm1 , a COBRA-Like Protein , Functions in Cellulose Assembly through Binding Cellulose Microfibrils. PLoS Genet **9**: 1–15

Maloney VJ, Shawn D. Mansfield (2010) Characterization and varied expression of a membrane-bound endo-β-1, 4-glucanase in hybrid poplar.pdf. Plant Biotechnol J **8**: 294–307

Martiniere A, Lavagi I, Nageswaran G, Rolfe DJ, Maneta-Peyret L, Luu DT, Botchway SW, Webb SED, Mongrand S, Maurel C, Martin-Fernandez ML, Kleine-vehn J, Frimi J, Moreau P, Runions J (2012) Cell wall constrains lateral diffusion of plant plasma-membrane proteins. Proc Natl Acad Sci **109**: 12805-12810

McLean BW, Boraston AB, Brouwer D, Sanaie N, Fyfe CA, Warren RAJ, Kilburn DG, Haynes CA (2002) Carbohydrate-binding Modules Recognize Fine Substructures of Cellulose. J of Biol Chem **277**: 50245-50254

Mcqueen-mason SJ, Cosgrove DJ (1995) Expansin Mode of Action on Cell Walls ’. Plant Physiol **107**: 87–100

Mitchell KJ, Lucanus R (1962) Growth of pasture species under controlled environment. New Zeal J Agric Res **5**: 135–144

Mongrand S, Morel J, Laroche J, Claverol S, Carde JP, Hartmann MA, Bonneu M, Simon-Plas F, Lessire R, Bessoule JJ (2004) Lipid rafts in higher plant cells: Purification and characterization of TX100-insoluble microdomains from tobacco plasma membrane. J Biol Chem **279**: 36277–36286

Morgan JLW, Strumillo J, Zimmer J (2013) Crystallographic snapshot of cellulose synthesis and membrane translocation. Nature **493**: 181–186

Murashige T, Skoog F (1962) A Revised Medium for Rapid Growth and Bio Assays with Tobaoco Tissue Cultures. **15**: 473–497

Nishi K, Saigo K (2007) Cellular internalization of green fluorescent protein fused with herpes simplex virus protein VP22 via a lipid raft-mediated endocytic pathway independent of caveolae and Rho family GTPases but dependent on dynamin and Arf6. J Biol Chem **282**: 27503–27517

Orlean P, Menon A (2007) Thematic review series: lipid posttranslational modifications. GPI anchoring of protein in yeast and mammalian cells, or: how we learned to stop worrying and love glycophospholipids. J Lipid Res **48**: 993–1011

Paredez AR, Somerville CR, Ehrhardt DW (2006) Visualization of cellulose synthase demonstrates functional association with microtubules. Science **312**: 1491–1495

Park J, Canam T, Kang K, Ellis DD, Mansfield SD (2008) Over expression of an *Arabidopsis* family A sucrose phosphate synthase (SPS) gene alters plant growth and fibre development. Transgenic Res **17**: 181–192

Park YB, Cosgrove DJ (2012) Changes in Cell Wall Biomechanical Properties in the Xyloglucan-Deficient xxt1/xxt2Mutant of *Arabidopsis*. Plant Phys **158**: 465-475

Paulick MG, Bertozzi CR (2008) The glycosylphosphatidylinositol anchor: a complex membrane-anchoring structure for proteins. Biochemistry **47**: 6991–7000

Pauly M, Albersheim P, Darvill A, York WS (1999) Molecular domains of the cellulose/xyloglucan network in the cell walls of higher plants. Plant J **20**: 629–639

Paux E, Carocha V, Marques C, Mendes de Sousa A, Borralho N, Sivadon P, Grima-Pettenati J (2005) Transcript profiling of Eucalyptus xylem genes during tension wood formation. New Phytol **167**: 89–100

Persson S, Paredez A, Carroll A, Palsdottir H, Doblin M, Poindexter P, Khitrov N, Auer M, Somerville CR (2007) Genetic evidence for three unique components in primary cell-wall cellulose synthase complexes in *Arabidopsis*. Proc Natl Acad Sci U S A **104**: 15566–15571

Persson S, Wei H, Milne J, Page GP, Somerville CR (2005) Identification of genes required for cellulose synthesis by regression analysis of public microarray data sets. Proc Natl Acad Sci U S A **102**: 8633-8638

Plomion C, Pionneau C, Baillères H (2003) Analysis of Protein Expression along the Normal to Tension Wood Gradient in Eucalyptus gunnii. Holzforschung **57**: 353–358

Qian Q, Yunhai L, Dali Z, Sheng T, Zhengke W, Xueyong L, Zhigang D, Ning D, Lei S, Jiayang L (2001) Isolation and genetic characterization of a fragile plant mutant in rice (itOryza sauva) L. Chinese Sci Bull **46**: 2082–2085

Reiterer A, Lichtenegger H (1999) Experimental evidence for a mechanical function of the cellulose microfibril angle in wood cell walls. Philos **79**: 2173–2184

Roland J-C, Vian B (1979) The wall of the growing plant cell. Int Rev Cytol **61**: 129–166

Roudier F, Fernandez AG, Fujita M, Himmelspach R, Borner GHH, Schindelman G, Song S, Baskin TI, Dupree P, Wasteneys GO, et al (2005b) COBRA, an *Arabidopsis* extracellular glycosyl-phosphatidyl inositol-anchored protein, specifically controls highly anisotropic expansion through its involvement in cellulose microfibril orientation. Plant Cell **17**: 1749-1760

Roudier F, Schindelman G, DeSalle R, Benfey PN (2002) The COBRA family of putative GPI-anchored proteins in *Arabidopsis*. A new fellowship in expansion. Plant Physiol **130**: 538-549

Ruel K, Nishiyama Y, Joseleau J (2012) Plant Science Crystalline and amorphous cellulose in the secondary walls of *Arabidopsis*. Plant Sci **194**: 48–61

Saka S, Goring DAI (1985) Localization of lignins in wood cells. In *Biosynthesis and Biodegredation of wood components*, ed. Higuchi T. Academic pp. 51-62

Sampathkumar A, Gutierrez R, Mcfarlane HE, Bringmann M, Lindeboom J, Emons A, Samuels L, Ketelaar T, Ehrhardt DW, Persson S (2013) Patterning and Lifetime of Plasma Membrane-Localized Cellulose Synthase Is Dependent on Actin Organization in *Arabidopsis* Interphase Cells 1 [W]. Society **162**: 675–688

Sato K, Suzuki R, Nishikubo N, Takenouchi S, Ito S, Nakano Y, Nakaba S, Sano Y, Funada R, Kajita S, et al (2010) Isolation of a novel cell wall architecture mutant of rice with defective *Arabidopsis* COBL4 ortholog BC1 required for regulated deposition of secondary cell wall components. Planta **232**: 257–270

Sato S, Kato T, Kakegawa K, Ishii T, Liu Y, Awano T, Takabe K, Nishiyama Y, Kuga S, Sato S, et al (2001) Role of the Putative Membrane-Bound Endo-1 , 4B -Glucanase KORRIGAN in Cell Elongation and Cellulose Synthesis in *Arabidopsis* thaliana. Dna Res **42**: 251–263

Sato K, Ito S, Fujii T, Suzuki R, Takenouchi S, Nakaba S, Funada R, Sano Y, Kajita S, Kitano H, Katayama Y (2011) The carbohydrate-binding module (CBM)-like sequence is crucial for rice CWA1/BC1 function in proper assembly of secondary cell wall materials. Plant Signaling & Behavior **5**: 1433-1436

Saxena IM, Brown RM (2005) Cellulose biosynthesis: current views and evolving concepts. Ann Bot **96**: 9–21

Scheible WR, Eshed R, Richmond T, Delmer D, Somerville C (2001) Modifications of cellulose synthase confer resistance to isoxaben and thiazolidinone herbicides in *Arabidopsis* Ixr1 mutants. Proc Natl Acad Sci U S A **98**: 10079–10084

Scheller HV, Ulvskov P (2010) Hemicelluloses. Annu Rev Plant Biol.61: 263-289

Schindelman G, Morikami a, Jung J, Baskin TI, Carpita NC, Derbyshire P, McCann MC, Benfey PN (2001) COBRA encodes a putative GPI-anchored protein, which is polarly localized and necessary for oriented cell expansion in *Arabidopsis*. Genes Dev **15**: 1115–1127

Schmid M, Davison TS, Henz SR, Pape UJ, Demar M, Vingron M, Schölkopf B, Weigel D, Lohmann JU (2005) A gene expression map of *Arabidopsis* thaliana development. Nat Genet **37**: 501–506

Schwab R, Ossowski S, Riester M, Warthmann N, Weigel D (2006) Highly Specific Gene Silencing by Artificial MicroRNAs in *Arabidopsis*. Society **18**: 1121–1133

Simpson PJ, Xie H, Bolan DN, Gilbert HJ, Williamson MJ (2010) The Structural Basis for the Ligand Specificity of Family 2 Carbohydrate-binding Modules. J of biol Chem **275**: 41137-41142

Sindhu A, Langewisch T, Olek A, Multani DS, McCann MC, Vermerris W, Carpita NC, Johal G (2007) Maize Brittle stalk2 encodes a COBRA-like protein expressed in early organ development but required for tissue flexibility at maturity. Plant Physiol **145**: 1444–1459

Singer SJ, Nicolson GL (1972) The fluid mosaic model of the structure of cell membranes. Science **175**: 720–731

Smith LG, Oppenheimer DG (2005) Spatial control of cell expansion by the plant cytoskeleton. Annu Rev Cell Dev Biol **21**: 271–95

Somerville C (2006) Cellulose synthesis in higher plants. Annu Rev Cell Dev Biol **22**: 53-78

Sugimoto K, Himmelspach R, Williamson RE, Wasteneys GO (2003) Mutation or drug-dependent microtubule disruption causes radial swelling without altering parallel cellulose microfibril deposition in *Arabidopsis* root cells. Plant Cell Online **15**: 1414-1425

Sugimoto K, Williamson RE, Wasteneys GO (2001) Wall architecture in the cellulose-deficient rsw1 mutant of *Arabidopsis* thaliana: microfibrils but not microtubules lose their transverse alignment before microfibrils become unrecognizable in the mitotic and elongation zones of roots. Protoplasma **215**: 172–183

Szymanski DB, Cosgrove DJ (2009) Dynamic coordination of cytoskeletal and cell wall systems during plant cell morphogenesis. Curr Biol **19**: 800–811

Tabuchi A, Li L-C, Cosgrove DJ (2011) Matrix solubilization and cell wall weakening by β-expansin (group-1 allergen) from maize pollen. Plant J **68**: 546–559

Takahashi J, Rudsander UJ, Hedenström M, Banasiak A, Harholt J, Amelot N, Immerzeel P, Ryden P, Endo S, Ibatullin FM, et al (2009) KORRIGAN1 and its aspen homolog PttCel9A1 decrease cellulose crystallinity in *Arabidopsis* stems. Plant Cell Physiol **50**: 1099–1115

Taylor NG (2007) Identification of cellulose synthase AtCesA7 (IRX3) in vivo phosphorylation sites—a potential role in regulating protein degradation. Plant Mol Biol **64**: 161–171

Taylor NG, Howells RM, Huttly AK, Vickers K, Turner SR (2003) Interactions among three distinct CesA proteins essential for cellulose synthesis. PNAS 100:1450-1455

Thumma BR, Matheson B a, Zhang D, Meeske C, Meder R, Downes GM, Southerton SG (2009) Identification of a Cis-acting regulatory polymorphism in a Eucalypt COBRA-like gene affecting cellulose content. Genetics **183**: 1153–1164

Turner SR, Somerville CR (1997a) Collapsed xylem phenotype of *Arabidopsis* identifies mutants deficient in cellulose deposition in the secondary cell wall. Plant Cell **9**: 689–701

Tuskan G a, Difazio S, Jansson S, Bohlmann J, Grigoriev I, Hellsten U, Putnam N, Ralph S, Rombauts S, Salamov a, et al (2006) The genome of black cottonwood, Populus trichocarpa (Torr. & Gray). Science **313**: 1596–1604

Vain T, Crowell EF, Timpano H, Biot E, Desprez T, Mansoori N, Trindade LM, Pagant S, Robert S, Höfte H, Gonneau M, Vernhette S (2014) The Cellulase KORRIGAN Is Part of the Cellulose Synthase Complex. Plant Phys **165**: 1521-1532

Varner JE, Lin LS (1989) Plant cell wall architecture Cell **56**: 231-239

Verbelen J, Vissenberg K, Fry SC, Pauly M, Ho H, Edinburgh T, Wall C, Building DR, Mu A, Cellulaire LDB, et al (2010) XTH acts at the microfibril – matrix interface during cell elongation. **56**: 673–683

Washusen R, Evans R (2001) THE ASSOCIATION BETWEEN CELLULOSE CRYSTALLITE WIDTH. **22**: 235–243

Wasteneys GO (2004) Progress in understanding the role of microtubules in plant cells. Curr Opin Plant Biol **7**: 651–660

Wasteneys GO, Fujita M (2006) Establishing and maintaining axial growth: wall mechanical properties and the cytoskeleton. J Plant Res **119**: 5–10

Wightman R, Marshall R, Turner SR (2009) A cellulose synthase-containing compartment moves rapidly beneath sites of secondary wall synthesis. Plant Cell Physiol **50**: 584–594

Wightman R, Turner SR (2008a) The roles of the cytoskeleton during cellulose deposition at the secondary cell wall. Plant J **54**: 794–805

Yamaguchi M, Goué N, Igarashi H, Ohtani M, Nakano Y, Mortimer JC, Nishikubo N, Kubo M, Katayama Y, Kakegawa K, et al (2010) VASCULAR-RELATED NAC-DOMAIN6 (VND6) and VND7 Effectively Induce Transdifferentiation into Xylem Vessel Elements under Control of an Induction System. Plant Physiol **153**: 906–914

Ye X, Kang B, Osburn LD, Cheng Z-M (2009a) The COBRA gene family in Populus and gene expression in vegetative organs and in response to hormones and environmental stresses. Plant Growth Regul **58**: 211–223

Yin Y, Huang J, Xu Y (2009) The cellulose synthase superfamily in fully sequenced plants and algae. BMC Plant Biol **9**: 99-110

Zhang D, Yang X, Zhang Z, Li B (2009) Expression and nucleotide diversity of the poplar COBL gene. Tree Genet Genomes **6**: 331–344

Zhou G, Nairn CJ, Wood-Jones A, Richardson EA, Zhong R, Pen MJ (2005) *Arabidopsis* Fragile Fiber8 , Which Encodes a Putative Glucuronyltransferase , Is Essential for Normal Secondary Wall Synthesis. Plant Cell **17**: 3390–3408